

Université du Québec
Institut National de la Recherche Scientifique
Centre Eau Terre Environnement

**Geology and chemo-stratigraphy of the Colomb-Chaboullié
greenstone belt, James Bay, Quebec**

Géologie et chimico-stratigraphie de la ceinture de roches vertes de Colomb-Chaboullié, Baie-James, Québec

Par

Sarah Galloway

Mémoire présenté
pour l'obtention du grade de Maître ès sciences (M.Sc.)
en Sciences de la Terre

Jury d'évaluation

Examinateur externe	Jonathan O'Neil Université d'Ottawa
Examinateur interne	Marc Richer-LaFlèche INRS Centre Eau Terre Environnement
Directeur de recherche	Pierre-Simon Ross INRS Centre Eau Terre Environnement

ABSTRACT

Archean greenstone terranes are key to understanding the geological processes active during early Earth history. These areas are also of economic interest due to their association with volcanogenic massive sulphide (VMS) deposits, and several other types of mineral deposits.

Geological, stratigraphic, petrographic and geochemical studies were carried out on the volcanic units of the Archean Colomb-Chaboullié greenstone belt, located between the Nemiscau and Opatica subprovinces of the Superior Province, Quebec, Canada. The Colomb-Chaboullié belt is considered to have potential for exploration of VMS deposits, orogenic gold, and Ni-PGE deposits, among others. The Colomb-Chaboullié greenstone belt presents a good opportunity to study the characteristics of a smaller and petrologically less complex greenstone belt, located to the north of the Abitibi greenstone belt. Such smaller greenstone terranes are understudied and underexplored compared to the Abitibi.

The Colomb-Chaboullié belt, which has undergone amphibolite facies metamorphism, is made up of three submarine volcanic units: the dominant pillowed to massive basaltic lavas (*Acch1*), massive to pillowed intermediate lavas (\pm intrusions) that are variably porphyritic (*Acch2* and *Acch2a*), and intermediate to felsic volcaniclastic rocks (*Acch3*). The basalts are divided here into five geochemical units that are tholeiitic to transitional in magmatic affinity. The three main basalt groups (*Acch1a*, *Acch1b*, and *Acch1c*) show a progressive influence of crustal contamination, suggesting that *Acch1a* had the most direct passage to the surface whereas *Acch1b* and *Acch1c* spent longer in the crust. However, most of the major element trends in the basalts are explained by crystal fractionation, independently of the degree of contamination.

The remaining volcanic facies are calc-alkaline in magmatic affinity. The intermediate lavas (*Acch2* and *Acch2a*) are geochemically similar to the intermediate volcaniclastic rocks (*Acch3a*), suggesting that petrologically, these rocks share the same origin. Trace

elements in the intermediate rocks show a distinct ‘arc’ signature, which can be interpreted either as the influence of a subduction zone, or as crustal contamination. Suitable contaminants are known from the adjacent Opatica Subprovince. If the crustal contamination hypothesis is correct, the intermediate rocks may simply be the more contaminated equivalents to the basalts. Yet Harker diagrams and the contrasting magmatic affinities indicate that the intermediate to felsic rocks are not related to the basalts by a simple assimilation-fractional crystallisation (AFC) trend. Instead, the andesites and felsic rocks must have evolved separately from the basalts, perhaps in a crustal magma chamber. The felsic volcaniclastic rocks (*Acch3b*), which are defined by high silica contents but relatively low Zr values, show the strongest volcanic arc signatures and/or have undergone the most intense crustal contamination of the Colomb-Chaboullié volcanic suite. Silicification and sericitisation may also have played a part in the evolution of these felsic rocks.

Au-Ag-Cu showings are present in the volcanic units of the Colomb-Chaboullié belt, especially in the basalt flows. This mineralisation, which occurs as massive, semi-massive and disseminated sulphide occurrences, shows evidence of a syn-volcanic origin. Detailed mapping of the gold-bearing Lac Marcaut VMS showing suggests that a favourable basalt-basalt contact may be present.

The Colomb-Chaboullié belt is compared to the Frotet-Evans and Lac des Montagnes greenstone belts of the Opatica and Nemiscau subprovinces, respectively. Although there is no perfect fit for the mafic samples of the Frotet-Evans belt, the intermediate lavas and volcaniclastic rocks are geochemically very similar to the intermediate rocks of the Colomb-Chaboullié belt. The Lac des Montagnes belt strongly resembles the Colomb-Chaboullié belt geochemically. However, currently available U-Pb geochronology suggests that the Lac des Montagnes belt is several tens of m.y. younger than the Colomb-Chaboullié belt, whereas the Frotet-Evans belt may have a similar age to the Colomb-Chaboullié.

RÉSUMÉ

Les ceintures de roches vertes archéennes sont essentielles à la compréhension des processus géologiques actifs au cours de l'histoire précoce de la terre. Ces terranes présentent également un intérêt économique en raison de leur association avec les gisements de sulfures massifs volcanogènes (SMV) et plusieurs autres types de gîtes minéraux.

Une étude géologique, stratigraphique, pétrographique, et géochimique a été réalisée sur les unités volcaniques de la ceinture de roches vertes archéennes de Colomb-Chaboullié, située entre les sous-provinces de Nemiscau et d'Opatica (Province du Supérieur), au Québec, Canada. La ceinture de Colomb-Chaboullié est considérée comme ayant un potentiel d'exploration pour les gites de SMV, d'or orogénique et de Ni-EGP, entre autres. La ceinture de roches vertes de Colomb-Chaboullié présente une opportunité d'étudier les caractéristiques d'une ceinture de roches vertes plus petite et moins complexe pétrologiquement, située au nord de la ceinture de l'Abitibi. Ces petites ceintures de roches vertes sont sous-étudiées et sous-explorées comparativement à l'Abitibi.

La ceinture de Colomb-Chaboullié, qui a subi un métamorphisme du facies amphibolite, est constituée de trois unités volcaniques sous-marines : les laves basaltiques massives à cousinées, qui sont dominantes (*Acch1*), les laves intermédiaires, massives à cousinées (\pm intrusions), qui sont variablement porphyriques (*Acch2* et *Acch2a*), et les roches volcanoclastiques intermédiaires à felsiques (*Acch3*). Les basaltes sont subdivisés en cinq unités géochimiques qui ont des affinités magmatique allant de tholéitique à transitionnelle. Les trois principaux groupes de basalte (*Acch1a*, *Acch1b* et *Acch1c*) montrent une influence progressive de la contamination crustale, ce qui suggère qu'*Acch1a* a eu le passage le plus direct vers la surface alors qu'*Acch1b* et *Acch1c* ont passé plus de temps dans la croûte. Cependant, la plupart des tendances d'éléments majeurs dans les basaltes s'expliquent par la cristallisation fractionnée, indépendamment du degré de contamination.

Les autres roches volcaniques sont d'affinité calco-alcaline. Les laves intermédiaires (*Acch2* et *Acch2a*) sont géochimiquement similaires aux roches volcanoclastiques intermédiaires (*Acch3a*), ce qui suggère que pétrologiquement, ces roches partagent la même origine. Les éléments en traces dans les roches intermédiaires, présentent une signature d'« arc » distincte, qui peut être interprétée soit comme l'influence d'une zone de subduction, soit comme une contamination

crustale. Des contaminants de composition appropriée sont connus dans la Sous-province d'Opatica, adjacente. Dans l'hypothèse d'une contamination crustale, les roches intermédiaires pourraient simplement être les équivalents plus contaminés des basaltes. Cependant, les diagrammes de Harker et les affinités magmatiques contrastantes suggèrent que les roches intermédiaires à felsiques ne sont pas reliées aux basaltes par une simple tendance d'assimilation-cristallisation fractionnée (AFC). Au lieu de cela, les andésites et les roches felsiques ont dû évoluer séparément des basaltes, peut-être dans une chambre magmatique crustale. Les roches volcanoclastiques felsiques (*Acch3b*), qui sont définies par des teneurs élevées en silice mais des concentrations en Zr relativement faibles, présentent les signatures d'arc volcanique les plus fortes et/ou ont subi la contamination crustale la plus intense de la suite volcanique Colomb-Chaboullié. La silicification et la séricitisation peuvent également avoir joué un rôle dans l'évolution de ces roches felsiques.

Des indices de Au-Ag-Cu sont présents dans les unités volcaniques de la ceinture de Colomb-Chaboullié, en particulier dans les coulées de basalte. Cette minéralisation, qui se présente sous la forme de sulfures massifs, semi-massifs ou disséminés, possède des caractéristiques suggérant une origine syn-volcanique. La cartographie détaillée de l'indice de SMV aurifère du Lac Marcaut suggère la présence possible d'un contact basalte-basalte favorable à la mise en place des minéralisations volcanogènes.

Les caractéristiques géochimiques des roches volcaniques de Colomb-Chaboullié sont comparées à celles des ceintures de roches vertes de Frotet-Evans et du lac des Montagnes des sous-provinces d'Opatica et de Nemiscau, respectivement. Bien qu'il n'y ait pas de correspondance géochimique parfaite pour les échantillons mafiques de la ceinture de Frotet-Evans, les laves intermédiaires et les roches volcanoclastiques de Frotet-Evans sont géochimiquement très similaires aux roches intermédiaires de la ceinture de Colomb-Chaboullié. Les roches volcaniques de ceinture du lac des Montagnes ressemblent fortement à la ceinture Colomb-Chaboullié géochimiquement. Cependant, les données géochronologiques U-Pb actuellement disponibles suggèrent que la ceinture du lac des Montagnes est plusieurs dizaines de millions d'années plus jeune que la ceinture de Colomb-Chaboullié, alors que la ceinture de Frotet-Evans pouvait avoir un âge similaire à celui de la ceinture de Colomb-Chaboullié.

ACKNOWLEDGEMENTS

I would like to sincerely thank my research director, Pierre-Simon Ross, for his supervision throughout this project, his help during field and lab work, support during the writing of this memoir, and his engaging discussions that were always food for thought.

I thank Daniel Bandyayera and Yannick Daoudene of the *Ministère de l'Énergie et des Ressources naturelles*, Quebec, for providing all necessary data to complete this project, making my time mapping with them a great learning experience and providing constructive comments on all publications. I would also like to thank all the field assistants who accompanied me during my fieldwork.

I would like to acknowledge Marc Richer-LaFlèche for his useful comments during my "Devis de recherche" and seminar, and also Jonathan O'Neil, both of whom agreed to evaluate this MSc thesis.

Some special words of gratitude go to my dad Charlie, mum Alison, and sister Emma who have supported me throughout this project and my studies and for their continuous encouragement, despite the distance. Finally, I would like to thank Adam and my friends, old and new for their good humour and encouragement throughout this project.

Funding for this MSc project came from the *Ministère de l'Énergie et des Ressources naturelles*, Quebec.

TABLE OF CONTENTS

ABSTRACT	III
RÉSUMÉ.....	V
ACKNOWLEDGEMENTS.....	VII
LIST OF FIGURES.....	XI
LIST OF TABLES	XIII
SOMMAIRE RÉCAPITULATIF	XIV
1 INTRODUCTION.....	1
1.1 Context and problem.....	1
1.2 Objectives	3
1.3 Methodology.....	3
1.3.1 Fieldwork	3
1.3.2 Laboratory work.....	5
1.4 Structure of the thesis and role of co-authors in chapter 3.....	11
1.5 Previous publications	12
2 GEOLOGICAL CONTEXT	13
2.1 Superior Province.....	13
2.2 Opatica Subprovince.....	15
2.2.1 Geology of the northernmost Opatica	17
2.2.2 Frotet-Evans greenstone belt	19
2.3 Nemiscau Subprovince	20
2.4 Colomb-Chaboullié greenstone belt	21
2.5 Metallogenic context: VMS deposits	27
2.5.1 VMS deposit characteristics	28
2.5.2 Au-rich VMS deposits	30

2.5.3 VMS emplacement mechanisms	31
3 THE COLOMB-CHABOULLIÉ GREENSTONE BELT VOLCANICS: GEOLOGY, STRATIGRAPHY, AND GEOCHEMISTRY	35
3.1 Introduction	35
3.2 Geological context.....	36
3.3 Methodology.....	41
3.4 Results	42
3.4.1 Lithofacies and petrography	42
3.4.2 Lithogeochemistry	45
3.4.3 Mineralisation	54
3.5 Discussion.....	59
3.5.1 Mode of emplacement for volcanic rocks.....	59
3.5.2 Mineralisation	59
3.5.3 Geochemical groups in the Colomb-Chaboullié greenstone belt and map refinement	60
3.5.4 Petrology	61
3.6 Comparison with the Frotet-Evans greenstone belt: geology, geochemistry and geochronology	65
3.6.1 Basalts.....	68
3.6.2 Intermediate rocks	68
3.6.3 Felsic rocks.....	71
3.6.4 Geochronology	72
3.7 Comparison with the Lac des Montagnes greenstone belt.....	72
3.8 Conclusions.....	76
REFERENCES.....	79

Appedices (on the CD):

Appendix A: Geological map of the study area showing 2015 and 2016 outcrop locations

Appendix B: 2015 and 2016 whole-rock geochemical data

LIST OF FIGURES

Figure 2.1	Superior Province showing the major subprovinces and subdivisions.....	14
Figure 2.2	Simplified geological map of the Superior Province in the James Bay region of Quebec.....	16
Figure 2.3	Simplified geology of the Lac Rodayer region.....	18
Figure 2.4	Geology of the Colomb-Chaboullié greenstone belt.....	22
Figure 2.5	Thematic maps showing the distribution of selected background mineralisation throughout the Colomb-Chaboullié greenstone belt.....	25
Figure 2.6	Compilation map of the Lac Marcaut showing of the Colomb-Chaboullié greenstone belt.....	28
Figure 2.7	Diagram of a present-day black smoker complex.....	30
Figure 2.8	Favourable locations for VMS mineralisation in a compressional tectonic regime.....	32
Figure 2.9	Generalised emplacement model for VMS deposits.....	33
Figure 3.1	Geological map of the Eastern Superior Province, Quebec, showing the location of the Colomb-Chaboullié greenstone belt (in red) at the contact between the Opatica and Nemiscau subprovinces.....	37
Figure 3.2	Geological map of the Colomb-Chaboullié greenstone belt.....	40
Figure 3.3	Basaltic and andesitic lava flows of the Colomb-Chaboullié belt.....	43
Figure 3.4	Pillowed andesite lava and volcaniclastic rocks of the Colomb-Chaboullié greenstone belt.....	44
Figure 3.5	Alteration box plot and Harker compositional diagrams for the Colomb-Chaboullié greenstone belt.....	46
Figure 3.6	Classification and magmatic affinity diagrams for the Colomb-Chaboullié greenstone belt.....	49

Figure 3.7	Extended multi-element plots for the mafic lavas of the Colomb-Chaboullié greenstone belt.....	50
Figure 3.8	Tectonic discrimination and rhyolite fertility diagrams.....	55
Figure 3.9	Extended multi-element diagrams for the intermediate extrusive lavas, and intermediate to felsic volcaniclastic rocks of the Colomb-Chaboullié belt, as well as possible contaminants from the Opatica Subprovince.....	56
Figure 3.10	Mineralisation of the Colomb-Chaboullié greenstone belt.....	57
Figure 3.11	Detailed map of the Lac Marcaut outcrop.....	58
Figure 3.12	Schematic diagram illustrating the emplacement of the mafic and intermediate lava flows of the Colomb-Chaboullié belt.....	64
Figure 3.13	Simplified geology of the Frotet-Evans and Lac des Montagnes greenstone belts.....	66
Figure 3.14	Extended multi-element plots for selected units of the Frotet-Evans greenstone belt.....	69
Figure 3.15	Geochemical plots showing the distribution of the Frotet-Evans greenstone belt samples.....	70
Figure 3.16	Geochemical plots of the Lac des Montagnes volcanic rocks.....	74
Figure 3.17	Extended multi element plots for the volcanic units of the Lac des Montagnes belt, superimposed over the Colomb-Chaboullié fields.....	75

LIST OF TABLES

Table 1.1	Analytical methods used in this study, with accompanying limits of detections and blank sample data.....	6
Table 1.2	Level of accuracy of the major oxide database for the Colomb-Chaboullié belt 2016 whole-rock geochemical samples.....	7
Table 1.3	Level of accuracy of the rare earth elements for the Colomb-Chaboullié belt 2016 whole-rock geochemical samples.....	8
Table 1.4	Level of accuracy of the other trace elements used for the Colomb-Chaboullié belt 2016 whole-rock geochemical samples.....	9
Table 1.5	Level of reproducibility of the major oxide database for the Colomb-Chaboullié belt 2016 whole-rock geochemical samples.....	10
Table 1.6	Level of reproducibility of the rare earth elements for the Colomb-Chaboullié belt 2016 whole-rock geochemical samples.....	10
Table 1.7	Level of reproducibility of the other trace elements used for the Colomb-Chaboullié belt 2016 whole-rock geochemical samples.....	10
Table 3.1	Average major oxide geochemical characteristics of the volcanic units of the Colomb-Chaboullié belt.....	47
Table 3.2	Average trace element and elemental ratio geochemical characteristics of the volcanic units of the Colomb-Chaboullié belt.....	48
Table 3.3	Total volcanic composition and magmatic affinity comparison of the Colomb-Chaboullié, Frotet-Evans, and Lac des Montagnes greenstone belts.....	71

SOMMAIRE RÉCAPITULATIF

Les pages suivantes (en chiffres romains) sont un résumé français de seize pages qui répond aux exigences du programme de maîtrise en sciences de la Terre de l'INRS. Ce mémoire est écrit en anglais, où la première page commence à la première page des chiffres arabes.

Introduction et problématique

Les ceintures de roches vertes archéennes donnent des informations clés pour comprendre les processus géologiques pendant l'Archéen (p. ex., Bickle et al., 1994; Bédard et Ludden, 1997; O'Neil et al., 2001, 2012, 2013). Ces ceintures de roches vertes présentent également un intérêt économique, notamment pour les gisements de sulfures massifs volcanogènes (SMV) (p. ex., Franklin et al., 2005; Galley et al., 2007; Mercier-Langevin et al., 2014). La ceinture de roches vertes de l'Abitibi de la Province du Supérieur, au Canada, est une zone importante pour les gisements de SMV (Galley et al., 2007). En conséquence, la géologie et les gisements de l'Abitibi ont été largement étudiés (p. ex., Laflèche et al., 1992; Hannington et al., 2005; Mercier-Langevin et al., 2007; Rogers et al., 2014). Toutefois, les petites ceintures de roches vertes, comme celles situées au nord de la ceinture de l'Abitibi, ne sont pas aussi bien étudiées, même si elles sont stratigraphiquement et probablement pétrologiquement moins complexes.

La ceinture de Colomb-Chaboullié est située entre les sous-provinces d'Opatica et de Nemiscau, dans la Province du Supérieur. Par conséquent, il n'est pas clair à laquelle de ces sous-provinces appartient la ceinture de Colomb-Chaboullié. La ceinture est composée de trois unités volcaniques sous-marines (Bandyayera et Daoudene, 2017) : des coulées de basalte massives à cousinées, des laves intermédiaires variablement porphyriques, et des roches volcanoclastiques intermédiaires à felsiques. Les autres lithologies de la ceinture de Colomb-Chaboullié comprennent des intrusions mafiques/ultramafiques et des faciès métasédimentaires. Une meilleure connaissance de

la chimico-stratigraphie, en particulier dans les basaltes, pourrait être utile pour l'exploration des SMV.

La ceinture de Colomb-Chaboullié contient des indices de sulfures massifs, semi-massifs et disséminés en Ag-Au-Cu, suggérant un potentiel pour l'exploration pour des gîtes de SMV. Toutefois l'origine de ces minéralisations (c. à. d. tectonique ou synvolcanique) n'était pas claire avant cette étude.

Objectifs

Les objectifs du projet de maîtrise sont de:

1. Améliorer les connaissances géologiques, stratigraphiques, pétrographiques et géochimiques des roches volcaniques de la ceinture de roches vertes de Colomb-Chaboullié;
2. Comparer la géochimie et la géochronologie des roches volcaniques de la ceinture de Colomb-Chaboullié à celles des ceintures de roches vertes des sous-provinces d'Opatica et de Nemiscau, spécifiquement les ceintures de Frotet-Evans et du Lac des Montagnes;
3. Déterminer l'origine des indices de sulfures polymétalliques et relier la minéralisation à des unités chimio-stratigraphiques spécifiques.

Méthodologie

La ceinture de Colomb-Chaboullié, mesurant 77 x 7 km, a été cartographiée en 2015 par le MERN (Bandyayera et Daoudene, 2017). La zone d'étude de ce projet de maîtrise, s'étendant sur 28,6 x 5,7 km, est située dans les feuillets SNRC 32N03 et 32N04. La zone d'étude choisie comprend la partie centrale de la ceinture et est traversée par la Route de la Baie-James. D'autres affleurements ont été visités en hélicoptère pour échantillonner toutes les lithologies, y compris quelques affleurements situés à l'extérieur

de la zone d'étude. Au total, 69 affleurements ont été visités en 2016, dont 39 étaient auparavant connus du MERN. Sur les 73 échantillons prélevés sur le terrain, 45 échantillons géochimiques et 34 échantillons de lames minces ont été préparés. Les nouvelles données géochimiques obtenues ont été combinées aux analyses géochimiques de la campagne cartographique 2015 du MERN. L'affleurement de l'indice de SMV du lac Marcaut, situé dans la partie ouest de la zone d'étude, a été cartographié plus en détail pour aider à établir l'origine de la lentille de sulfures massifs.

Contexte géologique

Province du Supérieur

Le plus grand terrane archéen terrestre est la Province du Supérieur au Canada (Benn et Moyen, 2008). La Province du Supérieur est divisée en sous-provinces en fonction de différentes caractéristiques géologiques (Card et Ciesielski, 1986) (Fig. 2.1). La ceinture de roches vertes de Colomb-Chaboullié est située au contact entre deux de ces sous-provinces, l'Opatica et le Nemiscau (Bandyayera et Daoudene, 2017) (Figs. 2.1 et 2.2).

Sous-province d'Opatica

L'Opatica est une sous-province composée majoritairement de granitoïdes et de tonalites très déformés (Davis et al., 1994). Elle est délimitée au sud par la Sous-province de l'Abitibi et au nord par la Sous-province de Nemiscau (Fig. 2.2). Le secteur nord de l'Opatica a été cartographié plus en détail en 2015 (Bandyayera et Daoudene, 2017) (Fig. 2.3) et contient le pluton du lac Rodayer (*Arod*). À 2829-2822 Ma, le pluton du lac Rodayer est la plus ancienne unité de la Sous-province d'Opatica (Davis et al., 1994), et pourrait être un contaminant potentiel pour les roches volcaniques de la ceinture de Colomb-Chaboullié. Un autre contaminant possible dans la Sous-province de l'Opatica est le Complexe de Théodat, constitué de granodiorite, tonalite, granite et pegmatite.

La ceinture volcano-sédimentaire de Frotet-Evans, qui fait 250 km de long, est située dans la partie centrale de la Sous-province d'Opatica (Sawyer et Benn, 1993). Cette ceinture est principalement composée de coulées de lave mafiques et intermédiaires, ainsi que de laves et roches volcanoclastiques calco-alcalines (Boily et Dion, 2002). L'âge U-Pb le plus récemment obtenu pour la ceinture de Frotet-Evans est de $2755,5 \pm 0,9$ Ma (Bandyayera et Sharma, 2001). Plusieurs types de minéralisation sont identifiées dans la ceinture de Frotet-Evans, y compris des indices de SMV (Gosselin, 1996). La mine d'or-cuivre de Troilus est située dans la partie nord-est de la ceinture (Goodman et al., 2005).

Sous-province de Nemiscau

Le Nemiscau est une sous-province métasédimentaire (Bandyayera et Daoudene, 2017) comprenant des paragneiss, des métatexites et des diatexites (Hocq, 1994). Une mince séquence volcano-sédimentaire est présente dans le Nemiscau, le Groupe du lac des Montagnes (Bandyayera et Daoudene, en préparation). Cette séquence de roches vertes est principalement composée de basaltes amphibolitisés avec des roches volcanoclastiques intermédiaires à felsiques et des formations de fer. Un échantillon felsique a donné un âge U-Pb sur zircons d'environ 2712 Ma (Bandyayera et Daoudene, en préparation).

Ceinture de roches vertes de Colomb-Chaboullié

Les unités volcaniques de la ceinture de roches vertes de Colomb-Chaboullié, qui font l'objet de cette étude, ont des compositions mafique, intermédiaire, et intermédiaire à felsique (unités *Acch1*, *Acch2*, et *Acch3*, respectivement) (Fig. 2.4). L'unité *Acch3* a donné des âges de $2756,8 \pm 4,4$ et $2760,3 \pm 6,4$ Ma (David et al., en préparation).

Les coulées basaltiques massives (*Acch1*) sont la lithologie dominante dans la ceinture de Colomb-Chaboullié (Bandyayera et Daoudene, 2017). Le faciès principal est coussiné et contient souvent des hyaloclastites inter-coussin. Les coulées d'andésite, situées dans la partie est de la ceinture, sont divisées en deux faciès en fonction des proportions de phénocristaux de plagioclase. *Acch2* (massif) contient de 10 à 30% de phénocristaux et

Acch2a (massif à coussiné) contient de 0 à 10% de phénocristaux. L'unité *Acch3* est formée de roches volcanoclastiques intermédiaires à felsiques, constituant des lentilles dans les coulées de basalte. Ce faciès comprend des tufs à lapillis et des tufs.

Les intrusions mafiques/ultramafiques de la ceinture de Colomb-Chaboullié sont constituées de roches gabbroïques (*Acch4*) ainsi que de périclites et pyroxénites (*Acch5*). Les séquences de roches sédimentaires sont composées d'une formation de fer (*Acch6*), d'une séquence de paragneiss (*Acch7*) et d'un conglomérat polymicte (*Acch8*).

Contexte métallogénique: les gisements de SMV

Caractéristiques des gisements

Les gisements polymétalliques de SMV sont associés à des séquences volcaniques sous-marines, mais des roches sédimentaires peuvent également être présentes dans l'encaissant (Franklin et al., 1981). Ces gisements sont composés de deux parties : une lentille massive à semi-massive et la zone du *stockwerk* sous-jacente (Galley et al., 2007) (Fig. 2.7). La lentille de sulfures massifs à semi-massifs montre une zonation métallique avec une base plus riche en Cu et un sommet plus riche en Zn. La zone de stockwerk contient un système de veinules de sulfures riches en cuivre et des roches altérées en chlorite et séricite (Franklin et al., 1981).

Classification et mécanismes de mise en place

Plusieurs classifications des gîtes de SMV ont été proposées dans la littérature scientifique. Dans le cadre de ce mémoire, nous avons utilisé un système de classification des SMV basé sur la nature des roches volcaniques associées (Franklin et al., 2005). Dans cette classification, cinq types sont proposés: 1) les séquences bimodales dont la composition dominante est mafique, 2) séquences mafiques, 3) séquences mafiques avec unités pélitiques, 4) séquences bimodales à dominance felsique, et 5) unités felsiques silicoclastiques.

Les gisements de SMV se forment lorsque des fluides hydrothermaux sont rejetés sur ou près du fond marin, où ils se refroidissent, permettant ainsi la précipitation des sulfures (Lydon, 1988). Ces fluides riches en métaux circulent dans la croûte à cause du flux de chaleur élevé et de la présence de grandes cellules de convection de l'eau de mer dans les roches volcanique et intrusives (Franklin et al., 2005) (Fig. 2.9). Les métaux sont extraits des zones de réaction par la circulation de l'eau de mer et peut-être des intrusions syn-volcaniques (Galley et al., 2007; Franklin et al., 2005). Des structures syn-volcaniques, comme des failles, sont nécessaires pour transporter les fluides vers la surface et déposer les métaux.

Résultats

Lithofaciès et pétrographie

Dans la ceinture de Colomb-Chaboullié, les basaltes coussinés et déformés (*Acch1*) sont dominants (Figs. 3.3a et b). Lorsqu'ils sont bien préservés, de la hyaloclastite peut être identifiée entre les coussins. Des sulfures disséminés et des grenats sont souvent présents dans le matériel inter-coussin (Figs. 3.10a et b). L'assemblage minéral de ces coulées mafiques est constitué de plagioclase-amphibolite \pm biotite \pm chlorite \pm minéraux opaques (Figs. 3.3c et d). Les coussins ne sont pas assez bien préservés pour déterminer la polarité. Dans les zones les plus déformées, les basaltes se présentent comme des schistes.

Les coulées de lave andésitiques porphyriques (\pm intrusions?) (*Acch2*) contiennent environ 20% de phénocristaux de plagioclase tabulaire, avec un peu de hornblende et quelques glomérophénocristaux de biotite (Figs. 3.3e et f). Ces coulées de lave se trouvent dans la partie est de la ceinture de Colomb-Chaboullié. La matrice des laves andésitiques est recristallisée et contient du plagioclase-quartz-amphibole \pm biotite \pm chlorite. La sous-unité *Acch2a* comprend des coulées de laves coussinées d'andésite déformées (Fig. 3.4a). Ce faciès contient moins de phénocristaux de plagioclase (<5%) que *Acch2*.

Les roches volcanoclastiques (*Acch3*) sont composées de tufs et tufs à lapillis, intermédiaires à felsiques. Ces roches forment des petites lentilles dans les coulées de basalte (Fig. 3.2). Certaines de ces roches volcanoclastiques sont stratifiées (Fig. 3.4b) avec des bandes riches en plagioclase et en chlorite, qui alternent. D'autres affleurements volcanoclastiques contiennent des lapillis allongés (Fig. 3.4d). Ces roches volcanoclastiques comprennent un assemblage de plagioclase-quartz ± muscovite ± chlorite ± biotite (Fig. 3.4c). Des bandes de chlorite sont également observées en lame mince dans l'unité laminée.

Lithogéochimie

Les données géochimiques présentées ici ont été utilisées pour améliorer la cartographie géologique. Tous les échantillons utilisés pour les analyses géochimiques ont été prélevés dans les zones les moins altérées de la stratigraphie. Par conséquent, ces roches présentent peu d'altération (Fig. 3.5a). En se basant sur les analyses lithogéochimiques disponibles, les basaltes ont été divisés en trois grands groupes (*Acch1a*, *Acch1b* et *Acch1c*) et deux groupes mineurs (*Acch1d* et *Acch1e*) (Tableau 3.1 et 3.2).

Les laves intermédiaires (*Acch2* et *Acch2a*) restent inchangées car cette subdivision est basée sur des observations de terrain et car les deux sous-groupes sont géochimiquement similaires. Les roches volcanoclastiques sont divisées ici en roches des compositions intermédiaires (*Acch3a*) et felsiques (*Acch3b*).

Les diagrammes de Harker suggèrent qu'il existe différentes tendances entre les roches mafiques, intermédiaires et felsiques de la ceinture de Colomb-Chaboullié (Figs. 3.5b à h). Quand la silice augmente, les roches mafiques présentent une réduction des concentrations de TiO_2 , Fe_2O_3 , et MgO , alors que CaO et Al_2O_3 restent constants. Les laves intermédiaires et les roches volcanoclastiques suivent les mêmes tendances que les laves mafiques, mais avec des pentes plus douces. Les roches de l'unité *Acch3b* ont des concentrations en silice les plus élevées, les concentrations en TiO_2 les plus faibles, et l' Al_2O_3 a une tendance à la baisse.

Sur un diagramme de classification des roches volcaniques, les laves mafiques sont principalement des basaltes sub-alcalins (Figs. 3.6a et b). Cependant, certains échantillons des groupes *Acch1a* et *Acch1c* sont présents dans le champ andésite/andésite basaltique (Fig. 3.6a) en raison de leurs concentrations plus élevées en silice, ce qui suggère une mobilité de cet élément car ces roches montrent de faibles rapports de Zr et TiO₂ (Fig. 3.6e). *Acch1c* a des rapports Zr/TiO₂ plus élevés que les autres basaltes (Tableau 3.2) (Fig. 3.6b). Bien que la majorité des échantillons d'*Acch1d* et d'*Acch1e* se trouvent dans le champ basaltique sub-alcalin, deux échantillons d'*Acch1e* ont des rapports Nb/Y plus élevés et se situent donc dans le champ des roches intermédiaires.

Les roches volcaniques des groupes *Acch2* et *Acch2a* forment une population séparée des basaltes en raison de rapports Nb/Y plus élevés (Fig. 3.6b). Ces laves intermédiaires se situent dans le champ andésite/andésite basaltique de la figure 3.6a et à la limite des basaltes sub-alcalins de la figure 3.6b, mais avec des rapports Zr/TiO₂ similaires à ceux du champ basaltique/andésitique indifférencié. Les roches volcanoclastiques de l'unité *Acch3a* se superposent aux compositions des laves intermédiaires (*Acch2* et *Acch2a*) sur les diagrammes de Winchester et Floyd (1977) (Figs. 3.6a et b).

Acch3b représente les seules roches volcaniques felsiques de la ceinture Colomb-Chaboullié (Figs. 3.6a et b). Ces roches montrent des concentrations en silice variant 66,3 à 80,5%. Sept de ces échantillons felsiques sont situés dans le champ des roches rhyodacitique/dacitique, et cinq échantillons tombent dans le champ rhyolitique (Fig. 3.6a). Cependant, cette unité felsique présente des concentrations de Zr relativement faibles (Fig. 3.6b), ce qui est typique des roches felsiques calco-alcalines modernes ou Archéennes. Par conséquent, ces échantillons se trouvent dans le domaine andésite à rhyodacite/dacite sur le diagramme de classification de Winchester et Floyd (1977) présenté à la figure 3.6b.

En termes d'affinité magmatique, *Acch1a* et *Acch1d* tombent dans le champ tholéïtique, tandis que *Acch1b*, *Acch1c* et *Acch1e* sont transitionnels (Fig. 3.6d). Toutes les laves

intermédiaires (*Acch2* et *Acch2a*) et les roches volcanoclastiques intermédiaires à felsiques (*Acch3a* et *Acch3b*) sont calco-alcalines.

Sur le diagramme TiO_2 vs Zr, les basaltes se situent le long de la tendance tholéïtique positive, avec des concentrations de TiO_2 croissantes (Fig. 3.6e). D'hypothétiques roches tholéïtiques intermédiaires et felsiques, produites par fractionnement d'un magma mafique, devraient suivre la même tendance que les échantillons mafiques de la ceinture Colomb-Chaboullié. Ces hypothétiques roches felsiques tholéïtiques seraient caractérisées par de faibles teneurs en TiO_2 et de fortes teneurs en Zr. Par contre, les roches intermédiaires et felsiques de Colomb-Chaboullié sont calco-alcalines et suivent une évolution distincte sur le diagramme TiO_2 vs Zr, tendance qui correspond à celle des arcs modernes. *Acch3b* montre une gamme de concentrations en Zr similaires à celles des unités intermédiaires, mais des concentrations sont plus faibles en TiO_2 . Cela suggère qu'*Acch3b* n'a pas été produit par le simple fractionnement des magmas intermédiaires.

En termes de diagrammes d'éléments en traces étendus, les roches d'*Acch1a* montrent des spectres relativement plats, semblables à ceux des N-MORBs (Figs. 3.7a et e). *Acch1b* et *Acch1c* montrent une augmentation progressive du Th, avec des anomalies négatives de Nb-Ta correspondantes (Figs. 3.7b et c). Les spectres d'éléments traces étendus pour *Acch1b* et *Acch1c* ressemblent aux spectres des basaltes de bassin d'arrière-arc (BABB) ou des tholéïites d'arc (IAT) (Fig. 3.7f). Sur les diagrammes d'éléments traces étendus, *Acch1d* est similaire à *Acch1b* alors qu'*Acch1e* est similaire à *Acch1c* (Fig. 3.7d). Sur le diagramme de Pearce (2008) (Fig. 3.8c), l'unité *Acch1a* se rapproche du pôle N-MORB tandis qu'*Acch1b* et *Acch1d* sont situés au-dessus de la tendance MORB-OIB.

Contrairement aux basaltes, *Acch2* et *Acch2a* présentent de fortes anomalies négatives en Nb-Ta et en Ti sur les diagrammes d'éléments traces étendus (Figs. 3.9a et b). Ces andésites tombent dans le champ des arcs volcaniques sur plusieurs diagrammes de discrimination tectonique (Figs. 3.8a et b). Sur le diagramme de Pearce (2008), les

andésites se situent près du pôle crustal archéen et des contaminants possibles de la Sous-province d'Opatica (Fig. 3.8c).

Les roches volcanoclastiques intermédiaires (*Acch3a*) chevauchent les compositions des roches volcaniques andésitiques sur tous les diagrammes d'éléments traces (Figs. 3.6a à e, Figs. 3.8a à c et Fig. 3.9c), ce qui suggère à nouveau que ces unités sont pétrologiquement reliées. Les roches felsiques tombent principalement près de la limite entre les domaines Fl et FII sur le diagramme de Hart et al. (2004), ce qui suggère que ces roches proviennent d'une source profonde contenant de grenat et/ou de l'amphibole.

Minéralisation

La minéralisation en sulfures de Au-Ag-Cu est principalement présente dans les basaltes, mais on en trouve aussi à des contacts lithologiques avec d'autres unités volcaniques. Cinq indices minéralisés sont présents dans les laves basaltiques, un dans l'unité volcanoclastique et un dans une séquence sédimentaire (voir figure 3.2). Dans le faciès basaltique coussiné, des sulfures disséminés sont présents dans le matériel inter-coussin et s'associent à une altération en grenat-chlorite (Figs. 3.10a et b). Dans les coulées massives, les sulfures sont présents dans les fractures (Fig. 3.10c).

Trois indices de sulfures massifs à semi-massifs sont présents dans la ceinture Colomb-Chaboullié. L'indice du lac Marcaut (Fig. 3.10d) est le plus connu. Cette lentille de sulfures massifs comprend des clastes arrondis, riches en silice, qui contiennent de la pyrite et de la chalcopyrite en traces, dans une matrice de pyrrhotite (Figs. 3.10e et f). On remarque aussi dans les lentilles de sulfures de petits clastes de chlorite et des fragments felsiques irréguliers. Une cartographie détaillée a été réalisée sur l'indice du lac Marcaut (Fig. 3.11). Ceci montre que la lentille de sulfures massifs est située à un contact chimique entre deux basaltes, provenant des unités *Acch1a* et *Acch1c*. On trouve également des sulfures dans le matériel inter-coussin, à l'intérieur de petites veines et sous forme de zones rouillées à la surface de l'affleurement.

La lentille de sulfures massifs du lac Marcaut, d'une épaisseur de 1,4 m, s'étend sur plus de 80 m le long de l'affleurement. Cet horizon de sulfures peut être suivi sur 3 km latéralement (Thorsen et al., 1993). La schistosité des basaltes encaissants est légèrement inclinée par rapport à la lentille de sulfures (Fig. 3.11). Une valeur de 27 g/t d'or a été obtenu sur un échantillon choisi (Thorsen et al., 1993).

Discussion

Environnement de dépôt des roches volcaniques

Les faciès coussinés dans les laves basaltiques et andésitiques, ainsi que la présence d'haloclastite dans les basaltes, indiquent que ces roches se sont déposées dans un environnement sous-marin. Comme les roches volcanoclastiques intermédiaires et felsiques forment de petites lentilles dans les coulées de laves basaltiques et andésitiques, elles ont dû aussi se former dans le même contexte sous-marin.

Minéralisation volcanogène

La lentille de sulfures massifs du lac Marcaut est située à un contact entre les unités basaltiques *Acch1a* et *Acch1c*. Ce contact pourrait être prospectif ailleurs dans la région. Concernant l'origine des sulfures, les observations suivantes sont importantes. D'abord, les sulfures à Au-Ag-Cu remplissent des espaces de porosité primaire entre les coussins. On les rencontre aussi dans des fractures du faciès basaltique massif, formant un stockwerk. Des lentilles de sulfures massifs à semi-massifs sont présentes à des contacts lithologiques. Finalement, la minéralisation est associée aux altérations en chlorite et grenat, et est située près de contacts lithologiques. Tout ceci suggère que la minéralisation est d'origine synvolcanique.

Géochimie et pétrologie

Les résultats géochimiques présentés ont été utilisés pour améliorer la carte géologique de la ceinture de roches vertes de Colomb-Chaboullié à l'échelle 1:50 000 (Fig. 3.2). Les unités de roches basaltiques prédominantes, qui étaient indifférenciées avant cette étude, resteront indifférenciées sur la carte géologique jusqu'à ce que l'échelle de la cartographie soit accrue. Cependant, les groupes géochimiques établis au cours de ce projet, ainsi que les indicateurs potentiels de polarité qui pourraient être établis dans le cadre de travaux futurs, permettront d'établir une chimio-stratigraphie complète des roches volcaniques de la ceinture de Colomb-Chaboullié.

Les basaltes ont été divisés en trois groupes principaux (*Acch1a*, *Acch1b* et *Acch1c*) et deux groupes mineurs (*Acch1d* et *Acch1e*), selon leurs caractéristiques géochimiques. Les roches volcaniques mafiques du secteur ouest de la ceinture Colomb-Chaboullié sont dominées par des basaltes *Acch1a* (Fig. 3.2). Le secteur central de la zone d'étude montre des compositions plus variées en ce qui concerne les basaltes. Les coulées de basalte dans la partie centrale du secteur d'étude, entre la route de la Baie-James et le lac Colomb, sont principalement composées des groupes *Acch1a* et *Acch1c* avec des occurrences d'*Acch1b* principalement près du lac Colomb. Les échantillons d'*Acch1c* sont situés au sud d'*Acch1b*. Dans l'est, les basaltes sont dominés par *Acch1a*. Les unités mineures de basalte, *Acch1d* et *Acch1e*, sont également présentes dans la partie est de la ceinture de roches vertes. Le groupe *Acch1d* se rencontre dans la région la plus à l'est de la zone d'étude, où il présente un faciès en coussin bien développé.

Les deux groupes de roches andésitiques (*Acch2* et *Acch2a*) sont géochimiquement similaires. La différenciation de ces groupes de roches intermédiaires est basée sur l'abondance des phénocristaux. Les données géochimiques actuelles ont permis d'identifier de petites unités *Acch2a* isolées, présentes dans les coulées basaltiques. *Acch3* a été divisé ici en *Acch3a* et *Acch3b* en fonction de la différence géochimique (compositions intermédiaire versus felsique).

Les roches de l'unité *Acch1a* montrent des concentrations des éléments traces similaires aux N-MORBs (Fig. 3.7a). Dans une perspective actualiste, elle pourrait avoir une origine similaire aux N-MORBs modernes, c'est-à-dire une dorsale médio-océanique ou un bassin d'arrière-arc très évolué (Figs. 3.8a et c). Les autres groupes de basaltes se trouvent au-dessus de la tendance MORB-OIB sur le diagramme de Pearce (2008) (Fig. 3.8c). Toujours dans une perspective actualiste, ceci pourrait témoigner de l'influence d'une zone de subduction sur les unités *Acch1b* à *Acch1e*. Cependant, si les processus tectoniques étaient différents pendant l'Archéen, la géochimie des basaltes pourraient s'expliquer par la cristallisation fractionnée avec, indépendamment, une composante de contamination crustale variable. Les basaltes n'ont subi qu'un faible degré de contamination crustale pendant l'ascension, *Acch1b* et *Acch1c* sont plus contaminés que *Acch1a* (Fig. 3.12).

Les roches andésitiques et les roches volcanoclastiques intermédiaires à felsiques ne sont pas directement reliées aux basaltes, ce qui est démontré par des rapports Nb/Y plus élevés, une affinité calco-alcaline et des anomalies négatives prononcées en Nb-Ta et Ti. Comme ces roches calco-alcalines sont intercalées dans coulées basaltiques, elles ont dû être produites dans un environnement tectonique similaire à celui des basaltes. Il semble que le magma ayant produit les andésites et les roches plus évoluées soit resté plus longtemps dans la croûte. Ce magma a évolué par assimilation et cristallisation fractionnée (AFC) dans une chambre magmatique crustale. Les basaltes auraient empruntés un chemin plus direct vers la surface.

Les roches intermédiaires de la ceinture de Colomb-Chaboullié se situent souvent au-delà du pôle crustal archéen (Figs. 3.8a à c). Ces roches ont donc dû être contaminées par une source plus riche en Th que la valeur moyenne de la croûte archéenne. Le Pluton du lac Rodayer et le Complexe de Théodat, de la Sous-province d'Opatica, pourraient être des contaminants appropriés pour expliquer la composition des roches intermédiaires à felsiques de Colomb-Chaboullié (Figs. 3.5, 3.6, 3.8, et 3.9). Spécifiquement, une contamination du magma par le Pluton du lac Rodayer pourrait expliquer les variations en éléments majeurs et traces de la plupart des roches volcaniques intermédiaires de la ceinture de Colomb-Chaboullié. Le Complexe de

Théodat chevauche géochimiquement une partie de l'unité felsique *Acch3b*, mais il n'explique pas toutes les roches *Acch3b*. Certaines de ces roches felsiques ont subi une silicification et une séricitisation, ce qui explique en partie leurs compositions (Fig. 3.5a)

Comparaison avec la ceinture de roches vertes de Frotet-Evans : géologie, géochimie et géochronologie

La ceinture de roches vertes de Frotet-Evans, qui est considérablement plus grande et plus complexe que la ceinture de Colomb-Chaboullié, est divisée en quatre segments. D'ouest en est, ces segments sont : 1) l'Evans-Ouagams, 2) le Storm-Evans, 3) l'Assinica et 4) le Frotet-Troilus (Fig. 3.13) (Boily, 1999). Plusieurs des faciès volcaniques observés dans la ceinture de Frotet-Evans ne correspondent pas à ceux observés dans les roches volcaniques de la ceinture Colomb-Chaboullié. Cependant, en général, les ceintures de roches vertes de Frotet-Evans et de Colomb-Chaboullié sont toutes deux dominées par des séquences volcaniques mafiques. De plus, les roches volcaniques présentent une affinité magmatique allant de tholéïtique à calco-alcaline (Tableau 3.2).

Les échantillons mafiques de la ceinture de Frotet-Evans utilisés dans cette étude comparative se retrouvent dans les quatre segments de la ceinture de roches vertes (Fig. 3.13). Ils comprennent des tholéïites magnésiennes de la Formation de Rabbit (segments Evans-Ouagama et Storm Evans) et des tholéïites magnésiennes appauvries du segment Frotet-Troilus. L'unité *Acch1a* de la ceinture de Colomb-Chaboullié ressemble à certaines unités mafiques de Frotet-Evans (Figs. 3.14a, b, et 3.15). Toutefois, il n'y a pas de correspondance complète entre les basaltes de Colomb-Chaboullié et les basaltes de Frotet-Evans.

Les échantillons intermédiaires des formations Le Gardeur et Storm (secteur Storm-Evans) montrent des similitudes important avec les roches intermédiaires et les roches volcanoclastiques intermédiaires de la ceinture de Colomb-Chaboullié (Figs. 3.14 et 3.15). Ceci suggère que ces roches intermédiaires ont pu être formées dans un contexte pétrogénétique similaire à celui de la ceinture Colomb-Chaboullié. Les roches felsiques

de la ceinture de Colomb-Chaboullié n'ont pas d'équivalent connu dans la ceinture de roches vertes de Frotet-Evans (Fig. 3.15a).

Pour la ceinture de Colomb-Chaboullié, deux âges U-Pb ont été obtenus à partir de l'unité volcanoclastique intermédiaire à felsique (*Acch3*) : $2756,8 \pm 4,4$ Ma et $2760,3 \pm 6,4$ Ma (David et al., en préparation). Dans la ceinture de Frotet-Evans, des âges U-Pb de 2793 et 2755 Ma ont été obtenus (Boily et Dion, 2002), mais il y a quelques doutes sur ces âges (D. Bandyayera et C. Dion, commun. pers., 2017). Dans la ceinture de Frotet-Evans, le meilleur âge U-Pb est $2755,5 \pm 0,9$ Ma pour une rhyodacite de la Formation de Storm (Groupe Evans) (Bandyayera et Sharma, 2001). Ceci correspond avec l'âge de la ceinture de Colomb-Chaboullié.

Comparaison avec la ceinture de roches vertes du lac des Montagnes

Une mince séquence de roches vertes est située dans la Sous-province de Nemiscau : le Groupe du lac des Montagnes. Il s'agit d'une séquence volcano-sédimentaire discontinue qui s'étend sur environ 75 km dans une direction est-ouest. Cette ceinture de roches vertes est simple sur le plan stratigraphique et se compose de roches qui ressemblent à celles de la ceinture de Colomb-Chaboullié. La ceinture de roches vertes du lac des Montages est principalement composée de coulées basaltiques (*Amo1*), de volcanoclastites felsiques à intermédiaires (*Amo2* et *Amo3*) et de formations de fer (*Amo4*) (Fig. 3.13).

Les roches basaltiques ont une affinité tholéïitique tandis que l'unité calco-alcaline *Amo1* a une composition d'andésite/andésite basaltique (Figs. 3.16a et b). Les basaltes tholéïitiques montrent plusieurs similitudes avec les basaltes de la ceinture de Colomb-Chaboullié (Figs. 3.16 et 3.17a, b et c). Les andésites/andésites basaltiques calco-alcalines du lac des Montagnes présentent également des caractéristiques géochimiques similaires à celles des laves intermédiaires de Colomb-Chaboullié (Figs. 3.16 et 3.17d).

Les roches volcanoclastiques du groupe du lac des Montagnes ont une large gamme de compositions, allant de mafique à felsique (Fig. 3.16a). Les roches volcanoclastiques intermédiaires et felsiques du lac des Montagnes montrent de nombreuses similitudes géochimiques avec celles de Colomb-Chaboullié (Figs. 3.17e et f), mais aucune roche volcanoclastique mafique n'a été identifiée dans la ceinture Colomb-Chaboullié.

Un échantillon volcanoclastique felsique du Groupe du lac des Montagnes a donné un âge U-Pb de $2712,6 \pm 5$ Ma (David et al., en préparation). Bien que les caractéristiques géochimiques des ceintures de roches vertes du lac des Montagnes et de Colomb-Chaboullié soient très similaires, il existe une différence d'âge considérable entre les deux.

Conclusions

Les coulées basaltiques massives et coussinées sous-marines de la ceinture de Colomb-Chaboullié sont interstratifiées avec des andésites massives, coussinées et porphyriques, et des roches volcanoclastiques intermédiaires à felsiques, moins abondantes. Plusieurs indices sulfures synvolcaniques à Au-Ag-Cu sont présents dans la ceinture.

Selon la géochimie, cinq groupes de basaltes ont été identifiés. L'indice de sulfures massifs du lac Marcaut est situé au contact de deux de ces groupes de basaltes. Ce contact minéralisé pourrait être localisé ailleurs dans la ceinture de Colomb-Chaboullié après une étude plus poussée. Les basaltes *Acch1a* montrent des similitudes aux N-MORBs alors que les basaltes *Acch1b* et *Acch1c* présentent de faibles fractionnement des HFSE-REE suggérant une légère contamination. Cependant, les roches intermédiaires (*Acch2*, *Acch2a* et *Acch3a*) et felsiques (*Acch3b*) ont une géochimie similaire à celle des contaminants de la Sous-province d'Opatica. Ces roches intermédiaires à felsiques auraient pu se former dans une chambre magmatique crustale, alors que les magmas basaltiques se sont mis en place d'une façon plus directe vers la surface.

Les roches volcaniques de la ceinture de Colomb-Chaboullié ont été comparées à la ceinture de roches vertes de Frotet-Evans dans la Sous-province d'Opatica et à la ceinture du Lac des Montagnes dans la Sous-province de Nemiscau. Bien que la ceinture du lac des Montages corresponde mieux à la ceinture de Colomb-Chaboullié sur le plan géochimique, la ceinture de Frotet-Evans a des dates plus comparables.

1 INTRODUCTION

1.1 Context and problem

Archean greenstone belts are important both in terms of academic geological research and mineral exploration. They provide a window into the composition of the early Earth and on mechanisms that occurred during the Archean (e.g., Bickle et al., 1994; Bédard and Ludden, 1997; O’Neil et al., 2011, 2012, 2013). Archean greenstone belts are often associated with volcanogenic massive sulphide (VMS) deposits (e.g., Franklin et al., 2005; Galley et al., 2007; Mercier-Langevin et al., 2014), as well as other mineral deposits such as komatiite-hosted Ni (e.g., Arndt et al., 2005; Eckstrand and Hulbert, 2007), or syn-volcanic to orogenic gold (e.g., Groves et al., 1998; Poulsen et al., 2000; Goldfarb et al., 2005).

The Superior Province of Canada hosts approximately 80% of the global tonnage of Archean VMS deposits (Mercier-Langevin et al., 2014). The Abitibi greenstone belt within the Superior Province hosts more than 600 Mt of VMS deposits (Galley et al., 2007). These Abitibi VMS deposits and their geological environments have been extensively studied and are increasingly well understood (e.g., Laflèche et al., 1992; Hannington et al., 2005; Mercier-Langevin et al., 2007; Rogers et al., 2014). However, the smaller greenstone belts situated to the north of the Abitibi greenstone belt are less understood, underexplored, and stratigraphically less complex. The Colomb-Chaboullié greenstone belt, the object of this study, is a NE-SW to E-W trending belt, located in the contact zone between the Nemiscau and Opatica subprovinces of the Superior Province, in the James Bay area of Quebec. As it is unclear to which of these subprovinces this greenstone belt belongs, we compare the geology, geochemistry, and geochronology of the Colomb-Chaboullié belt with the Frotet-Evans greenstone belt of the Opatica Subprovince and the Lac des Montagnes belt of the Nemiscau Subprovince.

The Colomb-Chaboullié greenstone belt was mapped by the *Ministère de l'Énergie et des Ressources naturelles du Québec* (MERN) at a scale of 1:50 000 during 2015 (Bandyayera et al., 2015). It is composed of volcanic¹ rocks, mafic/ultramafic intrusive bodies, and sedimentary units (Bandyayera and Daoudene, 2017). Three main volcanic units are identified in the Colomb-Chaboullié greenstone belt: the predominant basalt suite, variably porphyritic andesite flows, and felsic to intermediate volcaniclastic rocks (Bandyayera and Daoudene, 2017). These are map units suitable for presentation at 1:50 000 scale. There has been no attempt to further subdivide the basalts for example into stratigraphic or chemo-stratigraphic units. Yet a detailed stratigraphy would be useful for VMS exploration, since these deposits tend to occur along specific horizons (Gibson and Galley, 2007; Galley et al., 2007). Geochemistry could also be used to study the petrological processes that led to the variable composition of the magmas in the greenstone belt. This is particularly relevant because a small greenstone belt should be petrologically simpler than a large one such as the Abitibi.

The Colomb-Chaboullié belt contains a series of base and precious metal-bearing sulphide prospects that suggest a potential for exploration in this region (Bandyayera and Daoudene, 2017). Within this belt, sulphide mineralisation occurs as massive and semi-massive lenses, dominantly located in the volcanic units, and as disseminated sulphide zones infilling the inter-pillow material of the basalts. Sulphide veins also occur in massive basalt flows, infilling fractures. The Lac Marcaut gold showing is the best known showing in the Colomb-Chaboullié belt, with 8.37 g/t Au over 3.9 m of drill core obtained by Teck in 1992 (Riopel, 1994). Prior to this project it was uncertain whether the massive and semi-massive sulphide occurrences within the Colomb-Chaboullié belt were tectonic or volcanic in origin. This project therefore provides a great opportunity to determine the affinity of these sulphide showings and study their surrounding host rocks.

The Colomb-Chaboullié greenstone belt also contains Ni-Cu-PGE showings in mafic-ultramafic intrusions, but these are being investigated by other workers.

¹ All rocks of the Colomb-Chaboullié greenstone belt are metamorphosed to the amphibolite facies, but the prefix 'meta' will be omitted to lighten the text.

1.2 Objectives

The aims of this project are as follows:

1. Gain a better understanding of the volcanology, stratigraphy, petrography, geochemistry and petrology of the volcanic units in the Colomb-Chaboullié greenstone belt;
2. Compare the geochemistry and geochronology of the Colomb-Chaboullié belt to that of the Frotet-Evans greenstone belt in the Opatica Subprovince and the Lac des Montagnes greenstone belt in the Nemiscau Subprovince;
3. Determine the origin of the precious metal-bearing sulphide showings (volcanic or fault-related) and link the mineralisation with specific chemo-stratigraphic units using the geochemical data.

Overall, this study may help future exploration of the greenstone belts in the northern region of the Superior Province that are underexplored in comparison to the Abitibi greenstone belt.

1.3 Methodology

1.3.1 Fieldwork

The study area forms part of NTS sheets 32N03 and 32N04. During the summer of 2016, the author spent two weeks in the central part of the Colomb-Chaboullié greenstone belt, within a 28.6 x 5.7 km study area, in which only greenstone belt outcrops were visited. The main supervisor of this project was present during the second week. The *Route de la Baie-James* bisects the study area, which allowed numerous samples to be collected in a north-south transect.

Away from the main road, the majority of mapping was carried out via helicopter, either by traverses or by helicopter visits to more dispersed outcrops. Both the traverse and helicopter “jump” mapping were planned in advance using satellite images, the existing MERN geological map, and magnetic imagery in order to cover as much ground as possible, while also visiting a variety of different lithologies. The helicopter “jumps” enabled coverage of all lithological types within the 77 x 7 km greenstone belt, allowing the more distant lithologies such as the banded iron formation and the intrusive mafic rocks further west of the study area to be examined, in order to become familiar with all the rock types of the Colomb-Chaboullié greenstone belt.

In total, 69 outcrops were visited by the author, of which 39 were known outcrops from the MERN map and 30 were new. A total of 73 hand samples were collected in the field. This collection includes all the volcanic lithologies in the greenstone belt and some of the other (non-volcanic) lithological units in order to obtain a suitable selection for petrographic and lithogeochemical analysis. These samples included: massive to pillowd, mafic to intermediate lavas ($n = 41$), porphyritic andesite ($n = 4$), intermediate to felsic volcaniclastic rocks ($n = 13$), undifferentiated mafic schists ($n = 4$), gabbro ($n = 1$), paragneiss ($n = 4$), and massive to semi-massive sulphides ($n = 6$). Field names are used here, as opposed to geochemically verified names, since not all these samples were analysed.

The Lac Marcaut VMS-style outcrop (16-SG-3521), located at 316 632 m E and 5 662 111 m N (UTM Nad 83 zone 18U) in the western sector of the study region, is the best-known massive sulphide lens of the Colomb-Chaboullié greenstone belt. The lens itself extends laterally along an outcrop ridge for 80 m in an east-west direction, with a maximum thickness of 1.4 m (Thorsen et al., 1993). As a result, it was mapped in more detail with the tape and compass method, to help establish the origin and setting of the massive sulphide lens.

1.3.2 Laboratory work

Of the 73 samples collected in the field, 45 lithogeochemical and 34 thin section samples were prepared which covered the maximum geographical area possible of the Colomb-Chaboullié belt within the budget allowance. Four polished blocks of massive sulphides were also prepared at the INRS. The thin sections were prepared by Vancouver Petrographics in British Columbia. The lithogeochemical samples were cut using a rock saw into fist-sized “cubes” that contained as little weathered and fractured surfaces as each sample would permit, as some samples were highly fractured and therefore had some internal alteration surfaces. These blocks were then sent to Activation Laboratories Ltd. (ActLabs) in Ancaster, Ontario, where they were analysed with the standard geochemical package of the MERN. The requested analytical package comprises the ActLabs codes QC-tot major and trace elements fusion ICP/ICPMS/4B1-Total Digestion ICP/4B-INAA. As part of the preparation process, ActLabs crushes the samples to a 105 µm grain size (Activation Laboratories Ltd., 2017). Sand is used between each sample in order to reduce the risk of contamination.

Major oxides and Sr were analysed using ICP-OAS while the remaining trace elements were analysed using ICP-MS (Table 1.1), following a lithium metaborate/tetraborate fusion process, to ensure all phases were dissolved (Activation Laboratories Ltd., 2017). In-lab standards or certified reference materials are used for quality control (Tables 1.2 to 1.7).

Table 1.1

Analytical methods used in this study, with accompanying limits of detections and blank sample data.

Element	Method	L.O.D	Method blank
<i>Major oxides</i>		%	%
SiO ₂	FUS-ICP-OAS	0.01	-
Al ₂ O ₃	FUS-ICP-OAS	0.01	-
Fe ₂ O ₃ (T)	FUS-ICP-OAS	0.01	-
MgO	FUS-ICP-OAS	0.01	-
MnO	FUS-ICP-OAS	0.001	-
CaO	FUS-ICP-OAS	0.01	-
Na ₂ O	FUS-ICP-OAS	0.01	-
K ₂ O	FUS-ICP-OAS	0.01	-
TiO ₂	FUS-ICP-OAS	0.001	-
P ₂ O ₅	FUS-ICP-OAS	0.01	-
Cr ₂ O ₃	FUS-ICP-OAS	0.01	-
LOI	FUS-ICP-OAS	-	-
Total	FUS-ICP-OAS	0.01	-
<i>trace elements</i>		ppm	ppm
Sr	FUS-ICP-OAS	2	-
Rb	FUS ICP-MS	1	< 1
Y	FUS ICP-MS	0.5	< 0.5
Zr	FUS ICP-MS	1	< 1
Nb	FUS ICP-MS	0.2	< 0.2
Cs	FUS ICP-MS	0.1	< 0.1
La	FUS ICP-MS	0.05	< 0.05
Ce	FUS ICP-MS	0.05	< 0.05
Pr	FUS ICP-MS	0.01	< 0.01
Nd	FUS ICP-MS	0.05	< 0.05
Sm	FUS ICP-MS	0.01	< 0.01
Eu	FUS ICP-MS	0.005	< 0.005
Gd	FUS ICP-MS	0.01	< 0.01
Tb	FUS ICP-MS	0.01	< 0.01
Dy	FUS ICP-MS	0.01	< 0.01
Ho	FUS ICP-MS	0.01	< 0.01
Er	FUS ICP-MS	0.01	< 0.01
Yb	FUS ICP-MS	0.01	< 0.01
Lu	FUS ICP-MS	0.002	< 0.002
Hf	FUS ICP-MS	0.1	< 0.1
Ta	FUS ICP-MS	0.01	< 0.01
Th	FUS ICP-MS	0.05	< 0.05

Table 1.2

Level of accuracy of the major oxide database for the Colomb-Chaboullié belt 2016 whole-rock geochemical samples.

Analyte symbol	SiO ₂ (%)	Al ₂ O ₃ (%)	Fe ₂ O ₃ ^(T) (%)	MgO (%)	MnO (%)	CaO (%)	Na ₂ O (%)	K ₂ O (%)	TiO ₂ (%)	P ₂ O ₅ (%)	Cr ₂ O ₃ (%)
Relative Difference (%)											
NIST 694	0.8	5.0	6.3	3.0	12.1	1.7	0.0	7.8	8.2	0.1	10
DNC-1	0.0	2.1	0.6	1.6	2.7	0.4	1.1	6.0	2.9	14.3	
GBW 07113	2.8	2.4	1.6	12.5	0.7	0.0	4.3	1.1	6	20	
W-2a	2.0	0.1	2.6	1.7	3.1	2.1	4.2	1.0	3.1	0.0	
SY-4	1.1	3.1	2.7	9.3	0.0	0.1	2.3	0.6	3.1	8.4	
BIR-1a	0.5	2.2	3.0	0.2	1.7	1.5	0.0	33.3	3.4	4.8	

For concentrations that are typical of volcanic rocks, the accuracy for major oxides is typically better than 5% (relative difference), whereas Fe₂O₃ and TiO₂ are always better than 10%, and MgO and MnO are always better than 15% (Table 1.2). The accuracy for P₂O₅ can be quite poor, but this oxide is not used in the analysis of the Colomb-Chaboullié volcanic rocks. For the rare earth elements, as well as Sr, Nb, Cs, Hf, and Th, accuracy was often better than 5% and always better than 10% (Tables 1.3 and 1.4). For Ta and Rb, accuracy is better than or equal to 10%. Other trace elements were not used in this study.

Table 1.3

Level of accuracy of the rare earth elements for the Colomb-Chaboullié belt 2016 whole-rock geochemical samples.

Analyte symbol	Y ppm	La ppm	Ce ppm	Pr ppm	Nd ppm	Sm ppm	Eu ppm	Gd ppm	Tb ppm	Dy ppm	Ho ppm	Er ppm	Yb ppm	Lu ppm
<i>Relative Difference (%)</i>														
NIST 694	8.3	2.8					6.8						5.0	
GBW 07113														
LKSD-3	4.7		5.9		6.4					4.1		3.7	0.0	
TDB-1	1.4	0.0	2.9		5.7		0.0				5.6	1.3	2.9	
W-2a	10.4	13	6.1		0.8	3.0			1.6				0.0	0.0
SY-4														
CTA-AC-1	7.0				0.3	6.8	7.5	0.8	5.0				0.9	
BIR-1a	1.9	4.8	5.3			0.0		10		2.5			0.0	
NCS DC86312	1.7				3.8			1.8	1.4	4.4	7.2	0.1	6.3	3.8
NCS DC70009														
(GBW07241)	0.8	1.3	2.2	8.9	7.6	8.8		2.7	3.0	5.8		6.0	0.7	9.6
OREAS 100a (Fusion)	0.7	5.0	1.9	7.2	3.3	4.2	7.5			5.6	2.3	2.0	2.7	5.8
OREAS 101a (Fusion)	2.2	7.0	7.6		6.9	6.1	8.3				7.7	3.1	1.1	9.8
OREAS 101b (Fusion)	3.9	5.8	5.2	0.8	2.9	6.3	4.4		0.6	0.6	0.3	2.1	4.0	5.8
JR-1	10	2.0	2.5	6.8			4.7	2.0	0.2	8.1	5.3	8.1	8.5	

To give a measure of reproducibility, 2 to 4 duplicates were run for each session (Table 1.5). The relative difference between original and repeat analyses was typically less than 5% for major oxides (except P₂O₅), and for the rare earth and trace elements, was typically less than 5% and always less than 10% (except for Ta and Th) (Tables 1.6 and 1.7).

Table 1.4

Level of accuracy of the other trace elements used for the Colomb-Chaboullié belt 2016 whole-rock geochemical samples.

Analyte symbol	Sr ppm	Nb ppm	Cs ppm	Hf ppm	Ta ppm	Th ppm	Rb ppm	Zr ppm	Y ppm
<i>Relative Difference (%)</i>									
NIST 694	1.4						7.9	8.3	
GBW 07113	4.7								
LKSD-3			4.3	6.3	10.0	0.9		0.6	4.7
TDB-1							8.7	7.1	1.4
W-2a	5.3	0.0			10.0	0.0	4.8	1.1	10.4
SY-4	0.7								
CTA-AC-1						1.4		7.0	
BIR-1a									1.9
NCS DC86312						0.0			1.7
NCS DC70009 (GBW07241)			7.1			4.9	6.0		0.8
OREAS 100a (Fusion)						5.0			0.7
OREAS 101a (Fusion)									2.2
OREAS 101b (Fusion) JR-1	4.6	2.4		2.7		5.1	8.6	3.9	3.9 10

The new geochemical data obtained was then combined with the 78 geochemical analyses from the MERN from their 2015 mapping campaign, for a total of 121 analyses of volcanic rocks (Appendix B). These samples were processed in the same lab, using the same methods and lab standards as the 2016 database. The geochemical database was used to refine the chemo-stratigraphy of the Colomb-Chaboullié greenstone belt, as will be discussed in chapter 3. Based on the 2016 field work and detailed chemo-stratigraphy created as part of this project, the MERN 1:50 000 map was modified by Bandyayera, Galloway, Ross, and Daoudene in September 2017.

Table 1.5

Level of reproducibility of the major oxide database for the Colomb-Chaboullié belt 2016 whole-rock geochemical samples.

Analyte symbol	SiO ₂ (%)	Al ₂ O ₃ (%)	Fe ₂ O ₃ ^(T) (%)	MgO (%)	MnO (%)	CaO (%)	Na ₂ O (%)	K ₂ O (%)	TiO ₂ (%)	P ₂ O ₅ (%)	Cr ₂ O ₃ (%)
<i>Relative Difference (%)</i>											
67232	1.7	3.0	0.7	1.3	1.6	1.3	1.8	1.5	1.6	20	0.0
67249	2.2	2.3	2.0	0.2	1.8	0.3	2.0	0.0	5.0	20	0.0

Table 1.6

Level of reproducibility of the rare earth elements for the Colomb-Chaboullié belt 2016 whole-rock geochemical samples.

Analyte symbol	La ppm	Ce ppm	Pr ppm	Nd ppm	Sm ppm	Eu ppm	Gd ppm	Tb ppm	Dy ppm	Ho ppm	Er ppm	Yb ppm	Lu ppm
<i>Relative Difference (%)</i>													
67232	1.2	2.4	1.0	2.7	6.6	4.5	2.5	4.7	1.7	1.7	0.0	3.6	4.0
67249	3.3	1.1	6.1	3.3	1.4	5.7	1.0	2.8	0.4	2.0	0.0	5.7	2.5

Table 1.7

Level of reproducibility of the other trace elements used for the Colomb-Chaboullié belt 2016 whole-rock geochemical samples.

Analyte symbol	Sr ppm	Nb ppm	Cs ppm	Hf ppm	Ta ppm	Th ppm	Rb ppm	Zr ppm	Y ppm
<i>Relative Difference (%)</i>									
67232	2.0	0.0	1.6	0.0	0.0	6.7	0.0	5.4	0.6
67249	6.0	7.0	0.0	0.0	27	33	0.0	0.0	2.7

1.4 Structure of the thesis and role of co-authors in chapter 3

This is an MSc thesis by publication. Following this introductory chapter, the second chapter outlines the geological context of the study area, including an overview of the Superior Province, the Opatica and Nemiscau subprovinces, and the Colomb-Chaboullié greenstone belt. A more detailed context regarding VMS mineralisation is also included.

The third chapter is the core of the thesis and presents a typescript by S. Galloway, P.-S. Ross, D. Bandyayera and Y. Daoudene, ready for submission to Precambrian Research. The title is “The Colomb-Chaboullié greenstone belt volcanics: geology, stratigraphy, and geochemistry”. The typescript introduces the project, briefly summarises the geological context, contains all of the results of this study, presents the data interpretation (discussion), and ends with the conclusions.

This is followed by a final chapter containing all references cited in the thesis. Appendices on the CD include a geological map of the Colomb-Chaboullié belt containing all the outcrops visited during the 2016 field season and the whole-rock geochemical data from 2015 and 2016.

In the typescript presented in chapter 3, the first author (S. Galloway) was responsible for data collection including field mapping and whole-rock geochemical sampling, whole-rock and petrographic analysis, the integration of this data with existing MERN data, preparation of figures, typescript writing, interpretations, and conclusions. The second author (P-S. Ross) helped with field mapping and sample selection for analyses, contributed to the choice of figures, data presentation, discussion, conclusions, and typescript revision. The final two authors (D. Bandyayera and Y. Daoudene) provided input and comments during field work and typescript preparation. They also had an indirect influence on the typescript of chapter 3 through comments they made on drafts of two MERN reports discussed in the next section.

1.5 Previous publications

During the course of this study, the author of this memoir produced two reports for the MERN, in collaboration with several co-authors:

1. Galloway S, Ross P-S, Bandyayera D, and Daoudene Y (2017) The volcanic stratigraphy of the Colomb-Chaboullié greenstone belt and the emplacement context of the volcanogenic massive sulphides, James Bay: preliminary results. Ministère de l'Énergie et des Ressources naturelles du Québec, report MB 2017-10, 18 p.
2. Galloway S, Ross P-S, Bandyayera D, and Daoudene Y (2018) Chimico-stratigraphie volcanique et minéralisation volcanogène de la ceinture archéenne de Colomb-Chaboullié, Baie James. Ministère de l'Énergie et des Ressources naturelles du Québec, report MB 2018-06, 32 p.

All the data and ideas presented in these documents have been included in this thesis, which also contains supplementary observations and interpretations not included in these reports as a result of space limitations or because these were realised after the publication of the above documents.

In the MERN reports outlined above, the first author was responsible for data collection, including fieldwork, sample preparation and petrographic study. The first author also carried out the interpretation of the data, and composed the initial text and figures for these two reports. The second author contributed to field work and sample selection, contributed to data interpretation, and helped to revise these reports. The remaining co-authors provided advice during field work and made constructive comments and suggestions before the publication of these reports.

2 GEOLOGICAL CONTEXT

This chapter presents the geological and metallogenic background of the study. This includes an overview of the Superior Province and the Nemiscau and Opatica subprovinces. The study area in the Colomb-Chaboullié greenstone belt lies approximately 144 km north of the mining town of Matagami, and about 82 km east of the town of Waskaganish, in the James Bay area of Quebec. The main north-south transect of the study area extends between $51^{\circ}17'55.2''\text{N}$, $77^{\circ}22'42.4''\text{W}$ and $51^{\circ}02'58.6''\text{N}$, $77^{\circ}34'11.5''\text{W}$. This chapter also includes a summary of VMS deposits.

2.1 Superior Province

The Superior Province is the largest known Archean terrain and forms the core of the North American continent (Hoffman, 1988). The Superior Province is one of several provinces that make up the Precambrian Canadian Shield, and covers parts of Quebec, Ontario, Manitoba, also extending into the northern United States. The Superior Province is subdivided into smaller subprovinces (Fig. 2.1). These divisions are based on their structural features, dominant lithologies, degree of metamorphism, and geophysical characteristics. These subprovinces are classified into four main categories: 1) volcano-plutonic subprovinces dominantly composed of trondhjemite-tonalite-granodiorite derived gneissic assemblages, along with mostly mafic volcanic rocks, 2) metasedimentary subprovinces, 3) plutonic subprovinces, and 4) high-grade orthogneiss and paragneiss subprovinces (Card and Ciesielski, 1986). There are two main theories regarding the tectonic processes that were in play during the Archean. The first proposes the uniformitarian approach where modern-day tectonic processes were operating (Kröner, 1981; Turner et al., 2014; Ernst, 2017). The alternative theory posits that this tectonic style and therefore subduction environments had not been established in the Archean (e.g., Hamilton, 1998; Bédard et al., 2013; Bédard and Harris, 2014).

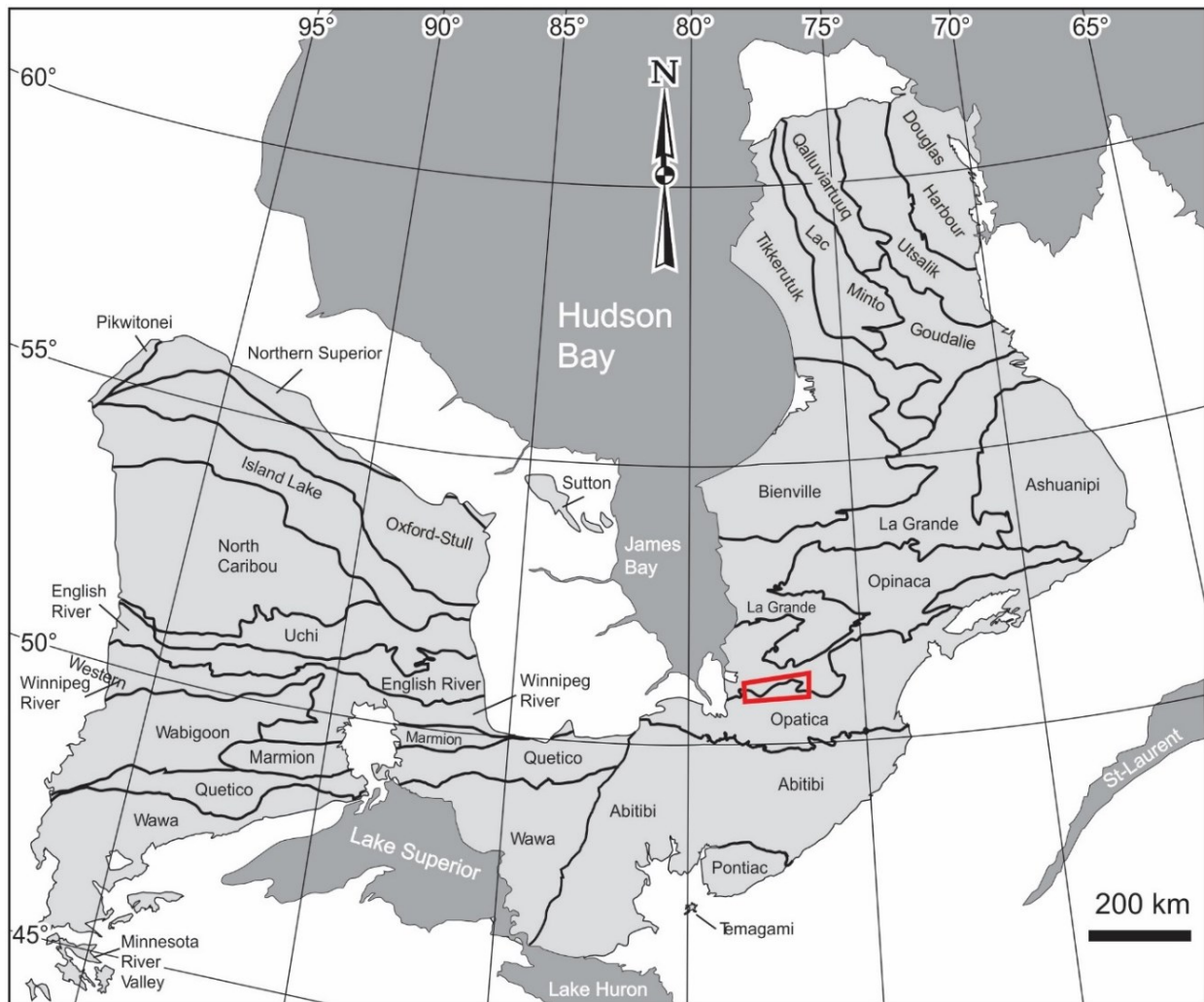


Fig. 2.1 Superior Province showing the major subprovinces and subdivisions. The approximate location of the Colomb-Chaboullié greenstone belt is shown in red. After Thurston et al. (2002).

The study area (Colomb-Chaboullié greenstone belt) is located between the Opatica and Nemiscau Subprovinces of the Superior Province (Figs. 2.1 and 2.2). Note that on figure 2.1, the Nemiscau Subprovince is included in the Opinaca Subprovince. The Nemiscau Subprovince is part of a metasedimentary complex that extends across the whole of the Superior Province (Morfin et al., 2014). This metasedimentary complex comprises four metasedimentary subprovinces: the Ashuanipi, the Opinaca, the Nemiscau, and the Quetico. Barring an increase in metamorphism in an easterly direction, these subprovinces are very similar, especially in terms of depositional age and geochemical

composition (Guernina and Sawyer, 2003). This suggests a similar origin, thus explaining why the Nemiscau is sometimes grouped with the Opinaca Subprovince.

2.2 Opatica Subprovince

The northeast trending Opatica Subprovince is composed mostly of plutonic rocks and stretches 800 km by 120 km (Bandyayera and Daoudene, 2017). The Opatica Subprovince is bounded by the Abitibi Subprovince to the south and the Nemiscau Subprovince to the north (Fig. 2.2). The Opatica has been interpreted as a deeply eroded part of an Archean collisional fold and thrust belt (Benn et al., 1992; Ludden et al., 1992; Sawyer and Benn, 1993; Lacroix and Sawyer, 1995). The majority of the Opatica is composed of deformed tonalite and granitoid rocks, with local migmatisation (Davis et al., 1994). In the northern part of the Opatica, the Lac Rodayer pluton, which is separated from the surrounding gneissic trondhjemite-tonalite-granodiorite suite by the Lac Rodayer thrust fault, has an age range of 2820-2825 Ma based on U-Pb dating (Davis et al., 1994). This is the oldest unit within the Opatica Subprovince. The Opatica shows a younging trend towards the south, where a monzodiorite plutonic suite, located adjacent to the Opatica-Abitibi contact, has an age range of 2696-2693 Ma (Gariépy and Allègre, 1985; Davis et al., 1995). The Opatica has undergone metamorphism to the amphibolite facies (Sawyer and Benn, 1992), with anatexis recorded by Sawyer and Benn (1993) in the central section of this subprovince.

An east-west trending, 250 km long sequence of sedimentary and volcanic rocks is located in the central part of the Opatica (Sawyer and Benn, 1993), representing an upper crustal nappe (Boily and Dion, 2002). This is known as the Frotet-Evans greenstone belt (Fig. 2.2), and described in section 2.2.2.

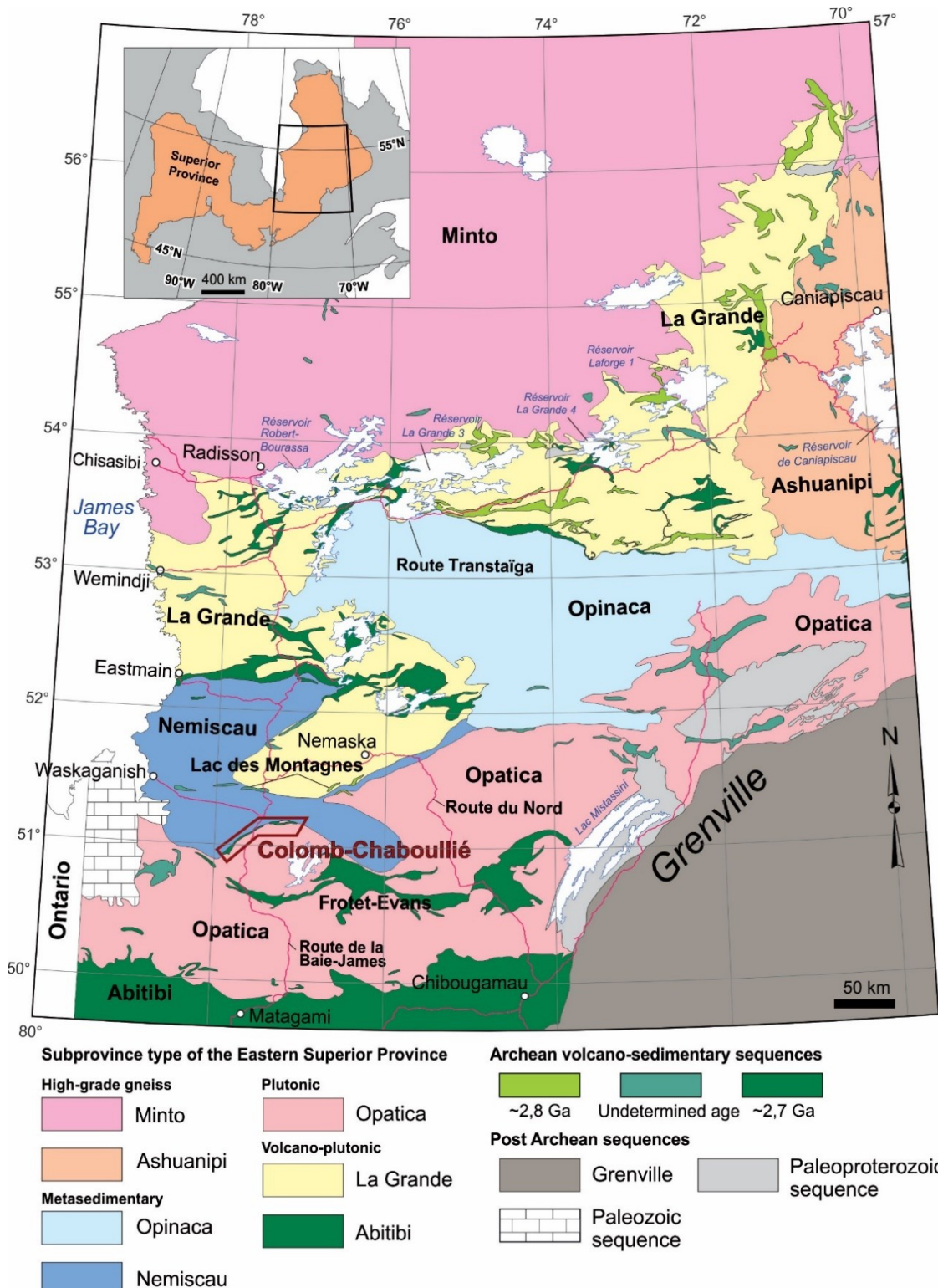


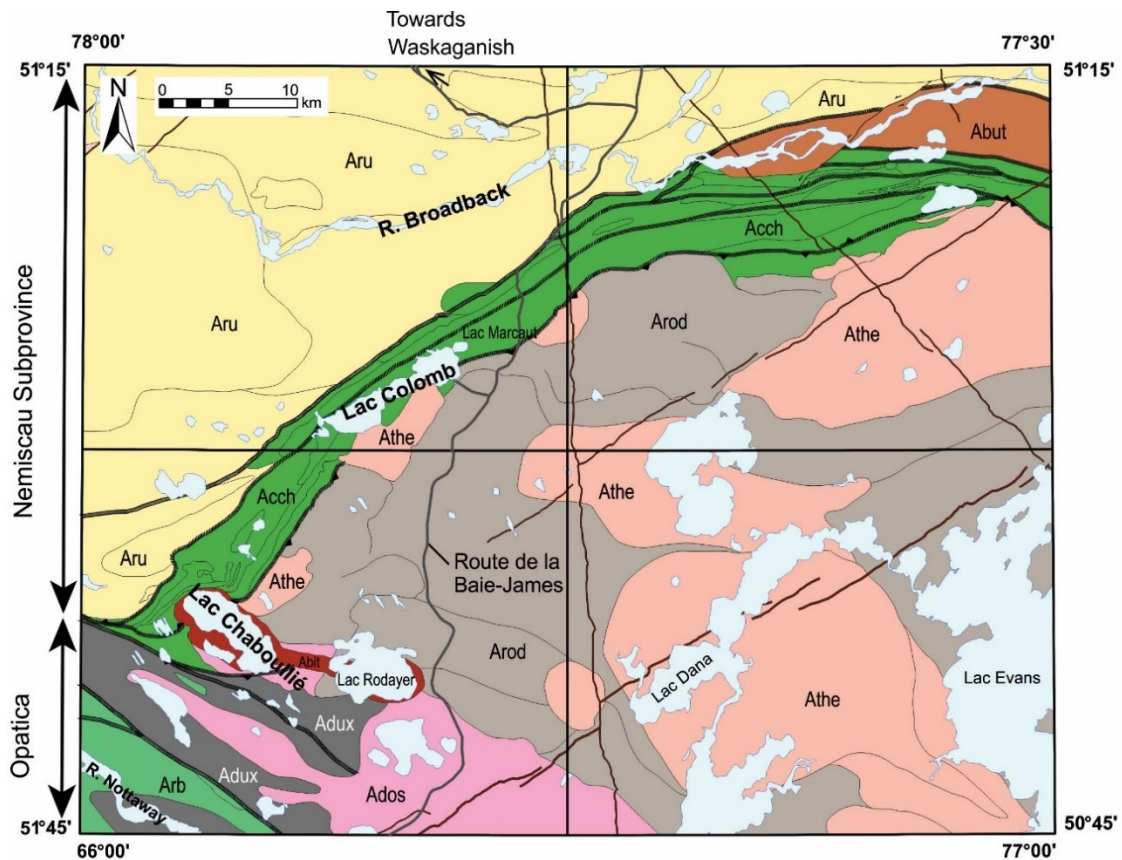
Fig. 2.2 Simplified geological map of the Eastern Superior Province in the James Bay region of Quebec. The Colomb-Chaboullié greenstone belt is highlighted in red. After Bandyayera and Daoudene (2017). Divisions of the Superior Province are based on Card (1990).

2.2.1 Geology of the northernmost Opatica

The northernmost Opatica Subprovince, immediately south of the Colomb-Chaboullié greenstone belt, is divided into six different plutonic units based on the work carried out by Bandyayera and Daoudene (2017) (Fig. 2.3):

- 1) the Syénite de Biteur, which is associated with a positive magnetic anomaly and is composed of alkaline feldspar syenite, syenite, quartz-syenite and monzonite (*Abit*);
- 2) the Desorsons Intrusion, composed of granites with some local occurrences of granodiorite (*Ados*);
- 3) the Lac Bout Intrusion (*Abut*), made up of foliated diorite and monzodiorite;
- 4) the Théodat Complex, which is a granodiorite-tonalite-granite-pegmatite unit, and their associated gneissic rocks (*Athe*);
- 5) a gneissic sequence that comprises tonalitic and granitic rocks, known as the Dusaux Complex (*Adux*). This suite also contains the volcano-sedimentary Rabbit Formation (*Arb*), consisting of basalt, volcaniclastic rocks, an iron formation, and thin sedimentary horizons (Brisson et al., 1998). The Rabbit Formation has been reoriented in a northwest-southeast direction by the Nottaway Shear Zone (Bandyayera and Daoudene, 2017), which may explain its presence within the plutonic *Adux* complex;
- 6) The Lac Rodayer Pluton (*Arod*), made up of tonalite, quartz-diorite and diorite lithologies.

Crustal contamination may be an important process that the magmas of the Colomb-Chaboullié were subjected to. The Lac Rodayer and Théodat Complex are likely contaminants, which is demonstrated in section 3.5.4.



Opatica Subprovince

Syenite de Bateau

Abit Syenite

Desorsons Intrusion

Ados Granite

Lac au Bout Intrusion

Abut Diorite and monzodiorite

Théodat Complex

Athe Granodiorite, porphyritic granodiorite, granite and pegmatite

Rabbit Formation

Arb Amphibolised basalt, banded amphibolised basalt, felsic tuffs

Dusaux Complex

Adux Gneissic tonalite and granite

Lac Rodayer Pluton

Arod Tonalite, diorite, quartz diorite

Nemiscau Subprovince

Rupert Group

Aru Paragneiss, metatexite, diatexite, granite injections

Diabase Dykes



Colomb-Chaboullié Group

Acch Amphibolised basalt, porphyritic andesite, felsic volcaniclastics, mafic and ultramafic intrusives, sedimentary units

Figure 2.3. Simplified geology of the Lac Rodayer region. The Colomb-Chaboullié greenstone belt is located between the Nemiscau and Opatica Subprovinces (after Bandyayera and Daoudene, 2017).

2.2.2 Frotet-Evans greenstone belt

The Frotet-Evans greenstone belt is described here because the Colomb-Chaboullié greenstone belt is compared with it in chapter 3. The Frotet-Evans greenstone belt is principally composed of Mg- and Fe-tholeiitic mafic to intermediate lavas and calc-alkaline rocks (Boily and Dion, 2002). The latter are dominantly composed of intermediate to felsic flow units and pyroclastic rocks. The Frotet-Evans is possibly the oldest greenstone belt in the Superior Province in Quebec with ages of 2793 and 2755 Ma recorded (cited by Boily and Dion, 2002), although there is some doubt over these ages (D. Bandyayera and C. Dion, pers. commun., 2017). A more recently obtained age for the “Rhyodacite de la Formation de Storm (Evans Group)” yielded 2755.5 ± 0.9 Ma (Bandyayera and Sharma, 2001).

The Frotet-Evans belt contains vein hosted Cu-Au showings, VMS mineralisation, intrusion-hosted Ni-Cu mineralisation, and iron formations (Gosselin, 1996). It most prominently hosts the Cu-Au Troilus Mine with geological resources of 1.08 g/t Au, 0.11% Cu, and 1.4 g/t Ag recorded from the main zone and total reserves estimated to be 50.8 Mt (Goodman et al., 2005). This mine is located in the northeastern section of the greenstone belt and is hosted in calc-alkaline rocks. Some authors describe it as an Archean porphyry-style deposit (Fraser, 1993; Rowins, 2000), although there is some disagreement over this idea (Goodman et al., 2005).

Based on structural and seismic studies carried out by Sawyer and Benn (1993) and Calvert et al. (1995), it is thought that the Frotet-Evans volcanism is a result of intra-oceanic activity, or occurred in an oceanic basin far from a continental mass. The metamorphic grade of this greenstone belt ranges from the upper greenschist facies to the amphibolite facies near the contact with the rest of the Opatica.

The basaltic and basaltic andesite volcanic rocks of the Frotet-Evans are characterised by a low titanium, high silica and Mg-rich composition (Boily and Dion, 2002). These basaltic rocks have a boninitic affinity due to their high $\text{Al}_2\text{O}_3/\text{TiO}_2$ ratios, U-shaped rare

earth element (REE) plots, negative Nb and Ta anomalies, and positive Zr and Hf anomalies. However, these rocks are not boninites in the strictest sense, based on the definition by Crawford et al. (1989), as they have a dominantly basaltic composition. Yet based on the geochemical signatures mentioned above, Boily and Dion (2002) propose that the volcanic rocks of the Frotet-Evans belt reflect a suprasubduction zone setting.

2.3 Nemiscau Subprovince

The Nemiscau Subprovince is a mostly metasedimentary subprovince (Bandyayera and Daoudene, 2017). The Nemiscau lies to the south of the La Grande Subprovince and is connected to the Opinaca by the Lac des Montagnes volcano-sedimentary sequence (Voliquette, 1975; Hocq, 1994). Little is known about this subprovince in the literature. The depositional age of the Nemiscau metasedimentary ensemble is estimated between 2698 Ma and 2688 Ma (Percival et al., 1992). However, a minimum age can be derived from Davis et al. (1995), who obtained a U-Pb zircon age of 2672 ± 2 Ma from a granite that cross-cuts the Nemiscau rocks.

According to Hocq (1994), the Nemiscau Subprovince can be subdivided into two different zones: a plutonic terrain that is composed of monzonite to granodiorite lithologies which contain remnants of paragneiss and amphibolites, and a metasedimentary terrain which itself can be further subdivided into three subunits (N-1, N-2 and N-3) based on magnetic features. A positive anomaly represents the N-2 subunit, which consists of paragneiss and amphibolite rocks that are orientated in an east-west direction. The N-2 subunit separates N-1 and N-3. These three high-grade metasedimentary domains are composed of paragneiss, metatexites, and diatexites, which mark the varying degrees of metamorphism that this subprovince underwent.

The Rupert Group, which corresponds with the N-1 subunit, has been introduced by Bandyayera and Daoudene (2017) based on the MERN fieldwork carried out in 2015. This group is made up of five units (not distinguished on Fig. 2.3): 1) a biotite and

hornblende rich paragneiss, 2) migmatised biotite and hornblende paragneiss, 3) a metatexite that contains between 30-50% melt pockets, 4) diatexite with 50-90% melt fractions and, 5) a granitic pegmatite that contains biotite ± garnet ± muscovite.

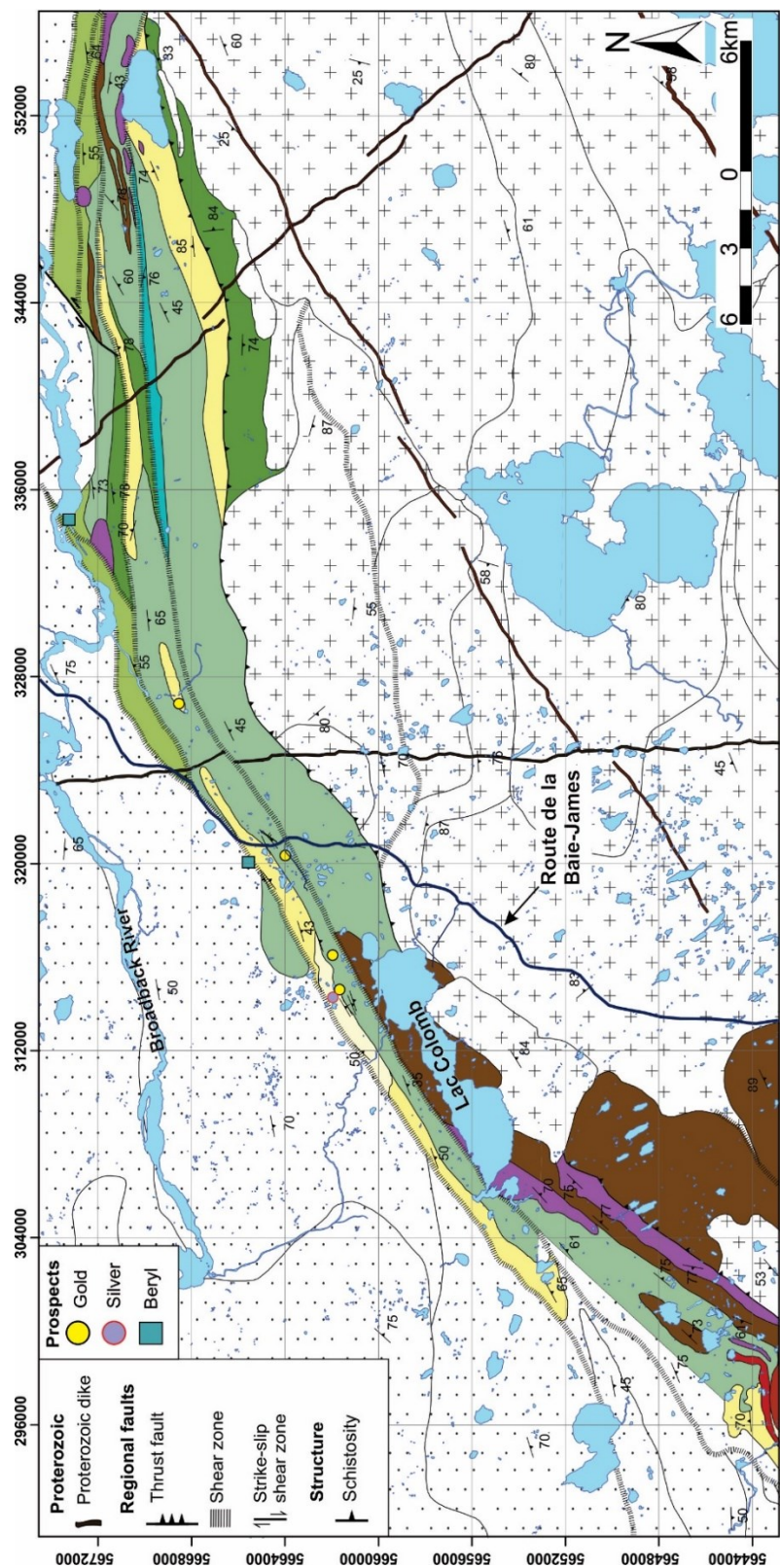
The narrow volcano-sedimentary Lac des Montagnes Group is located in the eastern part of the Nemiscau Subprovince, and connects this to the metasedimentary Opinaca Subprovince further east (Bandyayera and Daoudene, in preparation). The Lac des Montagnes Group is composed of massive to pillow basaltic flows and amphibolites derived from basalts, intermediate to felsic volcaniclastic rocks interstratified with the basalt flows, and iron formations.

2.4 Colomb-Chaboullié greenstone belt

Information in the present section is extracted largely from Bandyayera and Daoudene (2017). The Colomb-Chaboullié belt measures approximately 77 km in length and 5 km in horizontal width, with a maximum horizontal width of 7 km. It is composed of volcanic, sedimentary, mafic/ultramafic intrusive, and metamorphic units. The study area is dominantly composed of the volcanic units, which range from mafic, through intermediate, to felsic in composition (*Acch1*, *Acch2*, and *Acch3*, Fig. 2.4).

The dominant lithology throughout the whole belt is *Acch1*, which comprises about 80% of the total composition. This lithology is made up of basalts that are pillow or massive in nature. The pillows are dominantly elongate due to tectonic deformation, and are often surrounded by hyaloclastite material contained within the inter-pillow areas.

Acch2 is a porphyritic andesite which is located in the eastern part of the belt. The phenocrysts are plagioclase laths that range in size from 1 to 5 mm and make up to 10-30% of the rock. *Acch2a* is an andesite subunit which is located in the eastern side of the belt, adjacent to the Nemiscau Subprovince. It is characterised by lesser amounts of plagioclase phenocrysts (0-10%), and comprises predominantly pillow flows. The



Stratigraphic Legend		
Nemiscau Subprovince		
Undifferentiated Nemiscau Subprovince lithologies	Acch8 Polymict conglomerate	Peridotite and pyroxenite
Opatica Subprovince	Acch7 Paragneiss ($bi \pm hbl$)	Gabbro
Undifferentiated Opatica Subprovince lithologies	Acch6 Quartzite/iron formation	Felsic to intermediate volcanics
Colomb-Chaboullié Group		
Acch5	Acch4	Acch3
Undifferentiated Nemiscau Subprovince lithologies	Polymict conglomerate	Porphyritic andesite
Opatica Subprovince	Paragneiss ($bi \pm hbl$)	Andesite
Undifferentiated Opatica Subprovince lithologies	Quartzite/iron formation	Basalt

Fig. 2.4. Geology of the Colomb-Chaboullié greenstone belt. After Bandyayera and Daoudene (2015).

pillows in *Acch2a*, much like the pillows observed in *Acch1*, are elongate and measure up to 1 m in length.

Acch3 comprises volcaniclastic rocks that are felsic to intermediate in composition. These units occur as pods within *Acch1* (Fig. 2.4) and are made up of lapilli tuffs, crystal tuffs, and fine tuffs.

The *Acch4* and *Acch5* units represent the mafic and ultramafic intrusive bodies within the belt. These intrusive rocks make up about 10% of the greenstone belt. *Acch4* consists of medium- to coarse-grained gabbroic rocks. *Acch5* is made up peridotite and pyroxenite that occur in the western part of the belt. These intrusions occur as elongate bodies that follow the general stratigraphy of the region.

The Colomb-Chaboullié belt includes three sedimentary units. *Acch6* is a northeast-southwest trending unit of banded iron formation and quartzite, composed of interbedded iron-rich and quartzite layers. *Acch7* are biotite + hornblende bearing paragneiss rocks. This unit forms two small bands, one north of Lac Colomb (Fig. 2.4), and the other situated to the west of Lac Chaboullié (not shown on the map). As seen in figure 2.4, the *Acch7* band located to the north of Lac Colomb is located between the Colomb-Chaboullié volcanic units to the south and the metasedimentary rocks of the Nemiscau Subprovince to the north.

The final sedimentary lithology in the Colomb-Chaboullié greenstone belt is *Acch8*. This is a polymict conglomerate sequence that forms a thin band in the eastern part of the belt (Fig. 2.4). It is located between the *Acch1* and *Acch2* volcanic units. Polarities observed during the 2015 mapping campaign indicate that this conglomerate is situated in the centre of a syncline. *Acch8* is defined by rounded to sub-rounded fragments in a deformed, schistose, biotite-bearing paragneiss-like matrix. The clasts are dominantly composed of granitoid fragments (50-80%), with lesser amounts of fine-grained mafic clasts (1-10%), and chert (1%). The conglomerate is generally deformed where the

foliation moulds around the felsic clasts, while mafic clasts are strongly flattened in an east-west foliation.

Six different types of mineral occurrences were identified by the MERN in 2015. Volcanogenic polymetallic (Ag, Au, Cu) VMS showings and associated paleo-hydrothermal manifestations are found in *Acch1* (Bandyayera and Daoudene, 2017). The following thematic maps (Figs. 2.5a to d) show the Au, Ag, Cu and Zn values for the volcanic units of the Colomb-Chaboullié greenstone belt. Magmatic Ni-Cu type mineralisation is found within the gabbro and ultramafic peridotite and pyroxenite intrusions in the western sector of the belt. Known mineralisations of this type include the Horden Lake showing which has grades of 1.91% Cu and 0.4% Ni, and a projected reserve of 1,238,333 tonnes (Pearson et al., 1993). Therefore, a Ni thematic map is also included (Fig. 2.5e).

The Lac Marcaut horizon comprises a gold-bearing massive pyrrhotite-pyrite lens that stretches the length of the outcrop, and small sulphide filled veinlets and masses (Thorsen, 1993) (Fig. 2.6). Although anomalous gold values have been recorded throughout the massive sulphide lens, consistent high grades are recorded in the thin siliceous contacts at either side of the lens. Gold is also present in the sulphide veinlets and masses, which are thought to be a product of sulphide remobilisation after peak deformation and metamorphism. Along with the Lac Marcaut gold showing, a number of massive to semi-massive clusters are located in the central part of the belt, with grades up to 1 g/t Au recorded (Bandyayera and Daoudene, 2017).

Other mineralised zones within the belt include tectonic derived gold located within the deformation zones, rare earth element showings within alkaline intrusions, a thin corridor of banded quartzite and iron formation, and beryl-bearing pegmatites (Bandyayera and Daoudene, 2017).

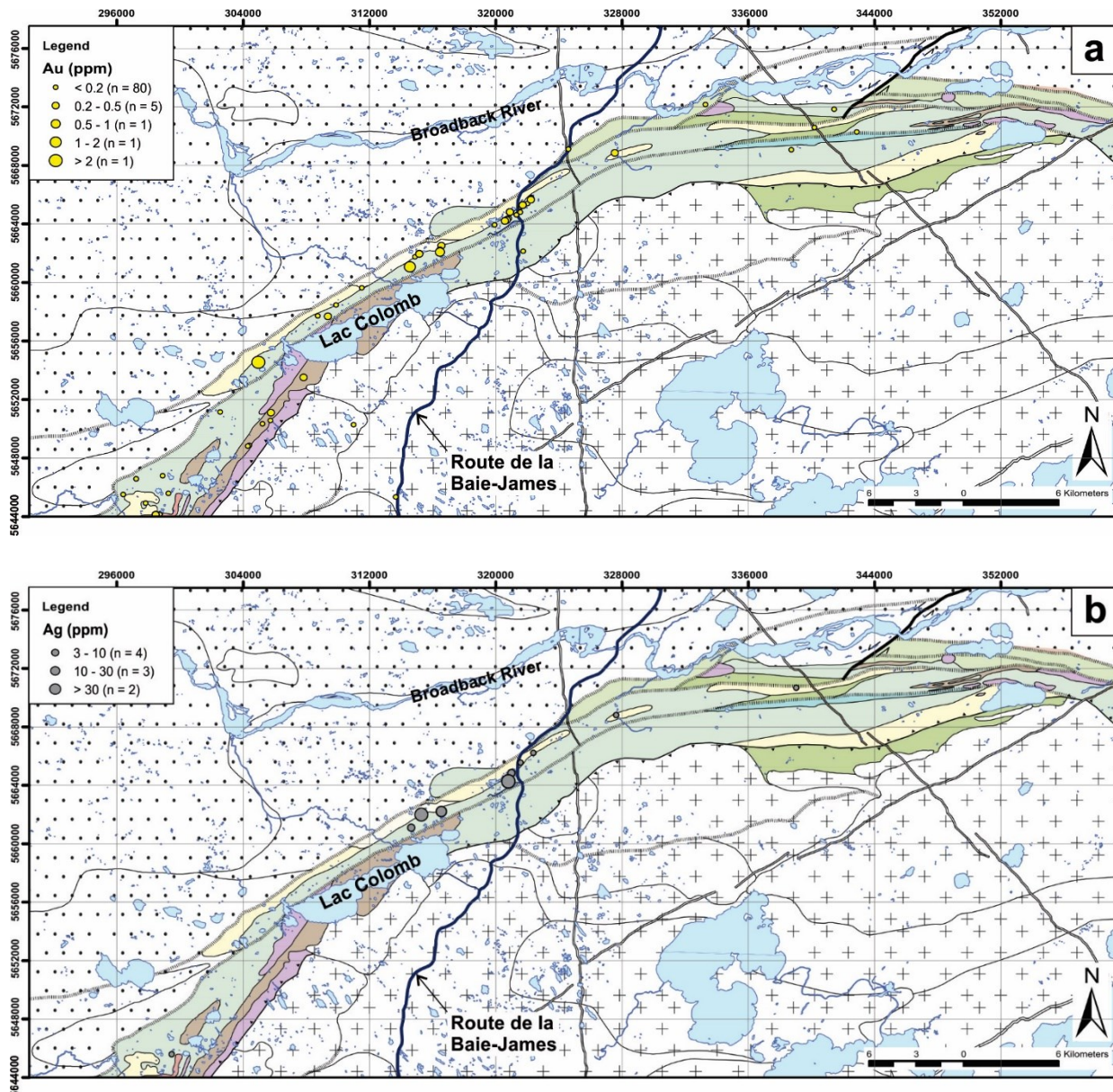


Fig. 2.5. Thematic maps showing the distribution of selected background mineralisation throughout the Colomb-Chaboullié greenstone belt. a) Background gold values and b) background silver values.

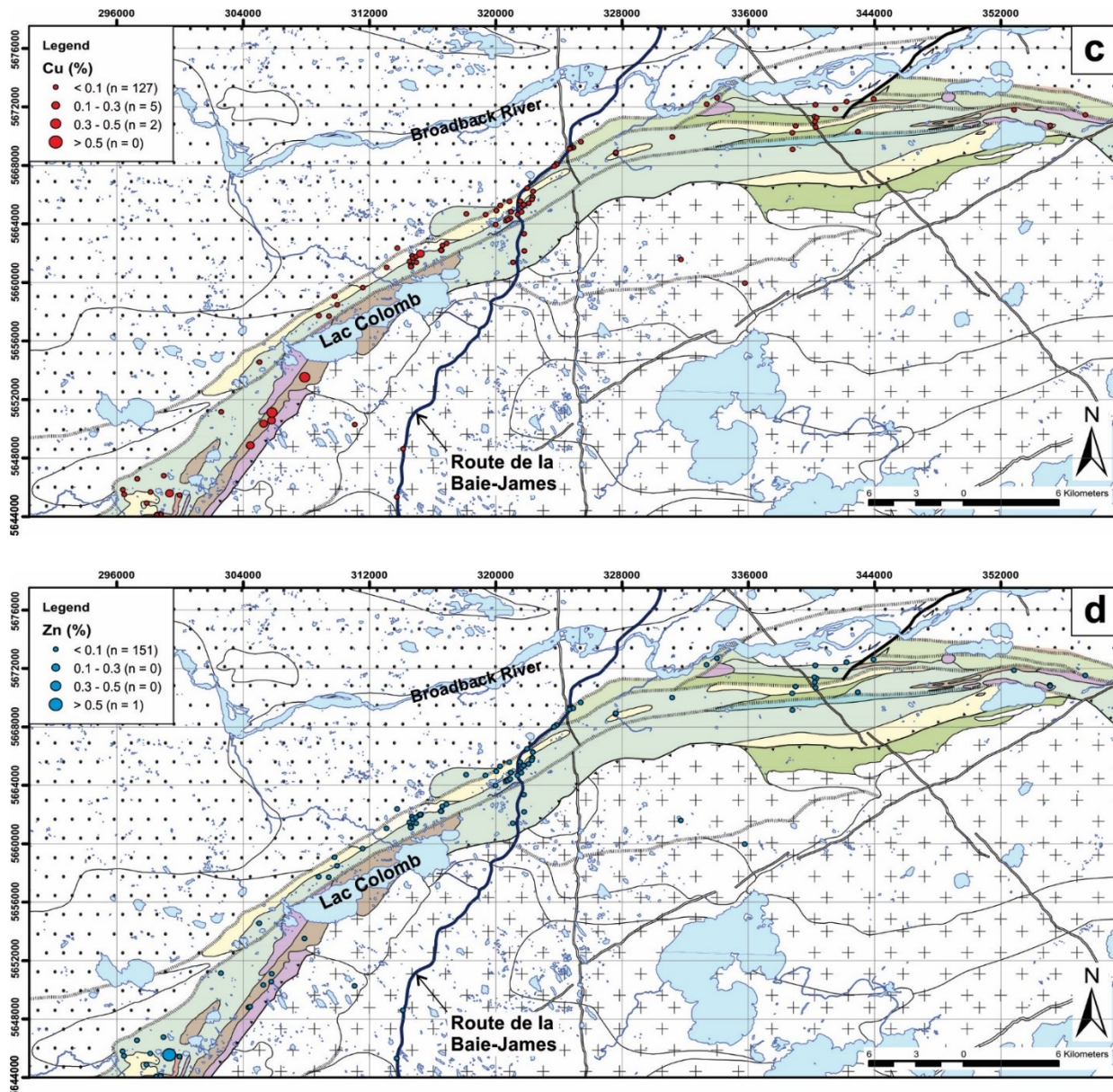


Fig. 2.5 cont. c) Background copper values and d) background zinc values.

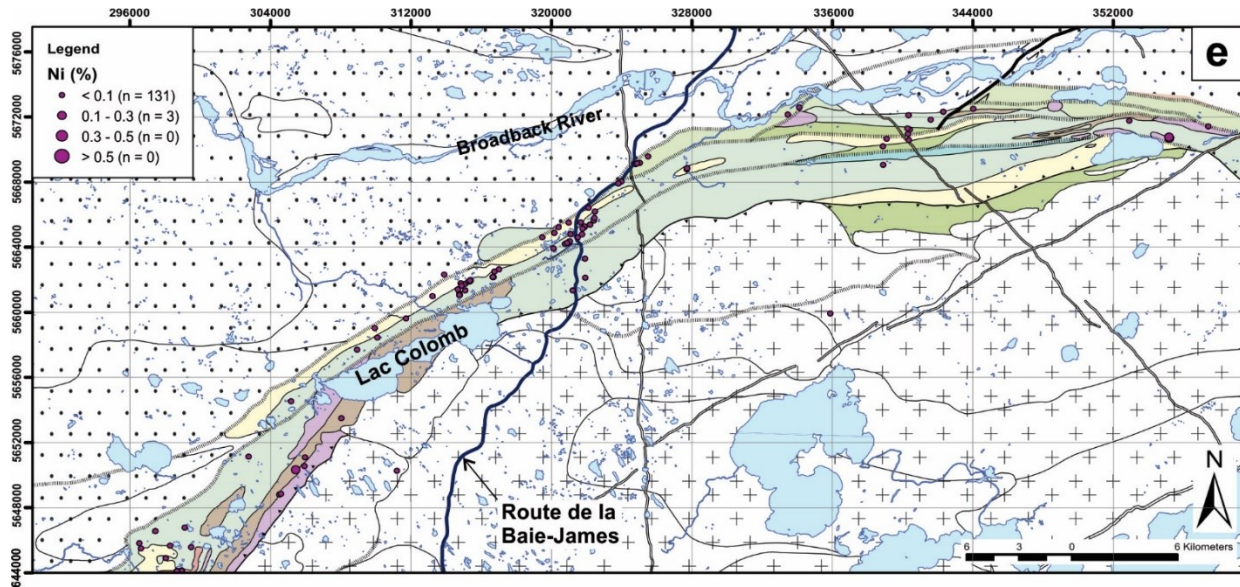


Fig. 2.5 cont. e) Background nickel values.

2.5 Metallogenetic context: VMS deposits

Volcanogenic massive sulphide (VMS) deposits are common in greenstone belts (Franklin et al., 2005; Galley et al., 2007), and the Colomb-Chaboullié greenstone belt contains a number of sulphide occurrences associated with Au-Ag-Cu anomalies within submarine volcanic rocks (Fig. 2.4), which signal VMS potential in the belt. Therefore, the present section summarises the characteristics and emplacement model for VMS deposits to provide metallogenetic context for this thesis. As mentioned in chapter one, the Lac Marcaut gold showing of the Colomb-Chaboullié has produced a high-grade drill sample in terms of Au (Riopel, 1994). Therefore a section on Au-rich VMS deposits has also been included here.

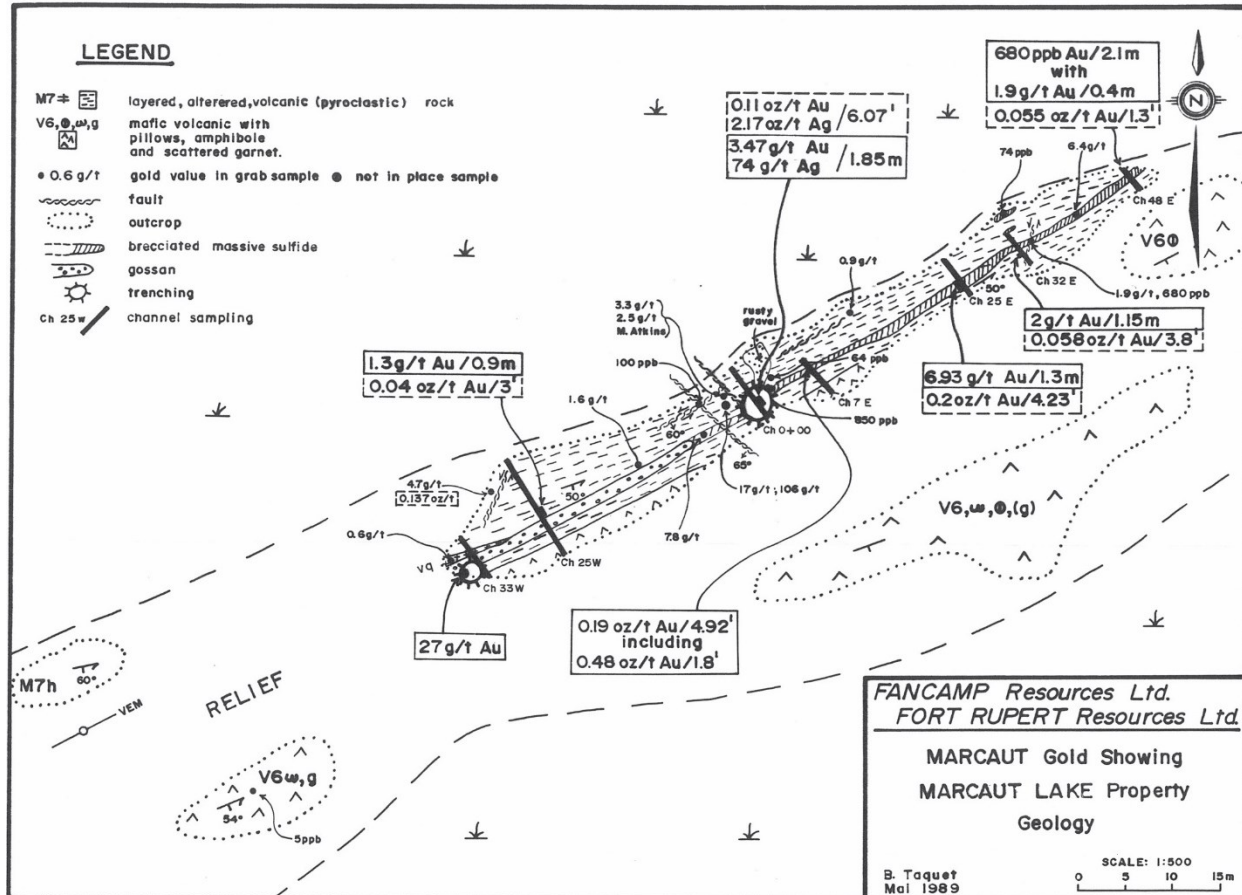


Fig. 2.6. Compilation map of the Lac Marcaut showing of the Colomb-Chaboullié greenstone belt. Principle outcrops, location of trenches, channel sample locations, and grab sample gold values are indicated (Taquet, 1989).

2.5.1 VMS deposit characteristics

VMS deposits are tabular to mound-shaped, syngenetic, polymetallic lenses that are produced via the release of hydrothermal fluids at or near the seafloor (Galley et al., 2007). They are major sources of Zn, Cu, Pb, Ag, and Au, with lesser amounts of Co, Sn, Se, Mn, Cd, In, Bi, Te, Ga, and Ge.

These deposits are associated with submarine volcanic sequences such as mafic to felsic lava flows and volcaniclastic rocks, however sedimentary host rocks are also common (Franklin et al., 1981). Chert-magnetite banded iron formations are often located near

VMS deposits, representing low-temperature hydrothermal events during a hiatus in volcanic activity (Gross, 1995). These horizons are also known as “exhalites” (e.g., Noranda camp) or “tuffites” (e.g. Matagami district) depending on their characteristics. The majority of VMS deposits in the Precambrian Canadian Shield are Cu-Zn dominated, located in bimodal volcanic terranes where mafic volcanic rocks comprise about 90% of the volcanic sequence (Galley et al., 2007). However, felsic volcanic rocks tend to be adjacent to the VMS mineralisation.

These deposits are made up of two parts, the massive to semi-massive sulphide lens and the underlying stringer zone (Galley et al., 2007) (Fig. 2.7). The lens contains 60 - 100% sulphide minerals (Franklin et al., 1981). The dominant sulphides are pyrite and/or pyrrhotite with lesser sphalerite, chalcopyrite, and galena. The massive sulphides may contain iron oxides, quartz and accessory phyllosilicates, and altered wall-rock fragments. The stringer zone is a Cu-rich stockwork veinlet system with disseminated sulphides and highly altered rocks (Franklin et al., 1981). However, this stringer zone is not always present or obvious.

The massive ore lens often contains a distinctive Cu-Zn metal zonation as a result of zone refining, caused by the increasing temperature of the VMS system. This allows lower temperature sulphides (pyrite-sphalerite) to migrate towards the edge of the sulphide lens, as they are replaced by copper sulphides (Kerr and Gibson, 1993; Gibson and Galley, 2007; Galley et al., 2007). This produces the classic polymetallic VMS deposits that have a Cu-dominant core and an outer Zn-rich zone, enclosed in a pyrite-rich rim. The stringer zone is encompassed in a vertically extensive alteration pipe (Galley et al., 2007) composed of either a sericitic + quartz or chlorite core with a chlorite- or sericite-rich outer zone (Franklin et al., 1981). Extensive alteration zones are also common beneath or surrounding the alteration pipe of many deposits (Franklin et al., 2005). These are most common in mafic dominant, bimodal-mafic and bimodal-felsic sequences. The alteration assemblages associated with these are: 1) regionally occurring diagenetic-zeolitic alteration, 2) carbonation, 3) spilitization, 4) silicification, and 5) epidote-quartz alteration.

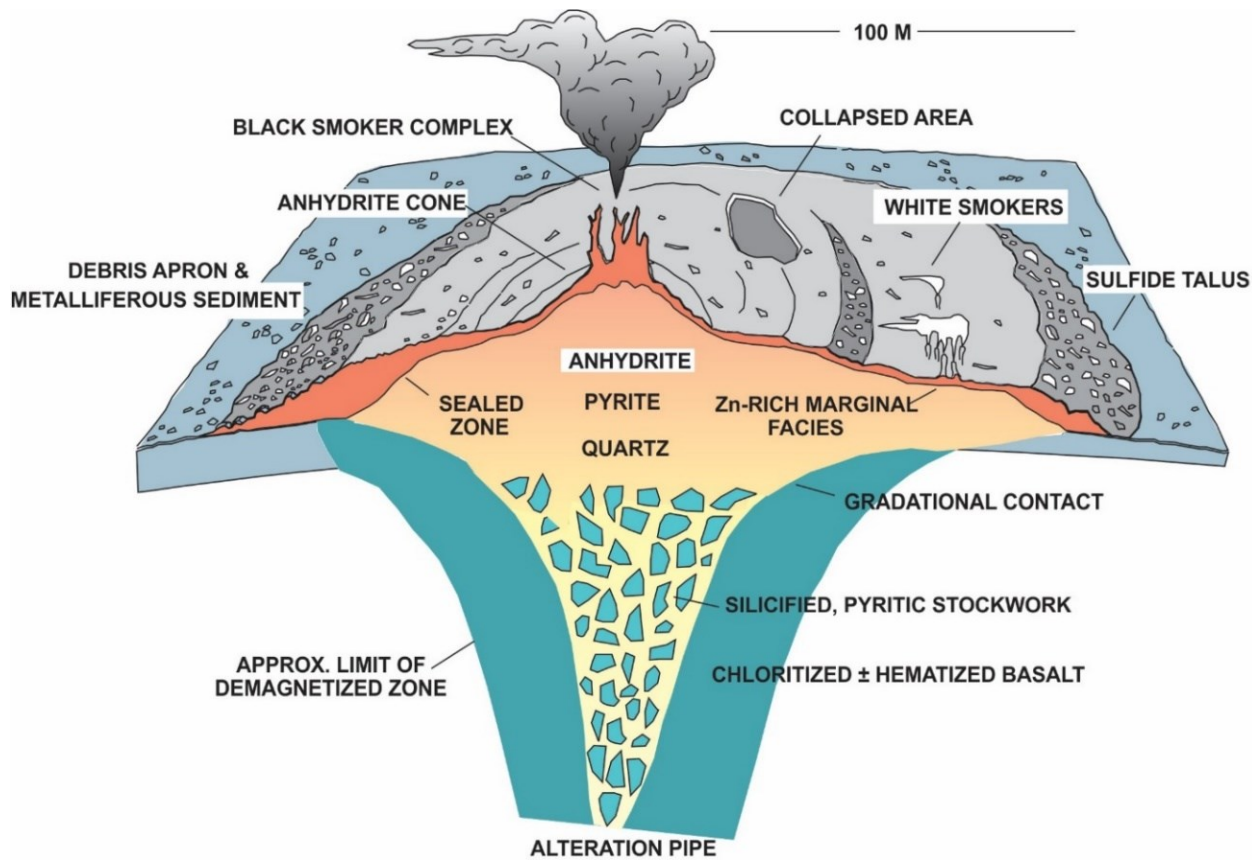


Fig. 2.7. Diagram of a present-day black smoker complex. The underlying cross-section representing the morphology of a VMS deposit, with a massive to semi-massive sulphide lens overlying a stringer zone, and the alteration pipe are illustrated (Galley et al., 2007).

2.5.2 Au-rich VMS deposits

Au-rich VMS deposits are important contributions to global gold reserves (Gosselin and Dubé, 2005). Au-rich Canadian VMS deposits amount to 870 t, equivalent to 10% of Canadian production and reserves (Dubé et al., 2007). There are two potential sources for this gold: 1) a syntectonic incorporation of Au during a regional deformation event into an Au-poor VMS deposit or 2) a synvolcanic precipitation of Au in the VMS system, produced by a chemical change in the hydrothermal fluids, perhaps via boiling (Dubé et

al., 2007). A magmatic contribution may also lead to Au-endowment of VMS deposits (Mercier-Langevin et al., 2014).

2.5.3 VMS emplacement mechanisms

Hydrothermal systems which drive VMS mineralisation develop in areas where there is high heat flow and cross-stratal permeability (Franklin et al., 2005). These conditions are present in several tectonic settings from back-arc basins, volcanic arc margins to mid-ocean ridge settings (Huston et al., 2011). The majority of ancient VMS deposits are associated with convergent tectonic settings (Fig. 2.8), as the preservation potential along spreading centres is low due to the recycling of this crust at subduction zones (Huston et al., 2011). However, the exact tectonic environment of Archean VMS deposits remains ambiguous. Therefore a classification system based on the volcanic and associated sequences was proposed by Franklin et al. (2005), which is as follows: 1) bimodal mafic dominated terranes, 2) mafic successions with little to no felsic volcanic units, 3) predominant mafic volcanics with numerous pelitic beds, 4) bimodal felsic terranes with lesser mafic and sedimentary sequences and, 5) siliciclastic-felsic units, containing a large proportion of terrigenous material.

These sulphide lenses are the result of growth, collapse, cementation, and replacement processes at hydrothermal vents, or near the paleo-seafloor (Franklin et al., 2005). In order for the VMS hydrothermal system to be established, a heat source must be available to initiate the circulation of hydrothermal fluids. This heat source may be a mafic or composite intrusion, located in the shallow sub-surface (Galley et al., 2007). This then allows large-scale hydrothermal systems to develop at temperatures of $>350^{\circ}\text{C}$, which leads to the precipitation and accumulation of massive sulphides. The ore metals are interpreted to have been leached from a high-temperature hydrothermal reaction zone via the circulation of evolved seawater or magma-derived fluids (Galley, 1993; Franklin et al., 2005) (Fig. 2.9). If these heat sources are located at shallow depths in the crust (between 2 to 5 km), they may also act as a source for metals (Franklin et al., 2005). The

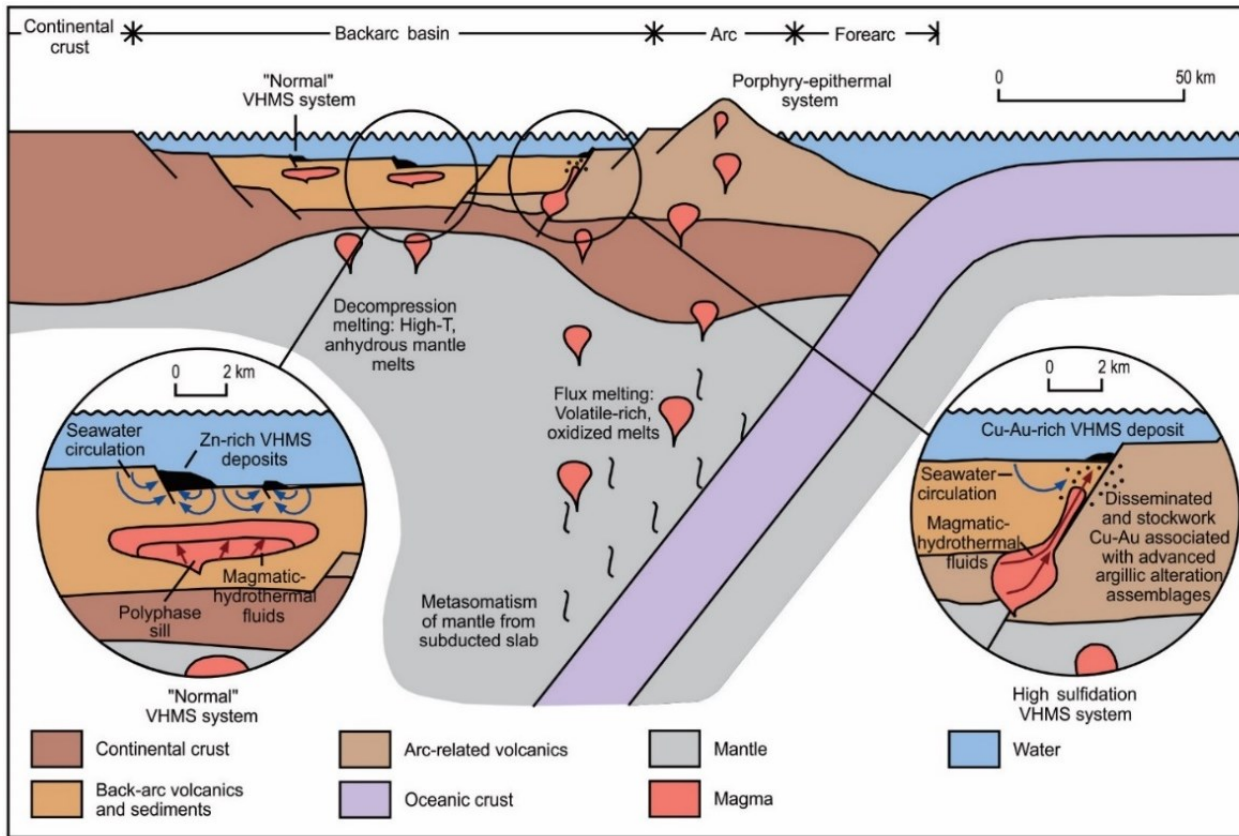


Fig. 2.8. Favourable locations for VMS mineralisation in a compressional tectonic regime. After Huston et al. (2011).

presence of synvolcanic structures, such as faults, are necessary to transport these metal endowed hydrothermal fluids towards the seafloor. These hydrothermal fluids are released onto, or near the seafloor through a volcanic edifice, sometimes into a pile of brecciated rock which is most likely produced from an initial, explosive hydrothermal eruption onto the seafloor (Lydon, 1988). As this hydrothermal fluid interacts with the surrounding rocks and seawater, it is cooled, allowing the sulphides to be precipitated.

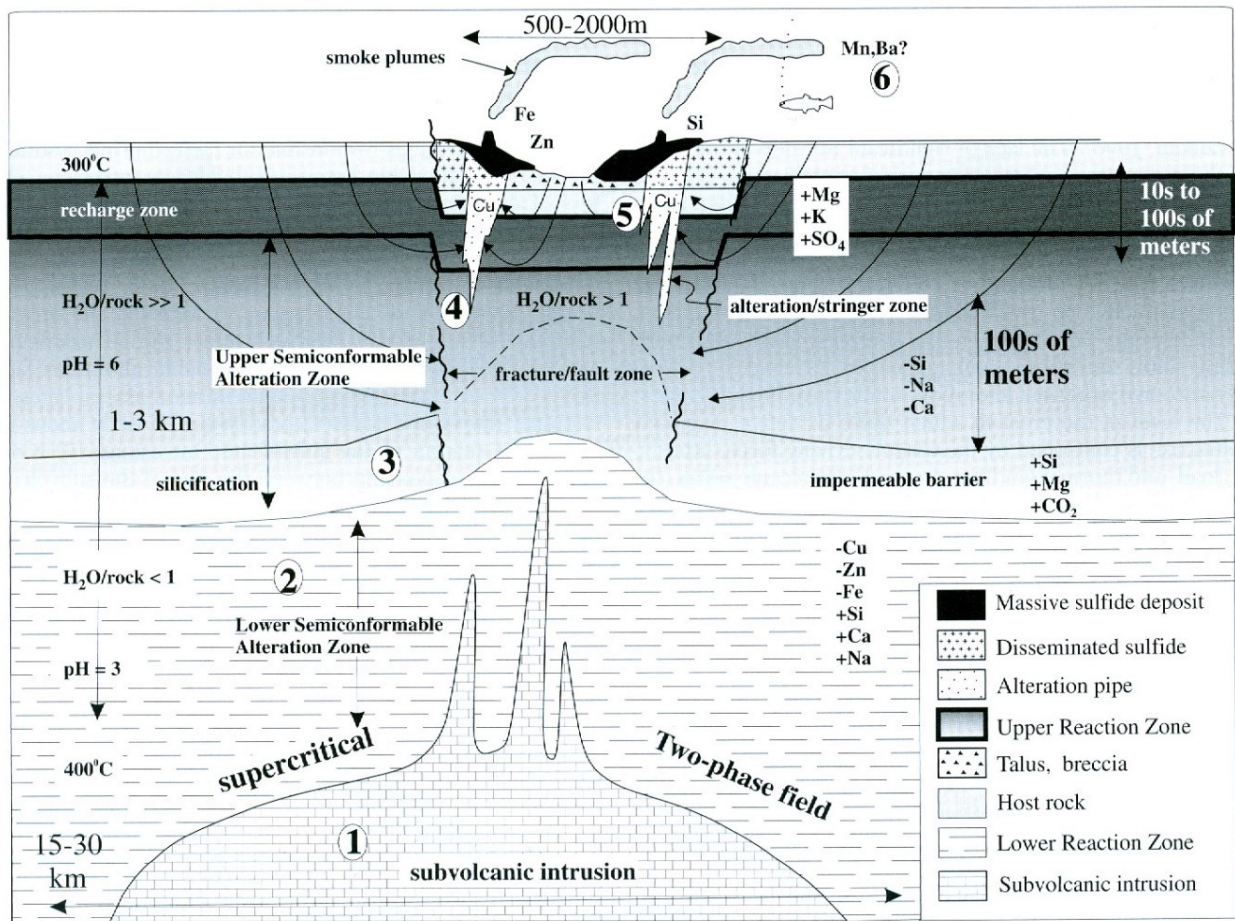


Fig. 2.9. Generalised emplacement model for VMS deposits. The hydrothermal fluid complex and the incorporation of seawater into the system are illustrated (Franklin et al., 2005).

3 THE COLOMB-CHABOULLIÉ GREENSTONE BELT VOLCANICS: GEOLOGY, STRATIGRAPHY, AND GEOCHEMISTRY

3.1 Introduction

Greenstone belts, which are areas of mostly mafic volcanic rocks surrounded by large granitoid terrains (Condie, 1981), are geologically important regions. They are key to understanding the geodynamic processes during the Archean, and even early life (e.g., Polat and Kerrich, 2001; Kerrick and Polat, 2006; Westall et al., 2006; O’Neil et al., 2011, 2012, 2013; Bédard et al., 2013; Bédard and Harris, 2014, Moyen and Laurent 2018; Smithies et al., 2018). They also host numerous mineral deposit types including volcanogenic massive sulphide (VMS) deposits (Franklin et al., 2005; Galley et al., 2007), Ni-Cu ± platinum-group element (PGE) sulphide deposits (Arndt et al., 2005; Maier and Groves, 2011), and orogenic gold deposits (Groves et al., 1998; Poulsen et al., 2000; Goldfarb et al., 2005). Large greenstone belts such as the Abitibi greenstone belt of the Superior Province in Canada and the Barberton belt in South Africa have provided ample data on their metamorphism, stratigraphy, geochemistry, and mineralisation (e.g., Laflèche et al., 1992; Powell et al., 1995; Thurston et al., 2008; Altigani et al., 2016). However, the study of smaller greenstone belts, such as the Colomb-Chaboullié of the Superior Province in Canada, is useful as these are stratigraphically, and hopefully petrologically less complex than larger greenstone belts. Another reason to map and study smaller greenstone belts is that they are economically underexplored; better knowledge of the volcanic stratigraphy for example, is a bonus for VMS exploration.

In this contribution, we present a geological, stratigraphic, and geochemical study of the Archean Colomb-Chaboullié greenstone belt. We speculate on the petrogenesis of the volcanic rocks based on the aforementioned information and propose that the intercalated tholeiitic basalts and calc-alkaline andesites have somewhat different magmatic histories. Because crustal contamination is potentially an important process in the origin of some

Colomb-Chaboullié volcanic rocks, we highlight some possible contaminants in the adjacent Opatica and Nemiscau subprovinces; the Lac Rodayer pluton and the Théodat Complex. We then compare the Colomb-Chaboullié belt with two other greenstone belts from the same general area: the Frotet-Evans greenstone belt located in the Opatica Subprovince and the Lac des Montagnes belt of the Nemiscau Subprovince. This study also looks at the origin of the Au-Ag-Cu sulphide showings throughout the greenstone belt, and uses geochemistry to determine any prospective contacts that may help future VMS exploration in the area.

3.2 Geological context

The Colomb-Chaboullié greenstone belt is located at the contact between the Nemiscau and Opatica subprovinces of the Superior Province, in the James Bay area of Quebec (Fig. 3.1). The Superior Province is one of the most extensive Archean cratons (Card, 1990; Benn and Moyen, 2008). The subdivision of the Superior Province into smaller subprovinces and domains is based on age differences and lithological, structural, metamorphic, and geophysical characteristics (Card and Ciesielski, 1986).

The Opatica Subprovince lies immediately south of the Colomb-Chaboullié greenstone belt. This is a high-grade volcano-plutonic subprovince, primarily composed of orthogneiss and granitoid rocks (Sawyer and Benn, 1993; Davis et al., 1995; Bandyayera and Daoudene, 2017). U-Pb ages for plutonic and gneissic rocks in the Opatica Subprovince range from 2820-2833 Ma (Davis et al., 1994) to 2678 ± 2 Ma (Davis et al., 1995). The Lac Rodayer pluton has an age range of 2833-2825 Ma, based on U-Pb ages (Davis et al., 1994). This is the oldest unit within the Opatica Subprovince. It is composed of four lithological subunits; *Arod1*, *Arod2*, *Arod3*, and *Arod4* (Bandyayera and Daoudene, 2017). *Arod2* and *Arod3* form spatially abundant bodies of the Lac Rodayer pluton located immediately adjacent to the Colomb-Chaboullié belt. These subunits comprise variably foliated tonalites, with quartz-diorite also present in *Arod3*. The 2822 Ma Théodat Complex (J. Davis, written communication, 2018) also borders the Colomb-Chaboullié,

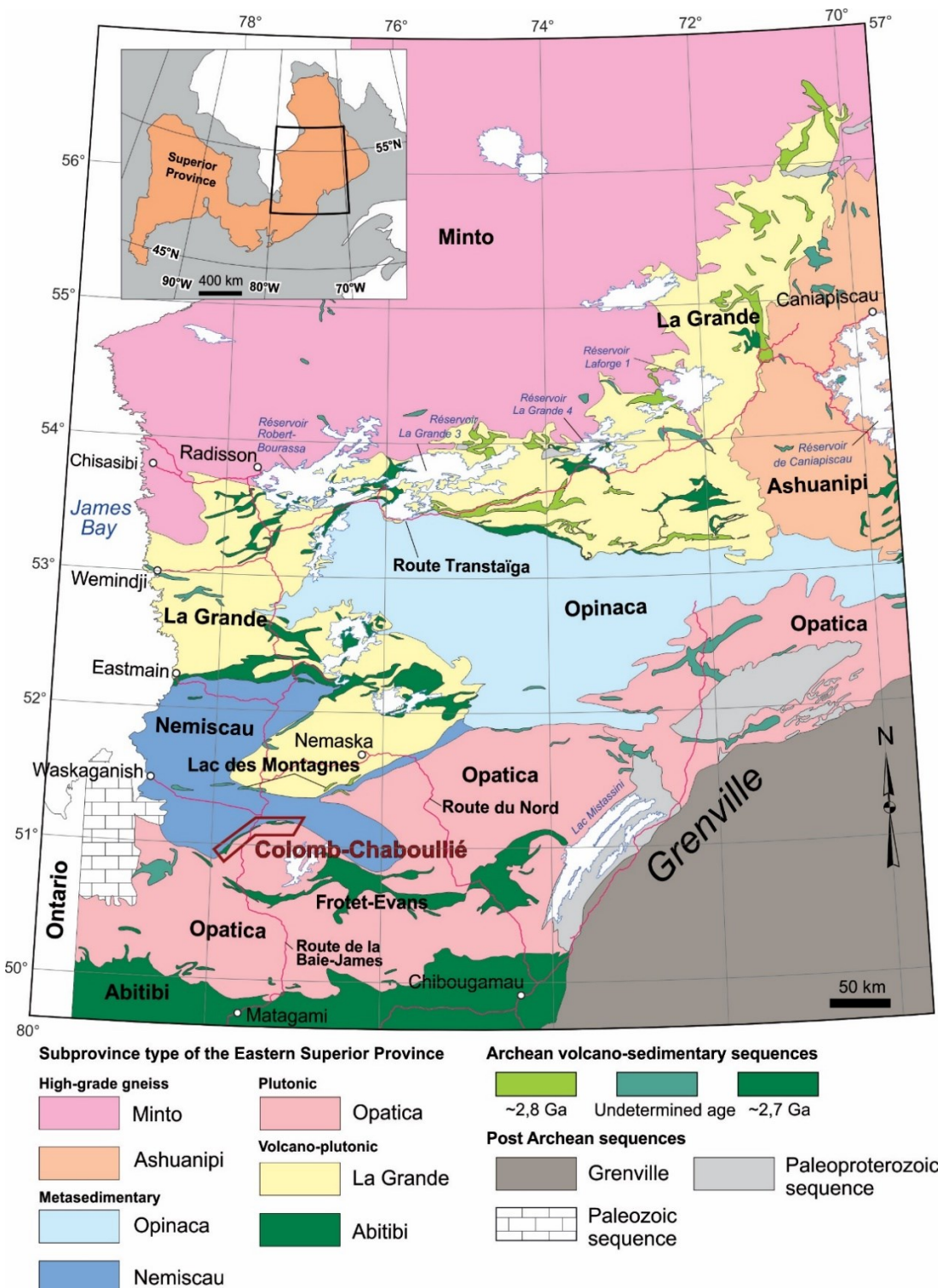


Fig. 3.1 Geological map of the Eastern Superior Province, Quebec, showing the location of the Colomb-Chaboullié greenstone belt (in red) at the contact between the Opatica and Nemiscau subprovinces. The location of the Frotet-Evans and Lac des Montagnes greenstone belts, to which the Colomb-Chaboullié is compared, is also highlighted. After Bandyayera and Daoudene (2017).

within the Opatica Subprovince. It is made up of six subunits; a biotite-rich gneiss (*Athe1*), a massive to gneissic granodiorite unit (*Athe2*), a magnetic porphyritic granodiorite unit (*Athe3*), a gneissic granodiorite unit (*Athe4*), a tonalite unit (*Athe5*), and a pegmatite and granite unit (*Athe6*).

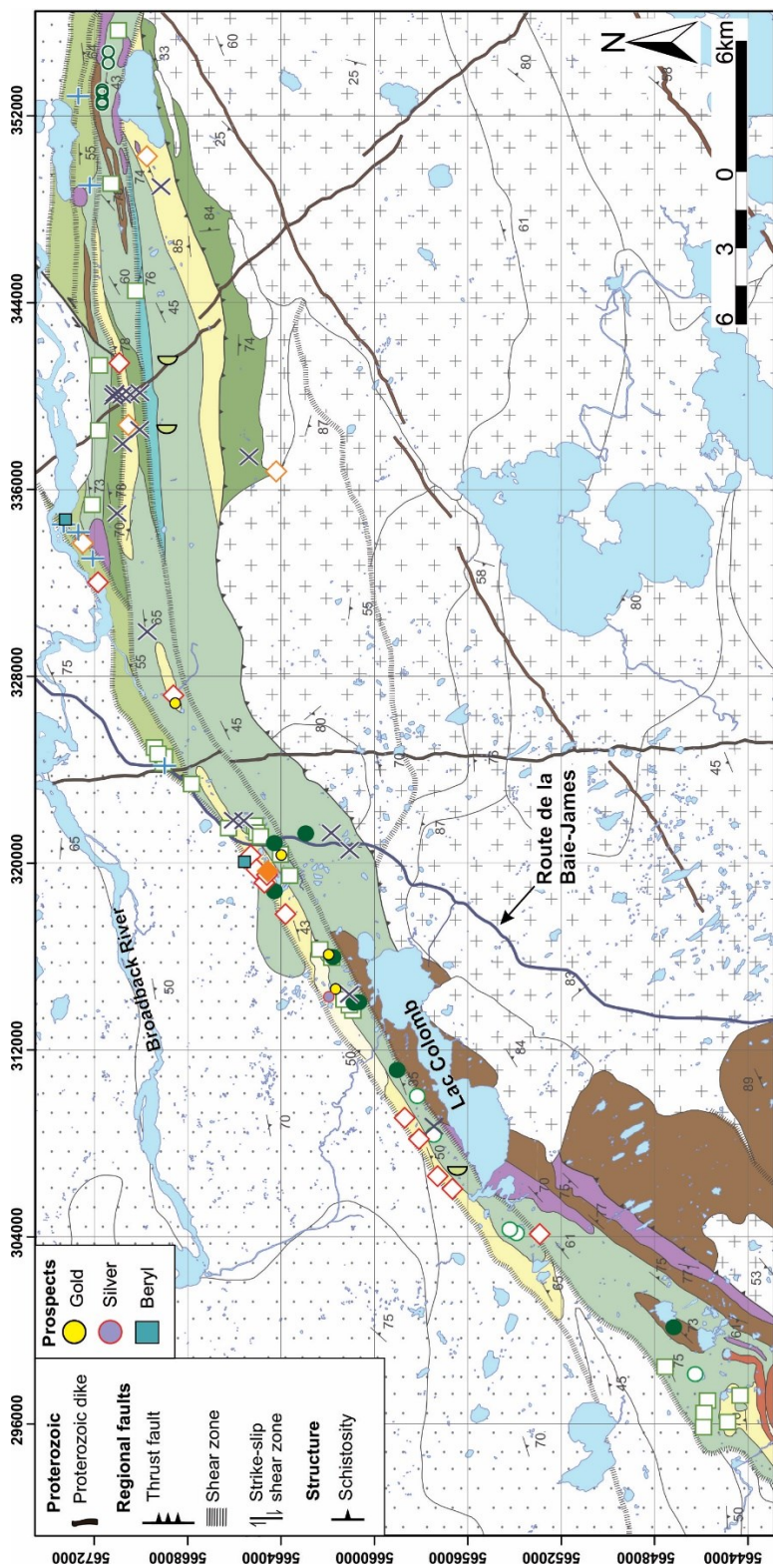
The 250 km long volcano-sedimentary Frotet-Evans greenstone belt is located in the central part of the Opatica Subprovince (Benn et al., 1992; Sawyer and Benn, 1993) (Fig. 3.1) and contains the Au-Cu Troilus mine (Goodman et al., 2005). This greenstone sequence is dominated by tholeiitic mafic to intermediate lavas and intermediate to felsic calc-alkaline lavas and pyroclastic sequences (Boily and Dion, 2002). An age of 2755.5 ± 0.9 Ma based on zircons has been obtained from a rhyodacite sample from the Storm Formation of the Evans Group, for volcanism in the Frotet-Evans greenstone belt (Bandyayera and Sharma, 2001).

The Nemiscau Subprovince is principally a high-grade metasedimentary terrain made up largely of paragneiss, metatexites, and diatexites (Hocq, 1994), situated to the north of the Colomb-Chaboullié belt. A U-Pb zircon sample derived from a granite that cross-cuts the Nemiscau yielded a minimum age of 2672 ± 2 Ma (Davis et al., 1995). A depositional age of the sediments of the Nemiscau Subprovince is estimated between 2698 and 2688 Ma (Percival et al., 1992). This is therefore not a viable source of magma contamination for the ~2.76 Ga Colomb-Chaboullié greenstone belt. The Nemiscau is subdivided into two principle regions; a plutonic terrane comprising monzonite and granodiorite rocks which contain remnants of paragneiss and amphibolites, and a metasedimentary terrain which itself is divided into three high-grade domains based on magnetic features (Hocq, 1994). The Nemiscau Subprovince contains the ca. 2712 Ma Lac des Montagnes volcano-sedimentary group (Valiquette, 1975; Hocq, 1994; Bandyayera and Daoudene, in preparation) (Fig. 3.1). This volcano-sedimentary sequence is composed of massive to pillowed basalt flows, with lesser amphibolites, intermediate to felsic volcaniclastic rocks, and iron formations.

The Colomb-Chaboullié belt was most recently mapped by the *Ministère de l'Énergie et des Ressources naturelles du Québec* (MERN) in 2015 (Bandyayera and Daoudene, 2017). This greenstone belt measures 77 x 5 km and is made up of volcanic, mafic/ultramafic intrusive, sedimentary, and metamorphic rocks (Bandyayera and Daoudene, 2017). It is dominantly composed of mafic, pillow to massive basaltic lava flows (Fig. 3.2). The remaining volcanic units include variably porphyritic, pillow to massive andesite flows and intermediate to felsic volcaniclastic rocks. These volcanic units have been metamorphosed to the amphibolite facies. U-Pb ages of 2756.8 ± 4 Ma and 2760.3 ± 6 Ma have been determined for zircons in these volcaniclastic rocks (David et al., in preparation). The intrusive bodies are located mostly in the west and are composed of gabbros, peridotites, and pyroxenites. There are three sedimentary units within the Colomb-Chaboullié belt. A small banded quartzite-iron formation is located to the west, two small bands of paragneiss are present, and a thin band of polymict conglomerate is located in the eastern part of the belt (Bandyayera and Daoudene, 2017).

The MERN compiled previously recorded and newly identified mineral prospects. Six Ni-Cu-PGE prospects in the mafic/ultramafic intrusives and six VMS-style Au-Ag-Cu prospects were confirmed or discovered in 2015. The presence of disseminated pyrite-arsenopyrite veins associated with shear zones suggests that orogenic gold mineralisation is also present in the Colomb-Chaboullié greenstone belt.

The Lac Marcaut massive sulphide showing is the best known VMS-style showing (Riopel, 1994), which extends laterally along an outcrop ridge for 80 m in an east-west direction, with a maximum thickness of 1.4 m (Thorsen et al., 1993). Borehole intersections and electromagnetic surveys show that the massive sulphide lens has a minimum strike length of 2.8 km (Thorsen et al., 1993). The electromagnetic data further suggests that this lens occurs discontinuously over a strike length of nearly 6 km. Gold contents are anomalous throughout the sulphide unit. Borehole grades of 3.52 g/t Au over 0.8 m and channel samples grades of 3.77 g/t Au across 1.85 m and 6.86 g/t Au across 1.3 m have been reported (Thorsen et al., 1993).



Stratigraphic Legend

Nemiscau Subprovince		Colomb-Chaboullié Group	
Undifferentiated Nemiscau Subprovince lithologies	Acch8	Peridotite and pyroxenite	Acch5
Undifferentiated Opatica Subprovince lithologies	Acch7	Paragneiss ($bi \pm hbl$)	Acch4
Quartzite/iron formation	Acch6	Felsic to intermediate volcanics	Acch3
			Acch1 Basalt
			Acch2 Andesite
			Acch2a Andesite
			Acch2b Porphyritic andesite

Fig. 3.2 Geological map of the Colomb-Chaboullié greenstone belt. The geology of the study area, the stratigraphic position of the geochemical samples used in this study, and the locations of previously recorded mineralisation are shown (after Bandyayera and Daoudene, 2017).

3.3 Methodology

Outcrop density in the study area is low due to woody or swampy terrain. Field mapping focused on the volcanic units of the Colomb-Chaboullié greenstone belt using the 1:50 000 scale geological map of NTS sheets 32N03 and 32N04 as a base map. Some 69 field stations were visited, of which 39 were new and 30 had been previously mapped by the MERN in 2015. The *Route de la Baie-James* crosscuts the greenstone belt in a north-south direction (Fig. 3.2), which allowed numerous samples to be taken along this transect. More remote samples were also collected via helicopter. Over 70 samples were collected and sawed to examine in the laboratory. From this set, 45 were selected for whole rock major and trace element analyses (see Fig. 3.2 for locations) at Activation Laboratories in Ontario, Canada, where they were crushed to a mesh size of 105 µm. Major oxides, along with Sr were analysed via ICP-OAS. All other trace elements were determined by ICP-MS following a lithium metaborate/tetraborate fusion process. These results were combined with pre-existing data from the MERN, using the same methods at the same laboratory, for a total of 121 analyses of volcanic rocks. Five outliers were excluded from the geochemical plots.

The Archean crustal pole average (AC) is plotted on all geochemical diagrams (after Rudnick and Fountain, 1995) to examine the possibility of crustal contamination for the Colomb-Chaboullié magmas. However, as this is a global average, it is not representative of the possible contamination conditions for these magmas. As a result, fields are also included on these diagrams for the Lac Rodayer pluton ($n = 18$) and the Théodat Complex ($n = 13$) in the Opatica Subprovince. *Athe1* to *Athe4* of the Théodat Complex were used to determine the degree of contamination as this was the lithogeochemical data available. Instead of averaging all of these samples from the potential contaminant lithologies, we drew fields comprising 80% of the data to show representative trends without visually overloading the plots.

The Lac Marcaut outcrop, located at 316 632 m E and 5 662 111 m N (UTM Nad 83 zone 18U), was mapped in more detail using the tape and compass method to establish the relationship between the massive sulphide lens and the surrounding host basalts.

3.4 Results

3.4.1 Lithofacies and petrography

Volcanic rocks in the study area (Fig. 3.2) consist of: (1) the predominant pillowed to massive submarine basalt lavas (*Acch1* in Bandyayera and Daoudene, 2017), (2) variably porphyritic intermediate lava flows (\pm intrusions?) (*Acch2* and *Acch2a*), and (3) felsic to intermediate volcaniclastic rocks (*Acch3*). The pillowed facies dominates the basalt lavas (Figs. 3.3a and b), with variably deformed pillows ranging in length from 30 cm to 2 m. Where primary textures are best preserved, hyaloclastite is recognised between the pillows, and consists of angular shards of former glass, now chloritised. Garnets (>5 mm) and disseminated sulphides are often present in the inter-pillow material. The lack of sufficiently well-preserved pillow shapes prevents the polarity (stratigraphic younging direction) from being determined. Schistose rocks are present in the most deformed areas of the stratigraphy. These fine-grained basalts have a plagioclase-amphibole \pm biotite \pm chlorite \pm epidote \pm opaques mineral assemblage (Figs. 3.3c and d).

Acch2 is a porphyritic andesite, which form massive lava flows and/or subvolcanic intrusions in the eastern sector of the Colomb-Chaboullié belt (Fig. 3.2). These are plagioclase-phyric (ca. 20%), with tabular phenocrysts ranging in size from 3 to 5 mm (Figs. 3.3e and f). Glomerophenocrysts of hornblende and lesser biotite are also present (5-8%, 3-5 mm). The groundmass is recrystallised and composed of plagioclase-quartz-amphibole \pm biotite \pm chlorite. *Acch2a* is characterised by pillowed andesite flows (Fig. 3.4a), containing a lower proportion of phenocrysts (0-10%). The pillows are deformed and measure up to 1 m in length. At microscopic scale, plagioclase phenocrysts comprise <5% of the composition of *Acch2a*, with an absence of hornblende-biotite

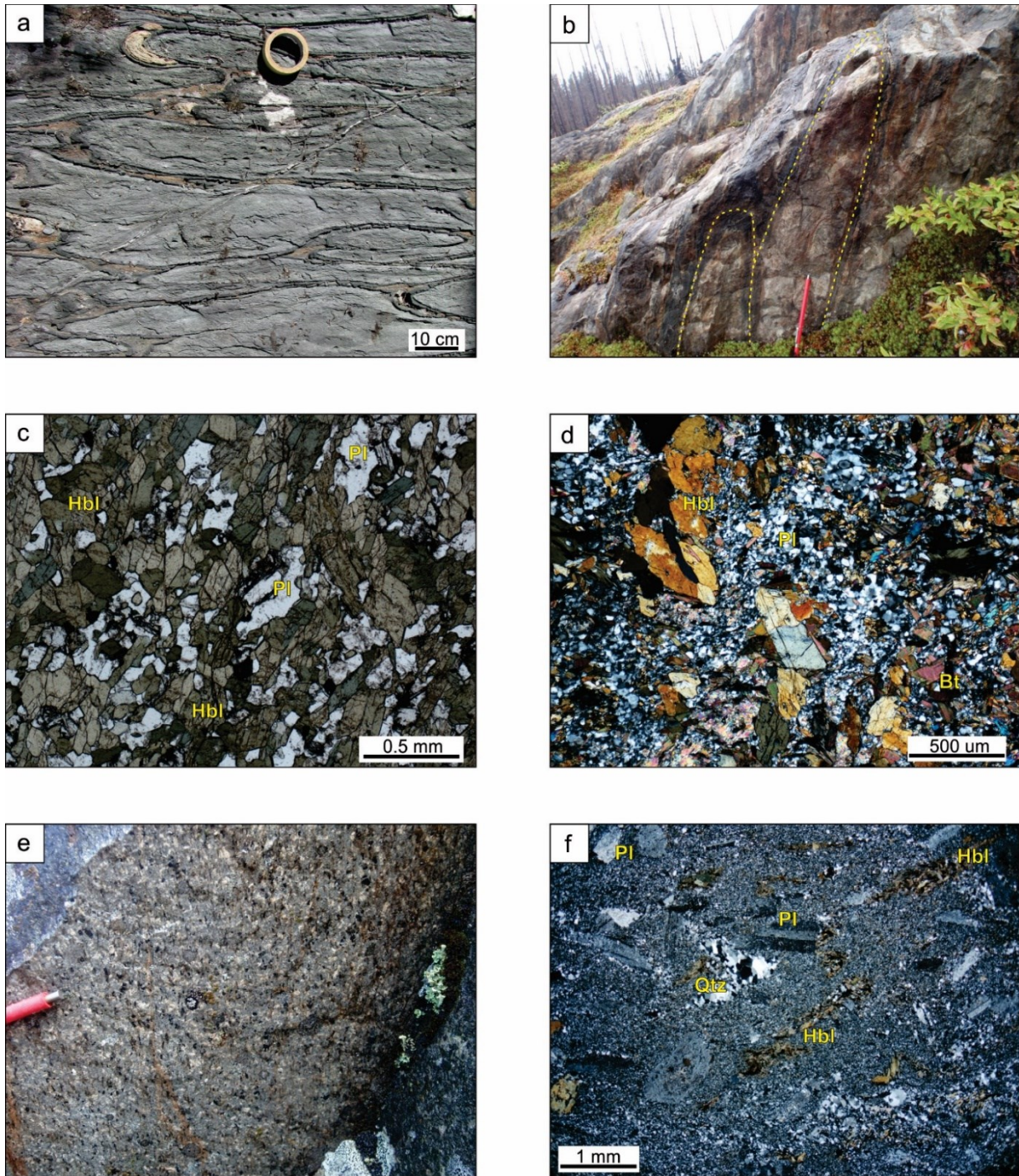


Fig. 3.3 Basaltic and andesitic lava flows of the Colomb-Chaboullié belt. (a) Best preserved pillows in the NE of the belt, (b) 3D view of highly deformed pillows, (c) – (d) photomicrographs of the basaltic lavas (plane polarized light and cross-polarized light, respectively). (e)-(f) Porphyritic andesite flows or subvolcanic intrusions in outcrop view and thin section (cross-polarized light). Abbreviations: Bt = biotite; Hbl = hornblende; Pl = plagioclase; Qtz = quartz. The red magnet is 12 cm-long.

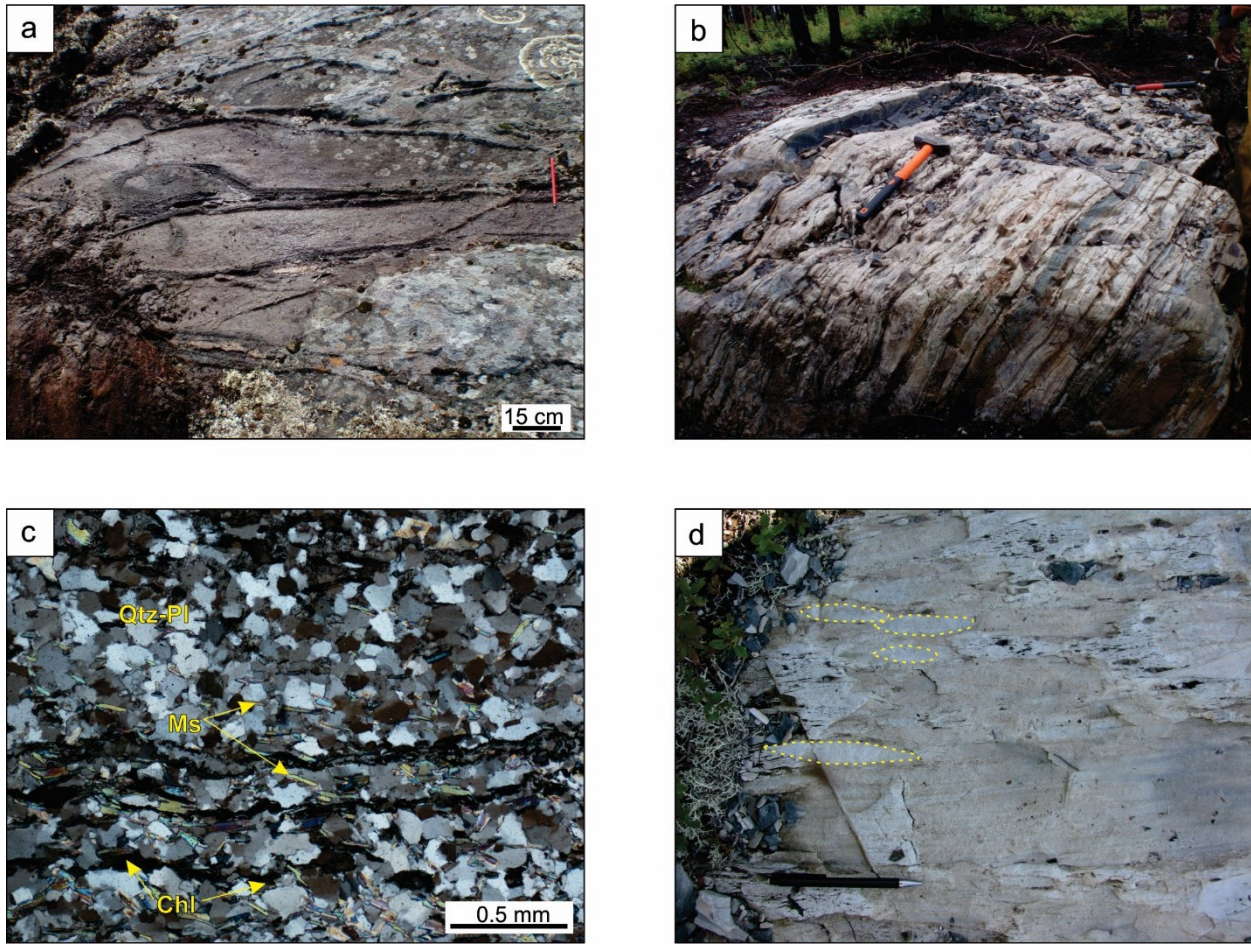


Fig. 3.4 Pillowed andesite lava and volcaniclastic rocks of the Colomb-Chaboullié greenstone belt. (a) Pillowed lava flows of *Acch2a* andesite, (b) and (c) outcrop and photomicrograph (cross-polarized light) of laminated volcaniclastic unit, and (d) lapilli tuff with some bombs (lapilli and bombs highlighted by dashed lines). Abbreviations: Chl = chlorite; Ms = muscovite; PI = plagioclase; Qtz = quartz. Orange hammer is 40 cm long, black pencil is 15 cm long.

glomerophenocrysts. This unit often shows a weak schistosity, defined by the alignment of elongate amphibole and biotite crystals, and in some cases chlorite. The groundmass mineral assemblage is comparable to that of *Acch2*.

Acch3 comprise intermediate to felsic tuffs and lapilli tuffs (Bandyayera and Daoudene, 2017). This lithofacies occurs as lenses within the basalt lavas (Fig. 3.2). Some *Acch3* rocks are finely bedded with well-developed centimetre to sub-centimetre stratification (Figs. 3.4b and c), where plagioclase-rich bands alternate with thinner bands rich in

chlorite. Where lapilli are present, they are elongate (Fig. 3.4d). These volcaniclastic rocks comprise a plagioclase-quartz ± muscovite ± chlorite ± biotite mineral assemblage, with chlorite-rich bands also present at microscopic-scale in the laminated unit (Fig. 3.4c).

3.4.2 Lithogeochemistry

The geochemical results presented here have been used to further refine the geological map, as presented in figure 3.2. The majority of the samples were taken from the least altered parts of the volcanic rocks, and only a few samples were taken near mineralised areas. On the alteration box plot (Fig. 3.5a), most of the analyses therefore show minimal alteration. Geochemistry allows the basalts to be sub-divided into three major groups (*Acch1a*, *Acch1b* and *Acch1c*) and two minor groups (*Acch1d* and *Acch1e*) (Table 3.1 and 3.2, Figs. 3.5 to 3.7). This division is based primarily on their extended multi-element profiles, and these groups were then verified using the various classification, magmatic affinity, immobile trace element, and tectonic discrimination diagrams, in particular the Ross and Bédard (2009) diagram, the TiO_2 vs Zr bivariate plot, the Wood (1980) diagram, and the Pearce (2008) plot (Figs. 3.5 to 3.7).

The *Acch1a* basalts are defined by their relatively flat extended multi-element patterns, tholeiitic affinity and lower Th/Yb ratios. *Acch1b* basalts are characterised by their more inclined multi-element pattern, with a small Nb-Ta negative anomaly and intermediate Th contents. *Acch1c* rocks have the lowest TiO_2 values of all the Colomb-Chaboullié basalts, which is also reflected in their high Zr/ TiO_2 ratios. They have the highest Th values and largest Nb-Ta negative anomalies of all the basalts. *Acch1d* basalts are defined by very high TiO_2 contents and *Acch1e* appear more intermediate in composition than other basalt groups, with higher Zr concentrations and Nb/Y ratios. The basalts are further described below.

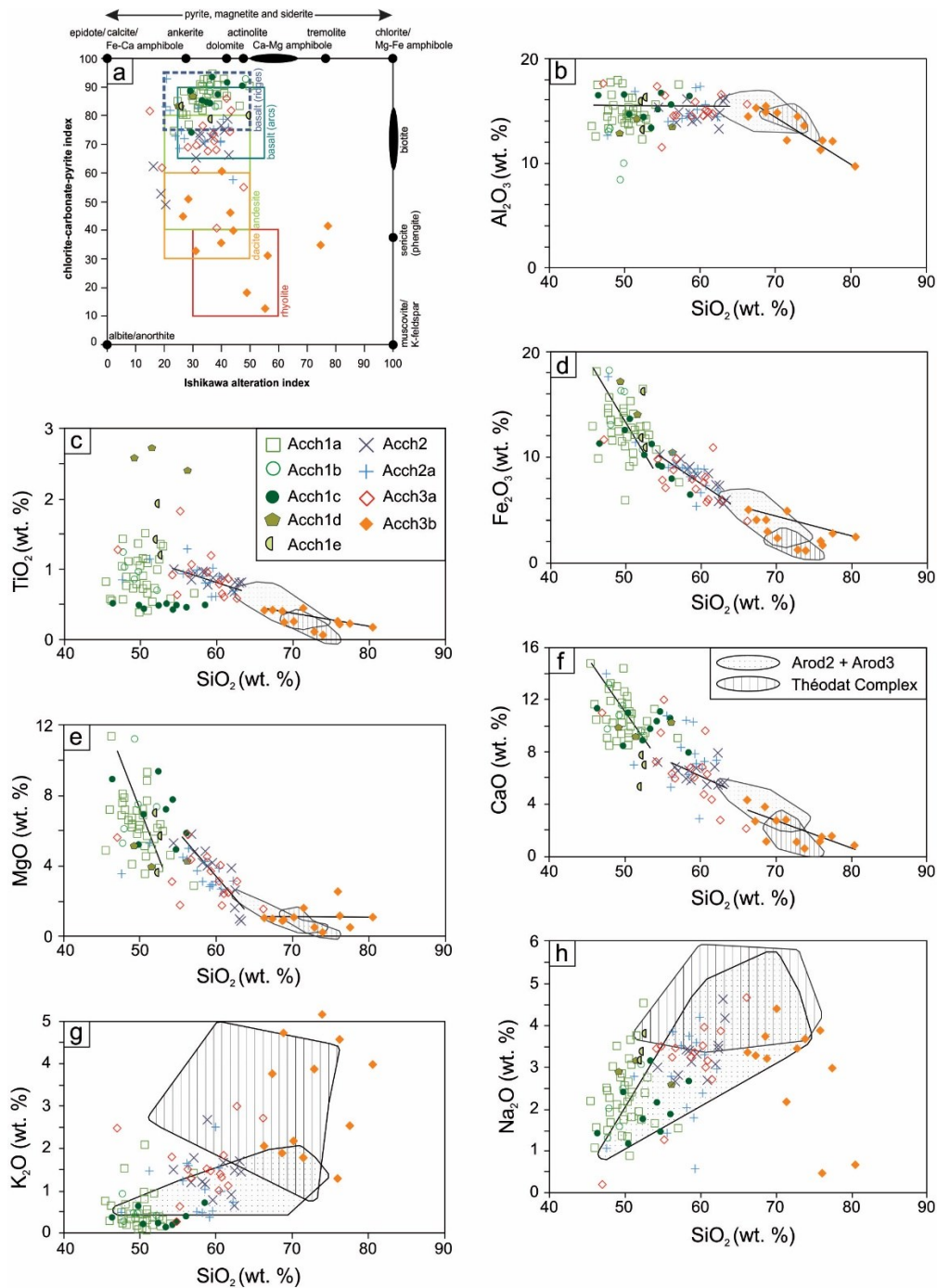


Fig. 3.5 Alteration box plot and Harker compositional diagrams for the Colomb-Chaboullié greenstone belt. (a) Al-CCPI alteration box plot (after Large et al., 2001). $\text{AI} = 100(\text{K}_2\text{O} + \text{MgO}) / (\text{K}_2\text{O} + \text{MgO} + \text{Na}_2\text{O} + \text{CaO})$; $\text{CCPI} = 100(\text{MgO} + \text{FeO}^\text{t}) / (\text{MgO} + \text{FeO}^\text{t} + \text{Na}_2\text{O} + \text{K}_2\text{O})$. The box for unaltered ridge basalts on the alteration box plot is from Rogers et al. (2014) and the least altered boxes for arc basalts to rhyolites are derived from Gifkins et al. (2005). The poles for biotite and various amphiboles are from Caté et al. (2015). (b) - (h) SiO_2 versus Al_2O_3 , TiO_2 , Fe_2O_3 , MgO , CaO , K_2O , and Na_2O . Trend lines are included on the Harker diagrams in order to provide visual aid between the mafic, intermediate and felsic trends. Abbreviations; Arod2 + Arod3: subunits of the Lac Rodayer pluton.

Table 3.1

Average major oxide geochemical characteristics of the volcanic units of the Colomb-Chaboullié belt.

	Acch1					Acch2		Acch3	
	Acch1a	Acch1b	Acch1c	Acch1d	Acch1e	Acch2	Acch2a	Acch3a	Acch3b
wt. %									
SiO ₂	50.0	49.4	52.0	52.3	52.2	59.0	57.4	58.4	72.4
TiO ₂	0.90	0.96	0.48	2.57	1.52	0.84	0.89	0.91	0.27
Al ₂ O ₃	15.0	11.8	15.4	13.5	15.1	14.7	14.9	15.2	13.3
Fe ₂ O ^T	12.7	15.0	10.3	14.0	13.1	8.44	9.13	7.93	2.93
MgO	6.38	7.50	6.67	4.45	5.47	3.86	3.68	3.80	1.05
MnO	0.30	0.31	0.26	0.25	0.18	0.14	0.18	0.17	0.05
CaO	10.8	11.0	9.93	9.75	6.69	6.55	7.83	6.76	2.01
K ₂ O	0.45	0.47	0.32	0.21	0.64	1.28	1.15	1.52	3.12
Na ₂ O	2.27	2.09	2.01	2.88	3.45	3.32	2.67	3.11	2.94
LOI	1.26	1.08	1.43	0.22	0.96	1.28	1.36	1.62	1.18
Total	100.1	99.6	98.8	100.1	99.3	99.4	99.2	99.4	99.3

The intermediate lava groups (*Acch2* and *Acch2a*) are similar to each other in terms of geochemical properties, however their division is based upon phenocryst populations. The volcaniclastic rocks are separated based on their composition (i.e. intermediate (*Acch3a*) and felsic (*Acch3b*)).

Harker diagrams show that overall, when SiO₂ increases, TiO₂, Fe₂O₃, MgO, and CaO decrease in concentration (Fig. 3.5). Na₂O and K₂O show more dispersed trends, but K₂O generally increases as a function of SiO₂. This suggests that potassium feldspar concentrations were low, or non-existent, and that albite abundances were also low (Winter, 2001). These Harker diagrams also show different trends between the mafic, intermediate, and felsic units. The mafic samples have flat Al₂O₃ concentrations and decreasing Fe₂O₃, MgO and CaO values. These basalts are predominantly rich in Fe₂O₃, with some high MgO contents (Figs. 3.5d and e). TiO₂ is variable in the mafic rocks: different subunits behave differently (Fig. 3.5c).

Table 3.2

Average trace element and elemental ratio geochemical characteristics of the volcanic units of the Colomb-Chaboullié belt.

	Acch1					Acch2		Acch3	
	Acch1a	Acch1b	Acch1c	Acch1d	Acch1e	Acch2	Acch2a	Acch3a	Acch3b
ppm									
Sc	39.4	30.0	46.6	40.2	24.7	20.8	16.9	17.9	11.6
Rb	19	14	11	4	25	70	39	57	95
Sr	131	137	81	141	192	344	352	387	250
Y	18.8	18.8	14.0	45.3	29.2	19.8	22.6	22.1	19.1
Zr	44	62	37	130	139	130	145	162	140
Nb	1.70	2.96	1.08	6.27	8.37	6.25	7.76	7.91	5.88
Cs	1.33	0.64	1.37	0.2	0.77	3.93	3.01	3.67	2.54
La	3.14	7.11	3.33	9.72	16.1	27.7	32.4	41.6	32
Ce	7.98	16.6	7.36	24.9	38.8	56	65.3	84.5	63.3
Pr	1.19	2.25	0.92	3.71	5.02	6.36	7.48	9.71	6.83
Nd	6.01	10.3	3.98	18.2	24	25.1	28.4	36.3	24.3
Sm	2.01	2.87	1.23	5.66	5.1	4.37	5.29	6.27	4.55
Eu	0.77	0.97	0.43	1.88	1.52	1.23	1.45	1.65	0.92
Gd	2.77	3.42	1.73	7.26	5.61	4.01	4.71	5.19	3.89
Tb	0.51	0.58	0.33	1.29	0.92	0.62	0.71	0.74	0.60
Dy	3.29	3.50	2.30	8.25	5.48	3.64	4.07	4.11	3.47
Ho	0.69	0.69	0.50	1.7	1.09	0.72	0.80	0.79	0.67
Er	2.04	2.02	1.53	4.99	3.18	2.10	2.34	2.25	2.01
Yb	2.06	1.91	1.62	5.1	3.25	2.12	2.28	2.09	2.06
Lu	0.33	0.30	0.26	0.8	0.51	0.33	0.36	0.33	0.34
Hf	1.29	1.56	1.03	3.63	3.30	3.19	3.51	3.80	3.58
Ta	0.14	0.25	0.10	0.44	0.60	0.53	0.60	0.60	0.74
Th	0.28	0.03	0.81	0.82	1.58	4.67	4.55	6.4	11.4
ratios									
Zr/Y	2.32	3.32	2.74	2.87	4.77	6.53	6.69	8.03	8.94
Th/Yb	0.14	0.55	0.51	0.16	0.49	2.24	2.11	3.99	8.15
Nb/Y	0.09	0.16	0.08	0.14	0.29	0.31	0.35	0.38	0.38
Zr/TiO ₂	50	66	78	51	96	162	166	190	546
La/Sm	1.51	2.50	2.70	1.69	3.15	6.16	6.04	6.56	6.87
Gd/Yb	1.35	1.82	1.08	1.42	1.73	1.90	2.08	2.70	2.40
Nb/Th	6.05	3.04	1.33	7.72	5.52	1.51	1.84	1.36	0.54

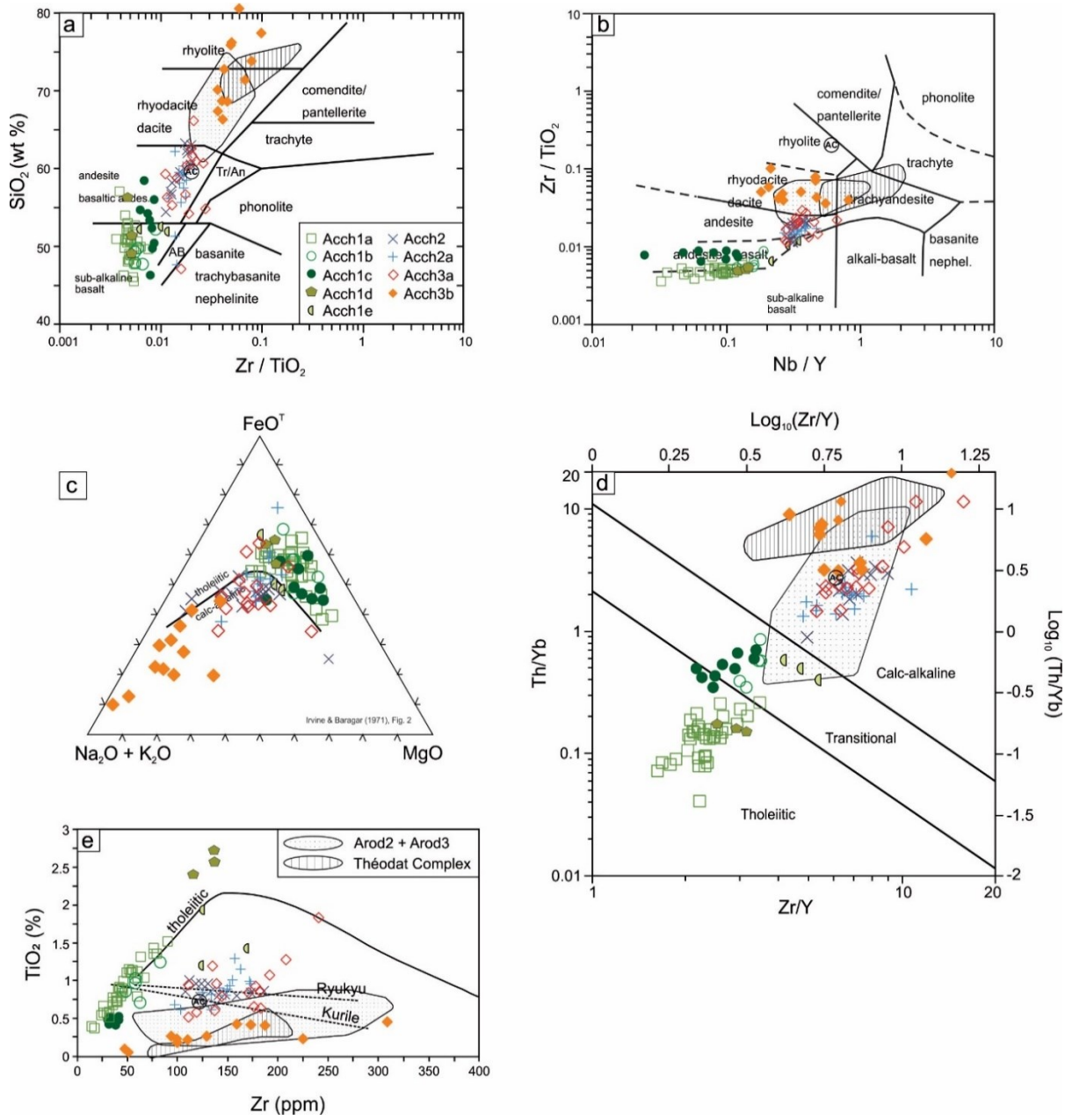


Fig. 3.6 Classification and magmatic affinity diagrams for the Colomb-Chaboullié greenstone belt. (a) and (b) Winchester and Floyd (1977) classification diagrams. (c) Alkali-total iron-magnesium (AFM) diagram. (d) Magmatic affinity diagram from Ross and Bédard (2009). (e) TiO_2 vs. Zr plot. AC; average Archean crust value, after Rudnick and Fountain (1995). The tholeiitic trend line is taken from MacLean and Barrett (1993). The calc-alkaline trend lines are based on mafic to felsic volcanic rocks from the Kurile and Ryukyu arcs, compiled from the GEOROC database (<http://georoc.mpch-mainz.gwdg.de/georoc/>). Analyses for the Kurile arc were initially obtained by Tsvetkov et al. (1985), Aoki et al. (1999), Takagi et al. (1999) and Frolova et al. (2001). Analyses for the Ryukyu arc are from Miyoshi et al. (2005, 2008, 2009, 2010) and Almberg et al. (2008). All modern arc data was plotted on the AFM diagram, and any samples in the tholeiitic field were eliminated to get a calc-alkaline trend in (e). Abbreviations; Arod2 + Arod3: subunits of the Lac Rodayer pluton.

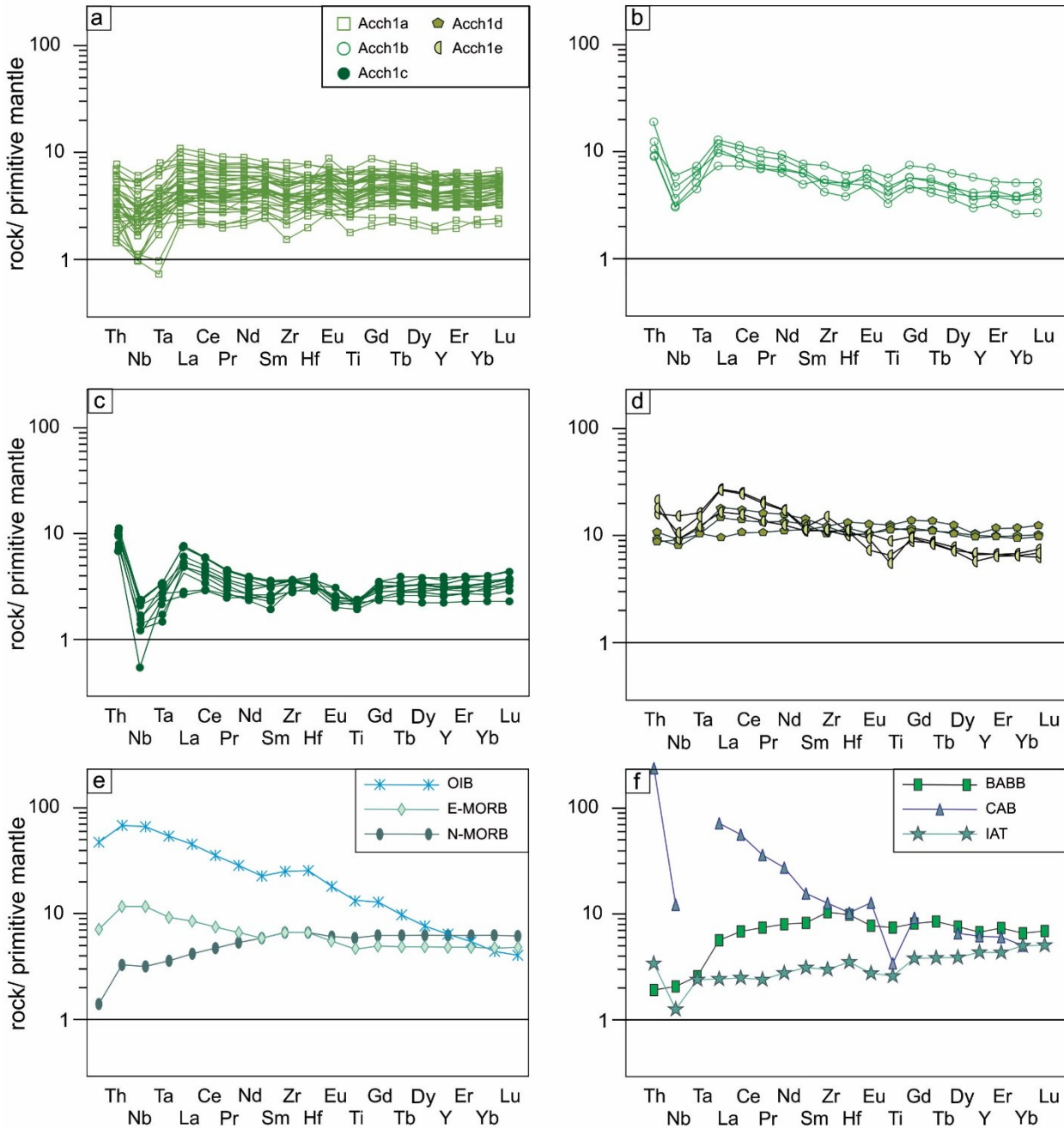


Fig. 3.7 Extended multi-element plots for the mafic lavas of the Colomb-Chaboullié greenstone belt. a) Acch1a, b) Acch1b, c) Acch1c, d) Acch1d and Acch1e, e) modern non-arc basalts, and f) modern arc basalts. Primitive mantle normalization values, normal mid-ocean ridge basalts (N-MORB), enriched mid-ocean ridge basalts (E-MORB), and ocean island basalts (OIB) are from Sun and McDonough (1989). The values for calc-alkaline basalts (CAB) and island arc tholeiites (IAT) are from Stolz et al. (1990), and for back-arc basin basalts (BABB) are from Ewart et al. (1994).

The intermediate lavas and *Acch3a* also have Fe₂O, MgO and CaO decreasing when SiO₂ increases, but with more gentle slopes compared to the mafic samples. Note that for MgO, the least evolved intermediate samples have higher values than the most evolved mafic samples. Al₂O₃ is flat in the intermediate samples, whereas TiO₂ decreases. *Acch3b* rocks have the highest silica contents, and have the smallest range in TiO₂, Fe₂O₃, MgO, and CaO. However, Al₂O₃ is used up in these rocks.

Classification and magmatic affinity

Both Winchester and Floyd (1977) classification diagrams are used here, rather than the total alkali-silica (TAS) diagram, to classify the Colomb-Chaboullié volcanic rocks. Although the geochemical samples used for this study are relatively fresh (Fig. 3.5a), the alkali elements used in the TAS diagram are very mobile and therefore not ideal for rocks of Archean age.

All the mafic samples are dominantly sub-alkaline basalts (Fig. 3.6a) and plot at the boundary between the sub-alkaline basalt and andesite/basalt fields of figure 3.6b. However, some of the *Acch1c* samples have higher silica contents and therefore plot in the andesite/basaltic andesite field of figure 3.6a. This might be due to silica mobility. *Acch1c* has a slightly elevated average Zr/TiO₂ ratio compared with the other two major basalt groups (Table 3.2), and is therefore slightly offset from the other mafic samples (Fig. 3.6b). *Acch1d* and *Acch1e* plot with the majority of the mafic samples as sub-alkaline basalts. In figure 3.6b, two *Acch1e* samples plot with *Acch2*, *Acch2a*, and *Acch3a*, a result of higher Nb/Y ratios.

Acch2 and *Acch2a* dominantly plot in the andesite/basaltic andesite field of figure 3.6a and in the andesite field of figure 3.6b. These samples also show a variation in their SiO₂ content, but are densely clustered together when Zr/TiO₂ is compared with Nb/Y. The Nb/Y ratios for these samples are higher than those of the mafic samples, and therefore *Acch2* and *Acch2a* plot as a separate group to the mafic rocks (Fig. 3.6b).

The *Acch3a* unit (intermediate volcaniclastic samples) plots with *Acch2* and *Acch2a* (intermediate lavas) on the Winchester and Floyd (1977) diagrams. This therefore shows that *Acch3a* rocks are more intermediate in composition compared to *Acch3b*. The latter represent felsic volcaniclastic rocks which have high silica contents (66.3 to 80.5 wt. %) (Fig. 3.6a), with seven samples plotting in the rhyodacite/dacite field and five samples plotting in the rhyolite field. In figure 3.6b, these samples solely plot in the rhyodacite/dacite to andesite fields due to relatively low Zr, as is typical of calc-alkaline felsic rocks.

On the alkali-total iron-magnesium (AFM) diagram (Fig. 3.6c), the basaltic samples dominantly plot in the tholeiitic field. This tholeiitic affinity is also observed on the Ross and Bédard (2009) magmatic affinity diagram for *Acch1a* and *Acch1d* (Fig. 3.6d). This particular diagram allows for the discrimination of rocks with a transitional magmatic affinity. *Acch1b*, *Acch1c*, and *Acch1e* are transitional in affinity. All the intermediate lavas (*Acch2* and *Acch2a*) and intermediate to felsic volcaniclastic rocks (*Acch3a* and *Acch3b*) are calc-alkaline. On a TiO₂ vs Zr diagram (Fig. 3.6e), most mafic samples from the Colomb-Chaboullié belt follow the positive slope of the tholeiitic trend, as titanium is initially incompatible in these magmas (Barrett and MacLean, 1999). However, *Acch1c* is characterised by low TiO₂ concentrations (Fig. 3.6e, Table 3.1), and as a result cluster at the base of the tholeiitic trend. If the intermediate to felsic samples were related to the mafic samples by simple fractionation, they would be expected to plot along the same trend, ending in very low Ti but very high Zr values typical of tholeiitic rhyolites (e.g., rocks from the Matagami or Chibougamau areas, MacLean and Barrett, 1993; Debreil, 2014; Boulerice, 2016). Instead, they follow a separate trend which parallels that of modern calc-alkaline arc rocks. Note however that *Acch3b* samples have a similar range of Zr values to the intermediate samples but consistently lower Ti, which suggests that *Acch3b* is not simply related by fractionation to the intermediate magmas.

Trace elements in mafic lavas (*Acch1a* to *Acch1e*)

On the extended trace element diagrams, *Acch1a* has a relatively flat profile (Figs. 3.7a and e). The profiles are slightly more inclined for *Acch1b* and *Acch1c*. *Acch1b* demonstrates a slightly negative heavy rare earth element (HREE) slope whereas *Acch1c* shows a flat to slightly positive HREE slope (Figs. 3.7b and c). Small negative Nb-Ta anomalies occur for these two basalt groups. In terms of profiles, *Acch1d* is most similar to *Acch1a*, whereas *Acch1e* is most similar to *Acch1b* (Fig. 3.7d). *Acch1a* and the two minor basalt groups straddle the MORB and volcanic arc (IAB or VAB) fields on the Agrawal et al. (2008) and Wood (1980) diagrams (Fig. 3.8a and b). *Acch1b* and *Acch1c* solely plot in the IAB and VAB fields. On the Pearce (2008) diagram, *Acch1a* plots at, or just above the N-MORB pole (Fig. 3.8c). *Acch1b*, *Acch1c*, and *Acch1e* have higher Th/Yb ratios and are situated above the MORB-OIB array.

Andesite trace elements (*Acch2* and *Acch2a*)

Extended trace element diagrams for *Acch2* and *Acch2a* show notable Nb-Ta and Ti negative anomalies (Figs. 3.9a and b), which are much more evident than in the basalt samples. *Acch2* and *Acch2a* both show light rare earth element (LREE) enrichment. The geochemical similarity between these two intermediate lava units is demonstrated by their comparable trace element profiles.

These andesites plot in the volcanic arc fields on tectonic discrimination diagrams (Figs. 3.8a and b). On the Pearce (2008) diagram, the andesites plot well outside the MORB-OIB array, near the Archean crustal pole and possible contaminants from the Opatica Subprovince (Fig. 3.8c).

Intermediate to felsic volcaniclastic rocks (*Acch3a* and *Acch3b*)

The intermediate volcaniclastic rocks (*Acch3a*) are chemically similar to the andesite lavas on all diagrams (Figs. 3.6a to e, Figs. 3.8a to c, and Fig. 3.9c), suggesting that these units are related.

A total of 12 felsic volcaniclastic rocks from the Colomb-Chaboullié greenstone belt (*Acch3b*) were analysed and positioned on the Hart et al. (2004) felsic volcanic rock classification diagram (Fig. 3.8d). These samples dominantly plot at the boundary between the FI and FII domains (Hart et al., 2004). The extended multi-element diagram (Fig. 3.9d) once again shows the distinctive Nb-Ta and Ti negative anomalies.

3.4.3 Mineralisation

Five showings are present in the basalt lavas, one in the volcaniclastic unit, and one in a sedimentary sequence (see Fig. 3.2). Sulphide mineralisation occurs as disseminated sulphides, veins, and massive to semi-massive occurrences. In the pillowed basalts, the sulphides are present within the inter-pillow material (Fig. 3.10a), often associated with chlorite and garnet alteration in the pillow margins (Fig. 3.10b). In the massive basalt flows, the sulphides are controlled by fractures, forming stockwork-style veins (Fig. 3.10c). Three massive to semi-massive bodies are identified in this greenstone belt, including the Lac Marcaut lens (Fig. 3.10d). These contain rounded, silica-rich clasts containing minor pyrite and chalcopyrite, in a pyrrhotite-rich matrix (Figs. 3.10e and f). These clasts may also comprise small chlorite clasts and irregular felsic fragments. The main Au-Ag-Cu showings of the Colomb-Chaboullié belt are situated close to lithological contacts, whether contacts are between lithological units (e.g., mafic-felsic) or internal contacts between basaltic subunits (Fig. 3.11).

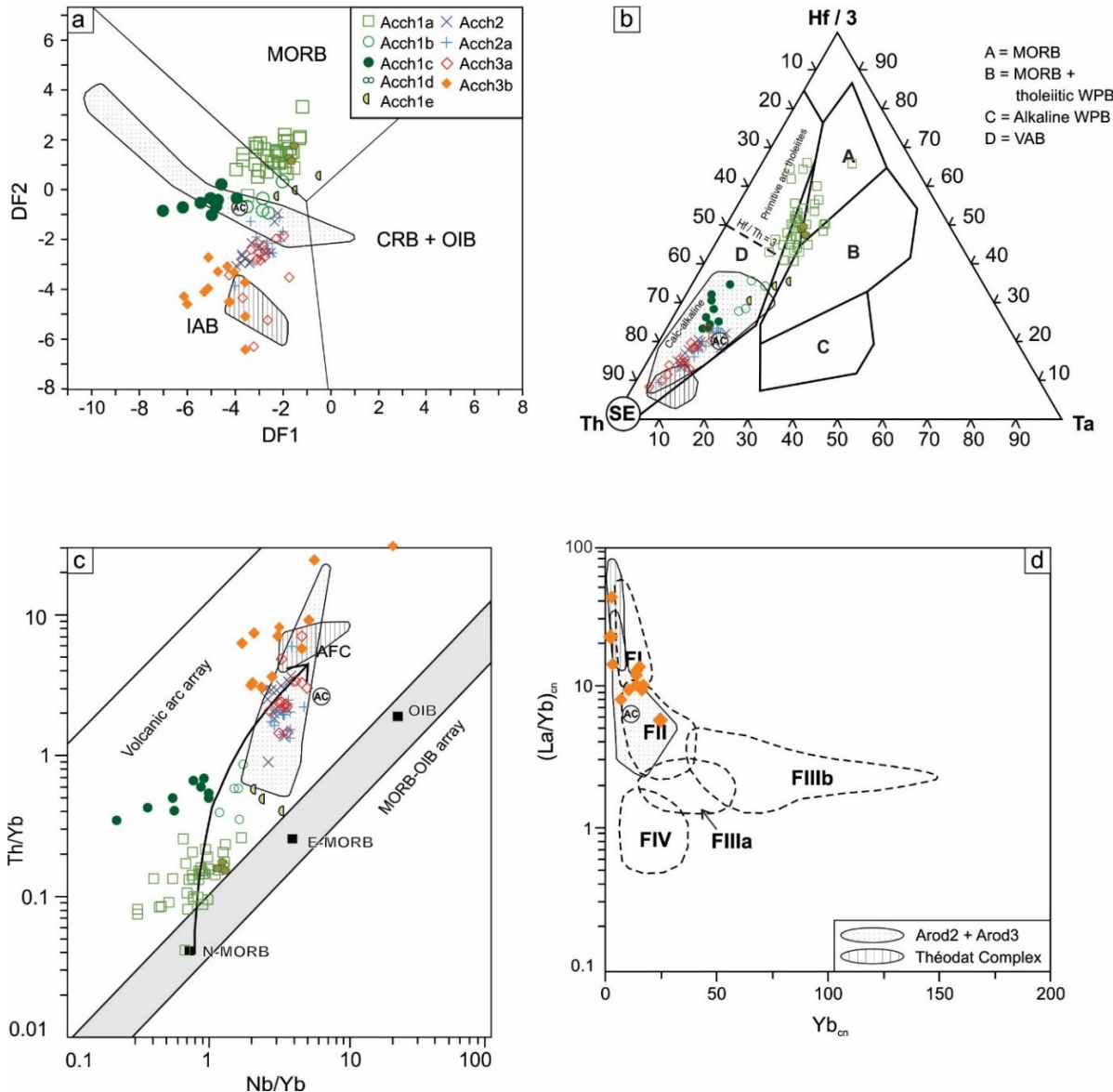


Fig. 3.8 Tectonic discrimination and rhyolite fertility diagrams. a) DF1-DF2 diagram of Agrawal et al. (2008). $DF1 = 0.3518 \log_e(La/Th) + 0.6013 \log_e(Sm/Th) - 1.3450 \log_e(Yb/Th) + 2.1056 \log_e(Nb/Th) - 5.4763$; $DF2 = -0.3050 \log_e(La/Th) - 1.1801 \log_e(Sm/Th) + 1.6189 \log_e(Yb/Th) + 1.2260 \log_e(Nb/Th) - 0.9944$. IAB: island arc basalts; MORB: mid-ocean ridge basalts; CRB: continental rift basalts; OIB: ocean island basalts. b) Th-Hf-Ta ternary diagram from Wood (1980). The Archean crust (AC); after Rudnick and Fountain (1995) and subduction enrichment (SE) values are indicated. N-MORB: normal mid-ocean ridge basalts; E-MORB: enriched mid-ocean ridge basalts; WPB: within-plate basalts, VAB: volcanic arc basalts. c) Th/Yb versus Nb/Yb diagram from Pearce (2008). AFC: assimilation-fractional crystallisation. d) $(La/Yb)_{cn}$ versus Yb_{cn} after Hart et al. (2004). F1: alkali dacites and rhyodacites; FII: calc-alkaline rhyodacites and rhyolites; FII: tholeiitic rhyolites; FIV: depleted rhyolites and high-silica rhyolites. Abbreviations: Arod2 + Arod3: subunits of the Lac Rodayer pluton.

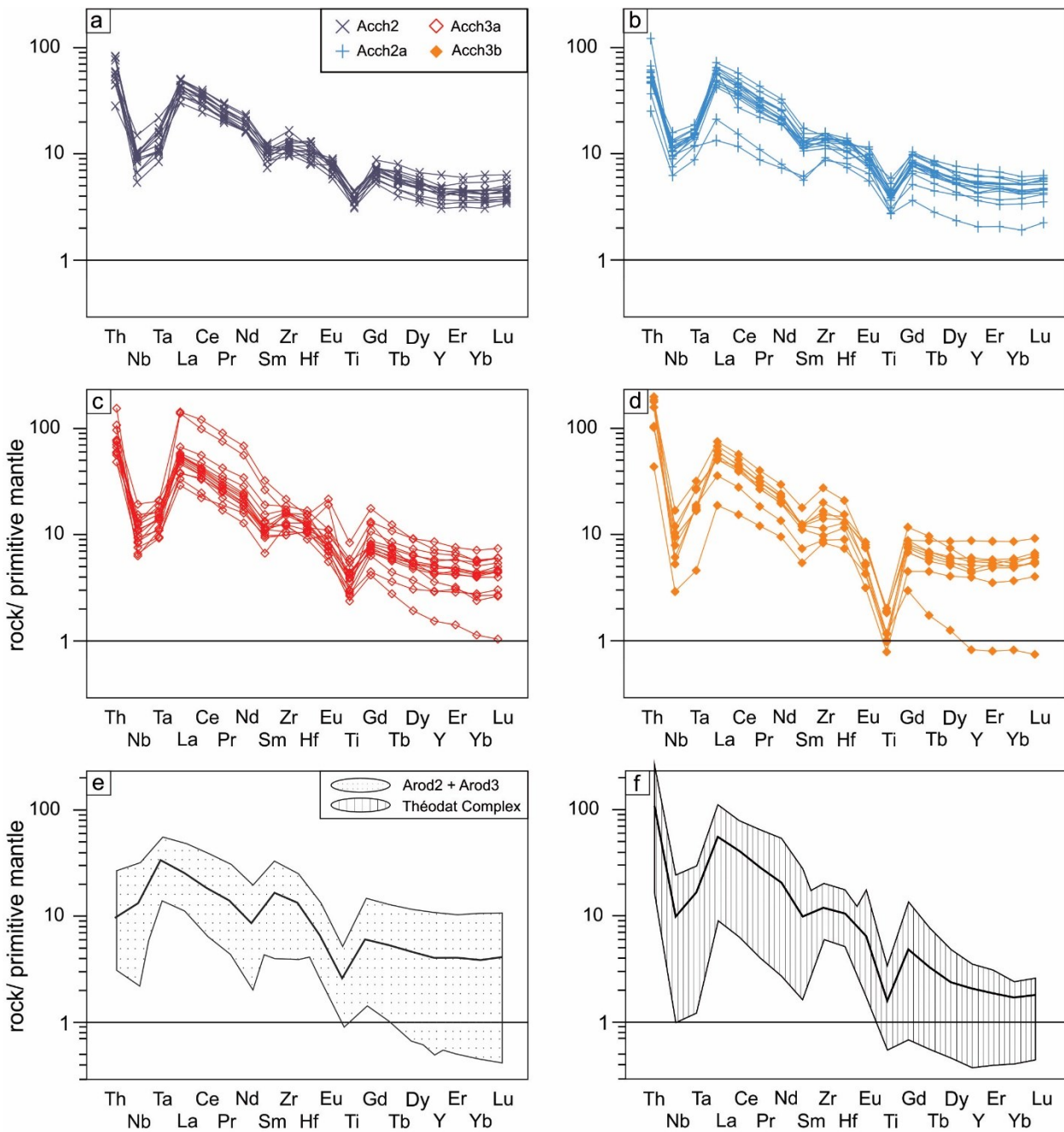


Fig. 3.9 Extended multi-element diagrams for the intermediate extrusive lavas, and intermediate to felsic volcaniclastic rocks of the Colomb-Chaboullié belt, as well as possible contaminants from the Opatica Subprovince. a) Acch2, b) Acch2a, c) Acch3a, d) Acch3b, e) Arod2 + Arod3, and f) Théodat Complex. Solid lines represent averages in (e)-(f). Primitive mantle normalisation values are from Sun and McDonough (1989). Abbreviations; Arod2 + Arod3: subunits of the Lac Rodayer pluton.

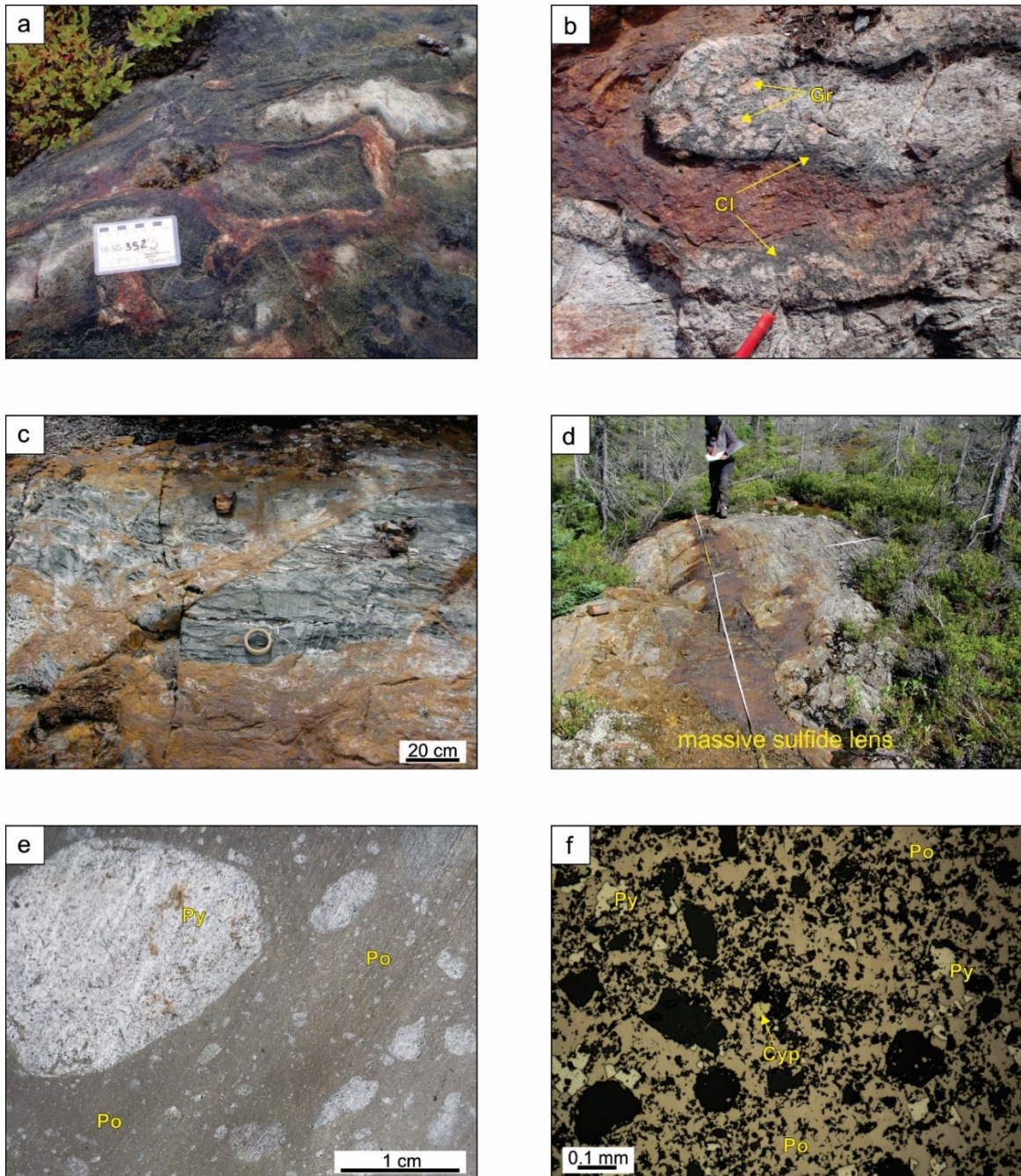


Fig. 3.10 Mineralisation of the Colomb-Chaboullié greenstone belt. **a)** Deformed pillow-shaped basalt with disseminated sulphides in the inter-pillow material, **b)** synvolcanic alteration of chlorite and garnet in the pillow margins, **c)** sulphide veins in a massive basalt flow, **d)** the Lac Marcaut sulphide lens containing gold values, **e)** rounded siliceous fragments containing pyrite, embedded in a pyrrhotite-rich matrix, and **f)** reflected light image of a massive sulphide sample from the Lac Marcaut showing. Abbreviations: Cl = chlorite, Cyp = chalcopyrite, Gr = garnet, Po = pyrrhotite, Py = pyrite.

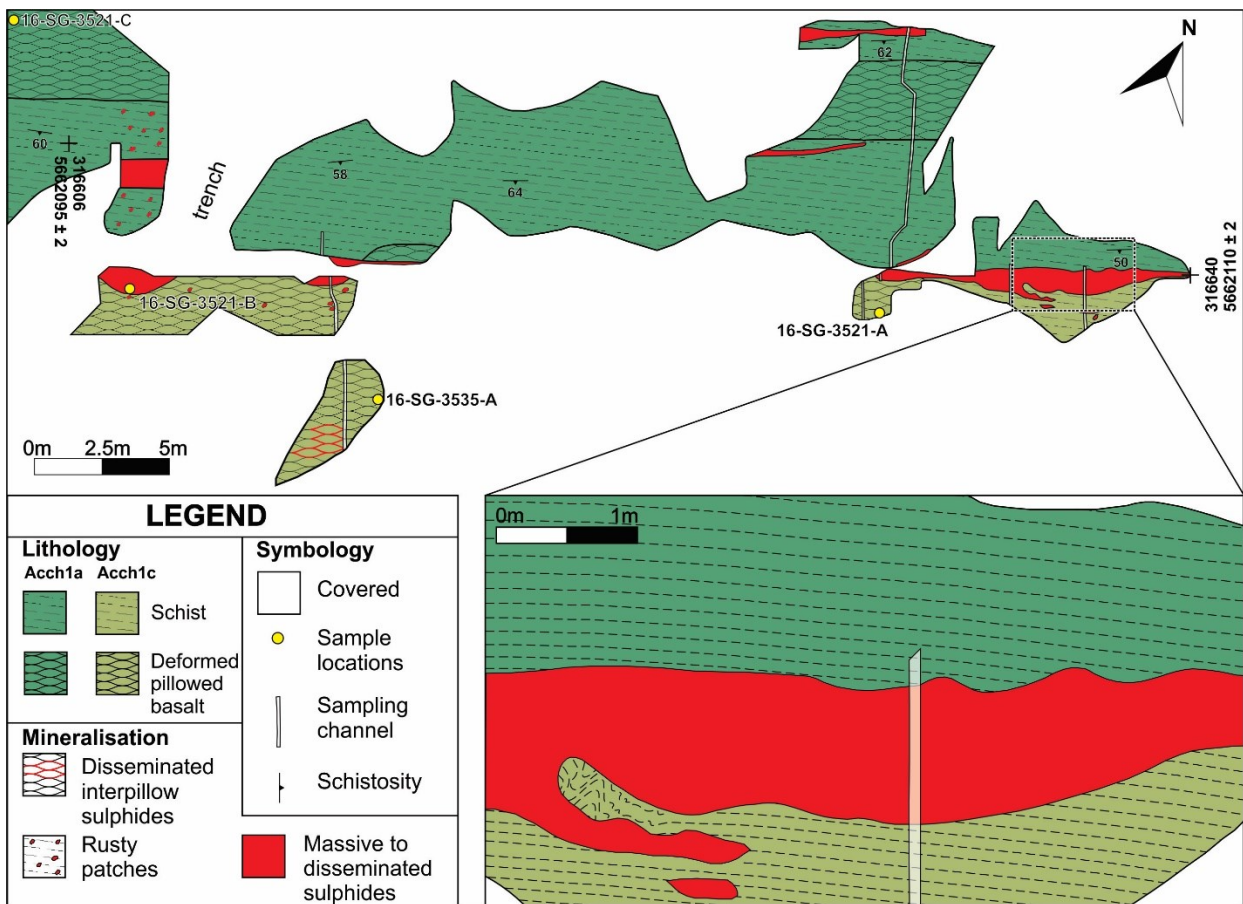


Fig. 3.11 Detailed map of the Lac Marcaut outcrop.

The Lac Marcaut outcrop was mapped in more detail as a typical example (Fig. 3.11). The massive sulphide lens, which runs along the length of the outcrop, was used as the baseline for the map as this is the closest feature to S_0 . This outcrop consists mostly of two types of basalts, *Acch1a* and *Acch1c*, with the sulphide lens at the contact. *Acch1a* is composed of both pillowed and schistose units. Sulphide occurrences are located in the schistose unit as rusty patches and thin sulphide veins. *Acch1c* is dominantly composed of deformed pillows. Sulphide patches are also present in this facies, along with disseminated sulphides in the inter-pillow material. The main sulphide lens has a maximum thickness of 1.4 m and can be followed laterally for 80 m along an outcrop ridge (Thorsen et al., 1993). Grab samples within this lens yield up to 27 g/t gold (Thorsen et

al., 1993). The schistosity of the host basalt lies at a slight angle relative to the sulphide lens (Fig. 3.11, inset).

3.5 Discussion

3.5.1 Mode of emplacement for volcanic rocks

The presence of pillowd basalt and pillowd andesite lava flows, along with hyaloclastites, indicates that the volcanic rocks of the Colomb-Chaboullié greenstone belt were deposited in a submarine setting. As the intermediate to felsic volcaniclastic rocks form lenses within the basalt flows, these were also most likely formed in the same submarine environment. The detailed mode of emplacement of the volcaniclastic rocks has not been investigated given the small number of outcrops available, the relatively high metamorphic grade, and penetrative tectonic deformation.

3.5.2 Mineralisation

We interpret the Au-Ag-Cu sulphide showings of the belt as synvolcanic (VMS-style) for the following reasons:

- sulphide lenses occur at or near geological contacts;
- chlorite alteration (some of which has recrystallised as garnet) is common;
- within pillow lavas, sulphides replace the inter-pillow material, indicating that primary porosity was still available when hydrothermal fluid circulation occurred;
- in the massive basalt facies, disseminated sulphides infill fractures forming a stockwork with chlorite and garnet, which is also a typical feature of volcanogenic mineralisation (Galley et al., 2007).

At the Lac Marcaut showing, the massive sulphide lens sits at a contact between *Acch1a* and *Acch1c* mafic lavas. The same contact may be prospective elsewhere in the Colomb-Chaboullié belt.

3.5.3 Geochemical groups in the Colomb-Chaboullié greenstone belt and map refinement

The geochemical results presented have been used to refine the 1:50 000 scale geological map for the Colomb-Chaboullié greenstone belt (Fig. 3.2). The basalt flows which dominate this greenstone belt were undifferentiated and given the scale of the geological map, they will have to remain so until the scale of mapping is eventually increased. However, the geochemical groupings established here, and potential stratigraphic younging indicators to be obtained in future work, will allow a full chemo-stratigraphy of the volcanic rocks to be established.

Geochemistry allows the basalts to be sub-divided into three major groups (*Acch1a*, *Acch1b*, and *Acch1c*) and two minor groups (*Acch1d* and *Acch1e*) (Table 3.1 and 3.2, Figs. 3.5 to 3.7). These groupings are based on their extended multi-element profiles, which were confirmed using major oxide concentrations, magmatic affinity, incompatible elements such as Th, and elemental ratios such as Zr/TiO₂ and Th/Yb. *Acch1a* is the dominant basalt unit and samples are distributed throughout the Colomb-Chaboullié greenstone belt (Fig. 3.2). *Acch1b* occurs in the western sector of the map. *Acch1c* occurrences are located in the central portion of the greenstone belt, dominantly to the south of *Acch1a* samples. *Acch1d* is defined by three samples which all occur in the far east of the map within a 1.6 km-long band, in a well-developed pillow unit. Although *Acch1d* and *Acch1e* are both defined by only three samples, they have been included here because they are chemically distinct from the rest of the mafic samples.

The intermediate lava flow units (*Acch2* and *Acch2a*), distinguished from one another based on phenocryst populations (section 3.4.1), are geochemically similar to each other. Based on the present geochemical dataset, a number of small, isolated *Acch2a* units have been identified in the mafic lava flows. These small intermediate lava lenses are located adjacent to *Acch3* lenses, or close to a contact with the felsic plutonic rocks of the Opatica Subprovince. *Acch3* has been divided here into *Acch3a* and *Acch3b* based on the differing geochemistry (intermediate versus felsic).

3.5.4 Petrology

The volcanic and volcaniclastic rocks of the Colomb-Chaboullié greenstone belt have compositions ranging from basalts to rhyolites (Figs. 3.6a and b). The basalts are tholeiitic to transitional in magmatic affinity whereas all intermediate and felsic rocks are calc-alkaline (Figs. 3.6c to e), therefore we discuss these rocks separately.

Basalts

The tholeiitic to transitional basaltic rocks of the Colomb-Chaboullié belt have high iron concentrations, with a maximum of 18.2 wt. % Fe_2O_3 (Fig. 3.5d). Overall, *Acch1a* samples show high Al_2O_3 , Fe_2O_3 and relatively high MgO concentrations (Figs. 3.5b, d, and e). Trace elements are somewhat similar to those of modern N-MORB, although the Th values are higher than those of N-MORB, the LREE have a flatter pattern and some samples have a negative Ti anomaly (Fig. 3.7a). Within tectonic discrimination diagrams, *Acch1a* samples dominantly plot in the MORB fields (Figs. 3.8a and b). This suggests that this basaltic unit comes from a mantle source similar to that of modern N-MORB. *Acch1b* and *Acch1c* have higher Th contents than *Acch1a* (Figs. 3.7b and c), so plot in the arc fields on the tectonic discrimination diagrams (Figs. 3.8a and b). *Acch1b* and *Acch1c* also plot further away from the MORB-OIB array, with higher Th/Yb ratios (Fig. 3.8c). On the Pearce (2008) diagram, the *Acch1a* through to *Acch1b* and *Acch1c* progression appears to form an assimilation-fractional crystallisation (AFC) trend that also extends to the andesites. Although it is tempting to assign all of the Colomb-Chaboullié volcanic rocks, from mafic through to felsic, to this AFC trend, the basaltic rocks are not a product of AFC. *Acch1c* is the most primitive basaltic unit based on low Zr and low TiO_2 (Fig. 3.6e). Compared to *Acch1a*, *Acch1b* and *Acch1c* also have higher average MgO contents (Table 3.1). Yet *Acch1b* and *Acch1c* show a higher degree of crustal contamination based on trace elements such as Th (e.g., 3.8b), and position on the Pearce (2008) plot (Fig. 3.8c). This suggests that rather than AFC producing the basalts of the Colomb-Chaboullié, fractionation and crustal contamination occurred mostly independently. We propose that crystal fractionation explains most of the major element

variations in the basalts (hence the tholeiitic trend on the TiO_2 -Zr diagram) while a negligible to moderate amount of crustal contamination (Tomlinson and Condie, 2001), largely independent of crystal fractionation, would explain most of the trace elements trends. Perhaps the basalts only experienced crustal contamination during ascent, with *Acch1b* and *Acch1c* experiencing the highest degree of contamination of the basalts.

The tectonic discrimination diagrams used in this study (Fig. 3.8) were designed to distinguish different Phanerozoic tectonic processes, and Archean tectonics may or may not have looked like Phanerozoic plate tectonics. In terms of modern tectonic environments, the Colomb-Chaboullié basalts could have formed in environments ranging from mid-ocean ridge to back-arc basins. Some basalts even look like arc tholeiites (Fig. 3.7), so a rifted arc could be considered. However, this study focuses on the petrogenesis of the Colomb-Chaboullié volcanic rocks and we therefore do not wish to speculate on the tectonic style during the Archean.

Andesitic lavas and intermediate volcaniclastic rocks

Beyond the more evolved compositions, the andesitic lavas (*Acch2* and *Acch2a*) and intermediate to felsic volcaniclastic rocks (*Acch3a* and *Acch3b*) are chemically very different from the basalts. These differences include their higher Nb/Y ratios (Fig. 6b), their calc-alkaline tendency on the TiO_2 versus Zr diagram (Fig. 6e), and their “volcanic arc” signature illustrated by their pronounced Nb-Ta and Ti negative anomalies (Figs. 9a to d). Harker diagrams show that the most SiO_2 -rich basalts have lower MgO concentrations than the most SiO_2 -poor andesites, and therefore have separate trends (Fig. 5e) and a different evolutionary history. The intermediate lavas and intermediate to felsic volcaniclastic rocks are intercalated with the basalt; both the basalts and andesite are lavas; and some of the volcaniclastic rocks are coarse, suggesting they are relatively proximal, and derived from a local vent. This means that we need to generate all of these rocks in a limited geographic area, and assigning a different tectonic environment to the basalts versus the andesites and more evolved rocks (e.g., arc versus ridge or back-arc) is not a good solution. In terms of modern tectonics, a back-arc basin would be a good

place to have a variable subduction influence, but that does not explain the Harker diagrams (e.g., SiO₂-poor andesites have higher MgO than SiO₂-rich basalts).

There is ample evidence for crustal contamination of the intermediate and felsic rocks of the Colomb-Chaboullié greenstone belt. This contamination trend is seen across all geochemical diagrams used in this study. For the intermediate rocks (lavas and volcaniclastic), the trace *and* major element variations we see in the database can be mostly explained by increasing AFC, hence the calc-alkaline trend (Figs. 3.5, 3.6e, 3.8c). These intermediate magmas might have spent a much longer time in the crust than the basalts, and may have been erupted due to the injection of fresh mafic magma into a pre-existing magma chamber (Fig. 3.12). This mixing of a mafic melt with more evolved melts was observed during the 2010 Eyjafjallajökull eruption in Iceland, which produced mafic, intermediate, and silicic compositions over only a few months (Sigmarsson et al., 2011; Tawasewicz et al., 2012). This model works regardless of the tectonic style during the Archean.

The Colomb-Chaboullié intermediate rocks often extend beyond the Archean crustal pole (Figs. 3.8a to c), so the andesites could have been contaminated by a composition richer in Th than the average Archean crust value. Both the Lac Rodayer pluton and the Théodat Complex, located south of the greenstone belt in the Opatica Subprovince, can be suitable contaminants from a geochemical point of view (Figs. 3.5, 3.6, 3.8, 3.9).

Felsic volcaniclastic rocks

In terms of major elements, some *Acch3b* samples plot outside the Lac Rodayer and Théodat Complex contamination fields and have higher SiO₂ concentrations. Two of the felsic samples which plot towards the sericite pole on the alteration box plot (Fig. 3.5a) show high SiO₂ abundances in the Harker diagrams, suggesting that silicification and sericitization may play a part in the evolution of these felsic rocks. These two samples also have low Na concentrations (Fig. 3.5h), which is typical of high-temperature VMS-related alteration.

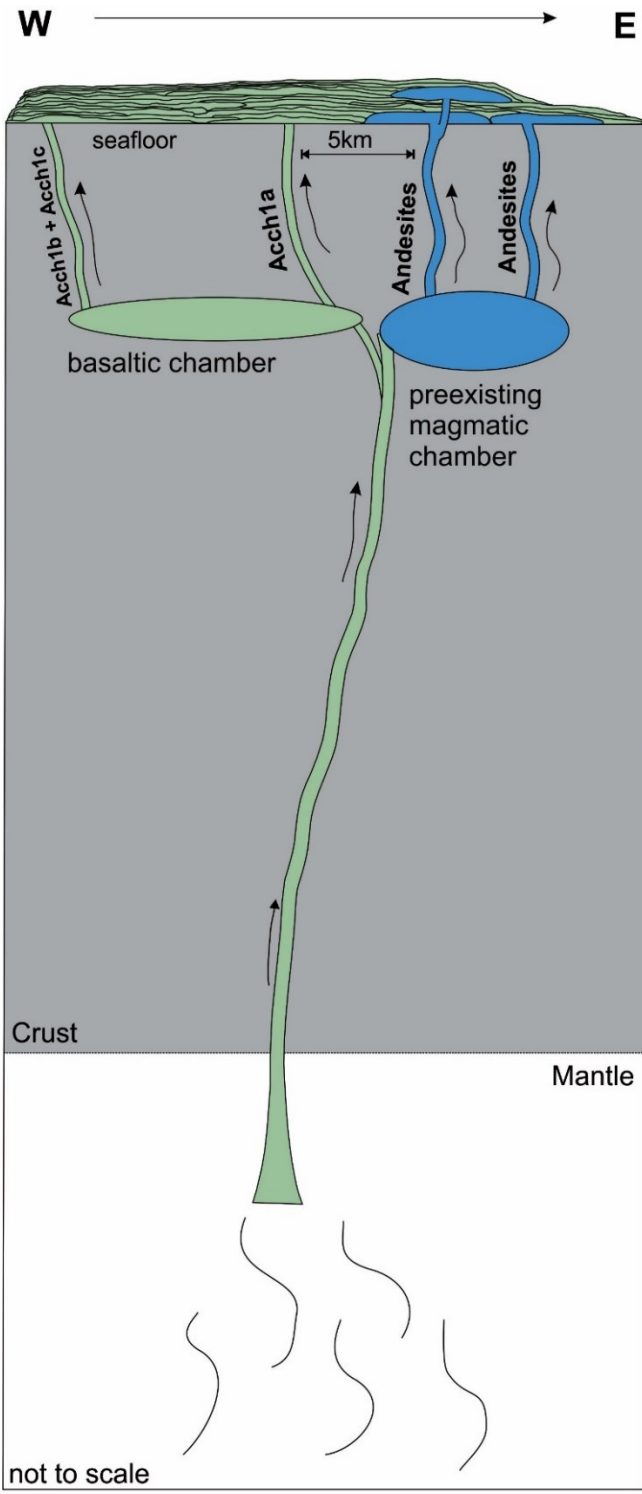
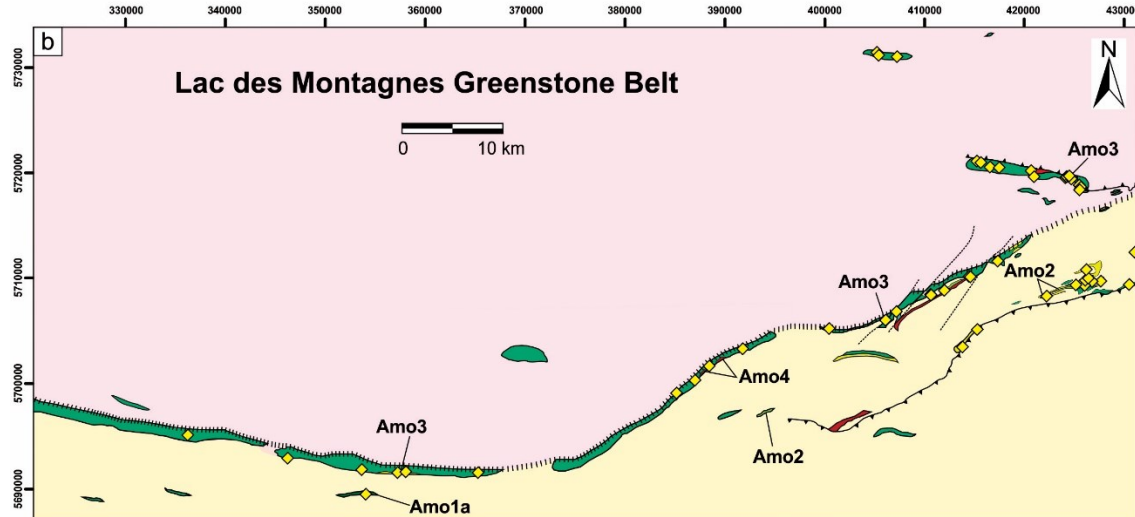
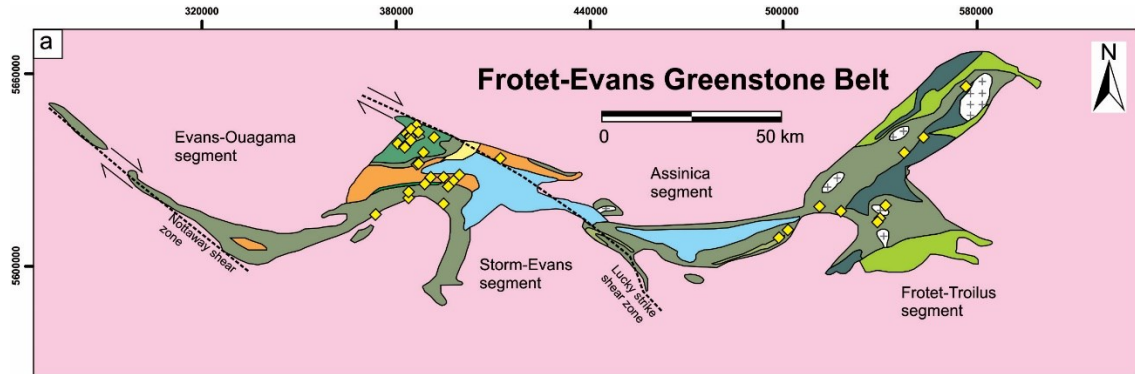


Fig. 3.12 Schematic diagram illustrating the emplacement of the mafic and intermediate lava flows of the Colomb-Chaboullié belt. Mixing in a pre-existing magma chamber may produce intermediate compositions. Inspired by Tawasewicz et al. (2012).

Acch3b are located at the boundary between the F1 and FII domains (Hart et al., 2004; Fig. 3.8d), which suggests that these rocks originated from a deep source. However, as all the volcanic rocks must have been produced in a similar environment during a relatively short period of time, a deep source for these samples would not be ideal for the formation of the hydrothermal cells which drive VMS generation. Alternatively, the high pressure signature may be explained by the partial melting of a garnet ± amphibole-rich metabasaltic source which would produce felsic magmas depleted in HREE and Y. This high pressure signature may be inherited from magmatic processes that are much older than the Colomb-Chaboullié greenstone belt.

3.6 Comparison with the Frotet-Evans greenstone belt: geology, geochemistry and geochronology

In this section we compare the Colomb-Chaboullié belt with the Frotet-Evans greenstone belt of the Opatica Subprovince. The Frotet-Evans belt is much larger than the Colomb-Chaboullié belt and is divided into four lithotectonic segments: the Evans-Ouagama, Storm-Evans, Assinica, and Frotet-Troilus segments (Fig. 3.13) (Boily, 1999). These segments are composed of volcanic rocks of varied compositions, many of which have no equivalent in the Colomb-Chaboullié belt. The two segments at the heart of the Frotet-Evans (Storm-Evans and Assinica) belt are dominated by volcano-sedimentary assemblages, whereas the two segments located at the eastern and western extremities are principally volcanic (Evans-Ouagama and Frotet-Troilus). In detail, the western Evans-Ouagama segment is made up of the Rabbit Formation, dominantly comprising massive to pillow basalt flows with minor gabbro-pyroxenite sills (Boily, 2000). Iron formation horizons are interstratified with the basalt, along with a small band of intermediate to felsic tuffs and andesite-dacite flows.



Stratigraphic legend		Structural legend
Frotet-Evans Greenstone Belt	Lac des Montagnes Group	<ul style="list-style-type: none"> Strike-slip shear zone Rupert River shear zone Albanal shear zone
Rabbit Fm Tholeiites of boninitic affinity, Mg-tholeiites, ferrotholeiites, transitional tholeiites, calc-alkaline basalts and andesites Storm Fm Calc-alkaline andesite-dacite flows Calc-alkaline andesitic to rhyolitic pyroclastics Calc-alkaline basaltic to andesitic flows. Calc-alkaline andesitic to rhyodacitic pyroclastics Le Gardeur Fm Calc-alkaline basaltic to dacitic flows Broadback Gp Wackes, conglomerates, and mudrocks Assinica Gp Calc-alkaline andesitic to dacitic pyroclastics Frotet-Troilus Segment "Adakite" andesitic to dacitic pyroclastics Mg-tholeiites and ferrotholeiites	Amo4 Iron formation Amo3 Felsic volcanics Amo2 Intermediate volcaniclastics Amo1 Basalt Amo1a Metatexite derived from amphibolite Opatica Subprovince Undifferentiated Opatica Subprovince lithologies Nemiscau Subprovince Undifferentiated Nemiscau Subprovince lithologies La Grande Subprovince Undifferentiated La Grande Subprovince lithologies	<ul style="list-style-type: none"> ◆ Lithogeochemical samples

Fig. 3.13 Simplified geology of the Frotet-Evans and Lac des Montagnes greenstone belts. a) Frotet-Evans belt of the Opatica Subprovince, after Boily and Dion (2002) and b) Lac des Montagnes belt of the Nemiscau Subprovince, after Bandyayera and Daoudene (in preparation) and the SIGEOM database (http://sigeom.mines.gouv.qc.ca/signet/classes/l1108_afchCarteIntr).

The centrally located Storm-Evans segment comprises the Evans Group, which is further divided into the Le Gardeur Formation, the Storm Formation, and the Rabbit Formation (Boily, 2000). The Le Gardeur Formation, located at the base of the Evans Group, is composed of calc-alkaline basalt, basaltic-andesite and andesite flows, with intermediate to felsic tuff beds. The Storm Formation, located at the top of the Evans Group, is composed of numerous lithologies including intermediate to felsic pyroclastic rocks, andesitic to rhyodacitic flows, calc-alkaline andesite flows, and tholeiitic basalts and gabbros. The Rabbit Formation extends into this segment from the Evans-Ouagama segment.

The Assinica segment, located to the east of the Storm Evans segment, contains the Assinica Group. This group is made up of tholeiitic basalts, siliceous Mg-basalts, and ferrotholeiites, intercalated with mafic to felsic tuffs. Felsic lavas are also present, which are interstratified with mafic to felsic tuffs and mudrock units. The Broadback Group, also found in this segment, consists of conglomerates, mudrocks, wackes, and volcanic-derived conglomerates.

The most easterly Frotet-Troilus segment is divided into four distinct volcanic phases (Boily, 1999). The first phase is composed of tholeiitic to ferrotholeiitic basalt and andesite lavas, calc-alkaline basaltic and/or andesitic lavas with some Mg-tholeiites and rare intercalations of intermediate to felsic pyroclastic tuffs. The Frotet-Evans Formation, forming the second phase, is essentially pyroclastic and calc-alkaline. The third phase contains several basaltic lavas, including tholeiites and ferrotholeiites, a siliceous high-Mg basalt suite, and basalts and Mg-andesites of a boninitic affinity. The final phase is made up of tholeiitic basalts, with minor sequences of felsic pyroclastic rocks.

In terms of total volcanic composition, both the Colomb-Chaboullié and Frotet-Evans belts are both mafic-dominated sequences, with rocks of varying magmatic affinities (Table 3.3). Only the geochemically best fit volcanic units from the Frotet-Evans belt will be used in the detailed geochemical comparison. These best fit samples account for 29% of the samples from Boily (1999) and Boily (2000).

3.6.1 Basalts

The chosen mafic samples represent 9% of the Frotet-Evans greenstone belt and are derived from the Rabbit Formation of the Evans-Ouagama and Storm Evans segments, the Assinica Group of the Assinica segment, and depleted Mg-tholeiites (siliceous high-Mg basalt subtype) from phase three of the Frotet-Troilus segment. Both the Rabbit Formation/Assinica Group Mg-tholeiites and the depleted Mg-tholeiites of the Frotet-Troilus Segment show a close correlation to *Acch1a* basalts in terms of trace element profiles (Figs. 3.14a and b).

Although the depleted Mg-tholeiites show a closer resemblance to the trace element profile of *Acch1a*, there is less overlap with *Acch1a* on the classification, affinity, and discrimination diagrams (e.g., Fig. 3.15b), when compared to the Mg-tholeiites of the Rabbit Formation/Assinica Group. Overall, there is not a perfect correlation between the Frotet-Evans best fit mafic samples and those of the Colomb-Chaboullié belt, suggesting that these are not geochemically identical.

3.6.2 Intermediate rocks

The intermediate samples considered here are from the Le Gardeur and Storm formations of the central Storm-Evans segment. The Le Gardeur Formation (calc-alkaline basalts-andesite-dacites) and units from the Storm Formation (*Asm1* and *Asm2*: lavas and tuffs, basalt-rhyodacite and andesite-rhyolite; *Asm3*: calc-alkaline andesites-dacites) are geochemically very similar to the intermediate lavas and intermediate volcaniclastic rocks (*Acch2*, *Acch2a*, and *Acch3a*) of the Colomb-Chaboullié belt, which is evident by their comparable extended trace element profiles (Figs. 3.14c to e), also showing the characteristic Nb-Ta and Ti negative anomalies. In terms of the classification, affinity and discrimination diagrams of figure 3.15, there is very close overlap between these rocks and the intermediate lava and volcaniclastic units of the Colomb-Chaboullié belt.

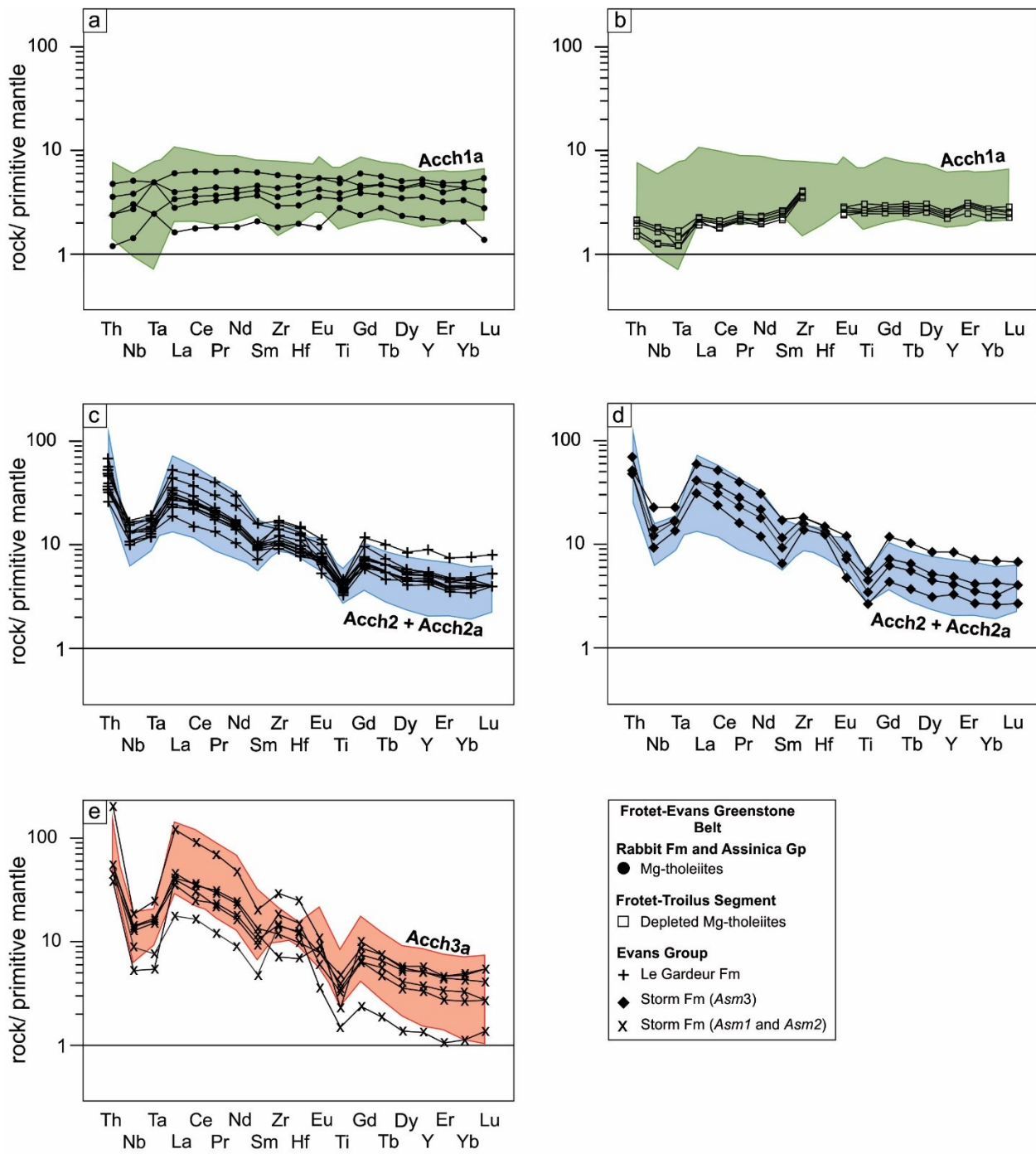


Fig. 3.14 Extended multi-element plots for selected units of the Frotet-Evans greenstone belt. **a)** Rabbit Formation and Assinica Group Mg-tholeiites, **b)** depleted Mg-tholeiites of the Frotet-Troilus segment, **c)** the Le Gardeur Formation, **d)** Asm3 of the Storm Formation, and **e)** Asm1 and Asm2 of the Storm Formation. The Frotet-Evans data is superimposed over the best fit fields of the Colomb-Chaboullié belt.

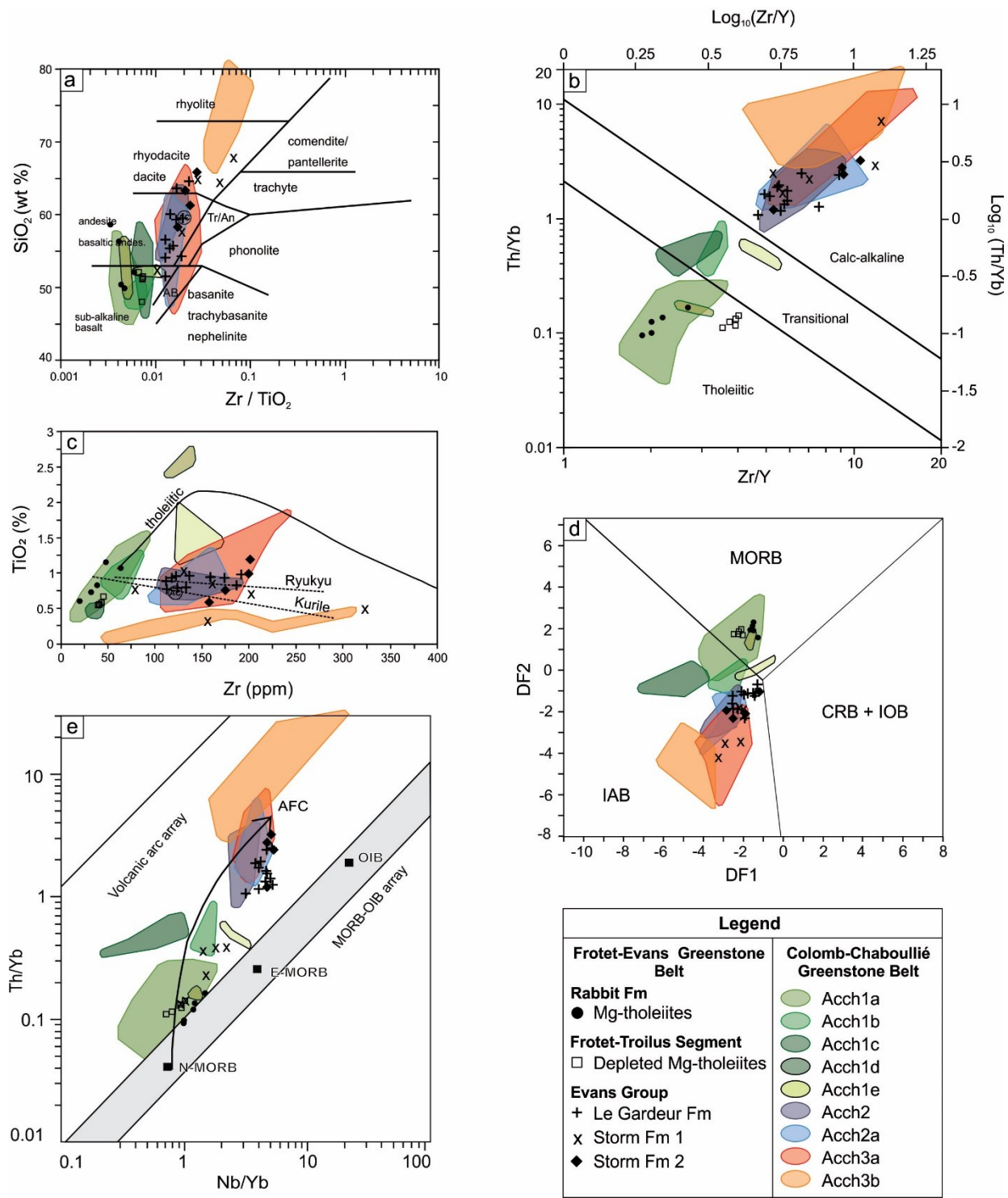


Fig. 3.15 Geochemical plots showing the distribution of the Frotet-Evans greenstone belt samples. a) Winchester and Floyd (1977) classification diagram, b) Ross and Bédard (2009) magmatic affinity diagram, c) TiO_2 vs. Zr plot, d) Agrawal et al. (2008), and e) Pearce (2008) diagrams. See figure 3.8 for abbreviations.

Table 3.3

Total volcanic composition and magmatic affinity comparison of the Colomb-Chaboullié, Frotet-Evans, and Lac des Montagnes greenstone belts.

	Composition (%) ¹					Magmatic affinity (%) ²		
	Bas	Bas and/ And	Dac/ Rhydac	Rhy	Other	Tholeiitic	Transitional	CA
Colomb- Chaboullié (n = 121)	45	38	8	4	5	38	13	49
Frotet-Evans (n = 110)	48	34	13	0	5	35	26	39
Lac des Montagnes (n = 63)	63.5	25	5	5	1.5	49	7	44

1. Composition established on figures 3.6, 3.15, and 3.16 of Winchester and Floyd (1977).

2. Magmatic affinity assessed on figure 3.6, 3.15, and 3.16 of Ross and Bédard (2009).

Abbreviations: bas = basalt, bas and = basaltic andesite, and = andesite, dac = dacite, rhydac = rhyodacite, rhy = rhyolite, CA = calc-alkaline.

3.6.3 Felsic rocks

Unlike the Colomb-Chaboullié belt where rhyolites occur (Table 3.3), rhyolitic rocks are not recognised in the Frotet-Evans belt. However some samples of the Evans group are dacitic-rhyodacitic in composition (Fig. 3.15 a), plotting at the SiO₂-rich end of the Colomb-Chaboullié *Acc3a* field. These roughly equate to the combined rhyolite/dacite-rhyodacite composition of the Colomb-Chaboullié belt. However, there is no overlap of the felsic rocks of the Colomb-Chaboullié belt and those of the Frotet-Evans greenstone belt.

3.6.4 Geochronology

For the Colomb-Chaboullié belt, two U-Pb zircon dates are available, both in the intermediate to felsic volcaniclastic unit (*Acch3*): 2756.8 ± 4.4 Ma and 2760.3 ± 6.4 Ma (David et al., in preparation). In the Frotet-Evans belt, U-Pb ages of 2793 and 2755 Ma have been obtained (cited by Boily and Dion, 2002), although there is some doubt over these ages (C. Dion, pers. commun., 2017). A more recently obtained age for a rhyodacite of the Storm Formation (Evans Group) yielded 2755.5 ± 0.9 Ma (Bandyayera and Sharma, 2001), which overlaps within error with the Colomb-Chaboullié belt.

Although the ages of the Colomb-Chaboullié and Frotet-Evans greenstone belts are similar (i.e., 2756.8 ± 4.4 and 2755.5 ± 0.9 Ma respectively), allowing a viable comparison in terms of age, a large proportion of the Frotet-Evans belt does not correspond with the geochemical constraints of the Colomb-Chaboullié volcanic units. Of the samples that are comparable, there is only partial overlap of the mafic samples. In general, the Evans Group samples have trace element, Zr and Th/Yb patterns and abundances that are similar to *Acch2*, *Acch2a*, and *Acch3a* intermediate rocks, including the characteristic Nb-Ta and Ti negative anomalies. This indicates that these intermediate rocks, at least, were formed during a similar geochemical context to those of the Colomb-Chaboullié belt.

3.7 Comparison with the Lac des Montagnes greenstone belt

The Lac des Montagnes Group is located at the contact zone between the Nemiscau Subprovince to the south and the plutonic Champion Complex of the La Grande Subprovince to the north. It forms a 1.5 km (N-S) by 75 km (E-W) discontinuous greenstone sequence dominantly composed of amphibolised ‘basalts’ (*Amo1*), with thin volcaniclastic (*Amo3*) and iron formation horizons (*Amo4*) interstratified with the ‘basalt’ (Bandyayera and Daoudene, in preparation; Fig. 3.13). New geochemical data from the MERN is used for this comparison.

Amo1 rocks are geochemically diverse and so are divided here into two distinct geochemical groups: tholeiitic basalts and intermediate calc-alkaline rocks (Figs. 3.16a and b). The tholeiitic basalts, here informally labelled *Amo1-TH*, have been further separated on spidergrams in order to match them with the *Acch1a* and *Acch1b* basalts of the Colomb-Chaboullié belt (Figs. 3.17a to c). In terms of the extended trace element profiles, there is no Colomb-Chaboullié *Acch1c* equivalent currently documented in the Lac des Montagnes, as this unit has an overall lower trace element abundance with a more marked Ta-Nb negative anomaly to the tholeiitic basalts of the Lac des Montagnes. The calc-alkaline group, here informally labelled *Amo1-CA*, dominantly consists of andesites/basaltic andesites, with strong Nb-Ta and Ti negative anomalies and similar TiO_2 and Th concentrations to the Colomb-Chaboullié andesites (Figs. 3.16 and 3.17).

The volcaniclastic rocks of the Lac des Montagnes sequence are also geochemically diverse and are separated here informally into mafic, intermediate and felsic groups (*Amo3-M*, *Amo3-I*, *Amo3-F*). There is significant overlap of the intermediate and felsic samples from this region and those of the Colomb-Chaboullié area (Figs. 3.17e and f), however mafic volcaniclastic rocks have yet to be identified in the Colomb-Chaboullié greenstone belt.

A U-Pb zircon sample from the *Amo3* volcaniclastic unit yielded a crystallisation age of 2712.6 ± 5 Ma (David et al., in preparation). Three additional ages have been established using statistical modelling, revealing ages of 2706.6 ± 5.1 Ma, 2755 ± 7.7 Ma, and 2810 ± 7.6 Ma. Based on the error margin, the youngest statistical age corresponds to the U-Pb age (Bandyayera and Daoudene, in preparation).

Overall, the geochemistry of the Lac des Montagnes belt strongly resembles that of the Colomb-Chaboullié belt, suggesting that these volcano-sedimentary sequences were formed by similar magmatic processes, or formed in a similar tectonic environment. However, the significant age difference between these two greenstone belts means that they can't be correlated given the currently available geochronology data.

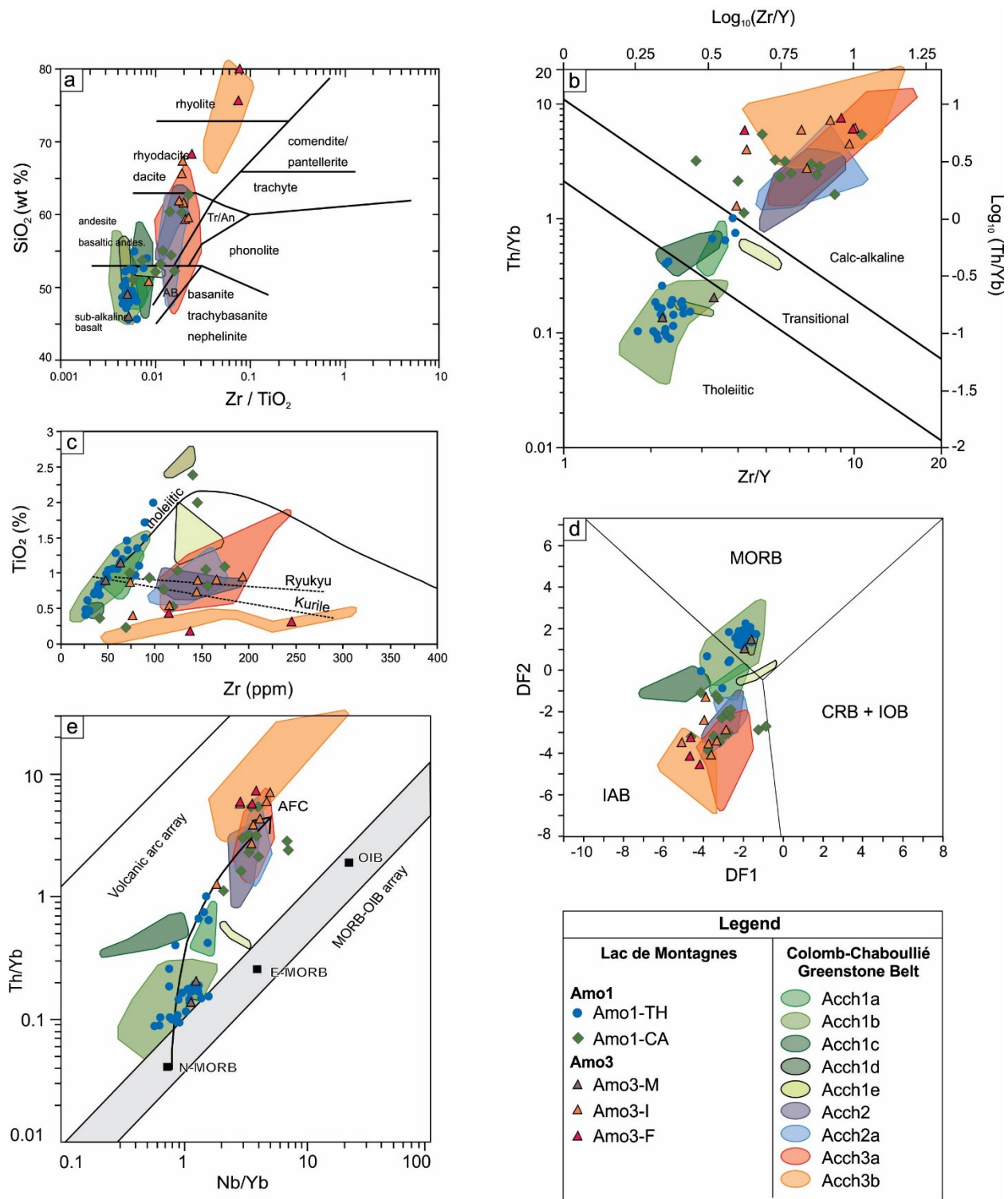


Fig. 3.16 Geochemical plots of the Lac des Montagnes volcanic rocks. a) Winchester and Floyd (1977), b) Ross and Bédard (2009), c) TiO₂ vs. Zr, d) Agrawal et al. (2008), and e) Pearce (2008). See figure 3.8 for abbreviations.

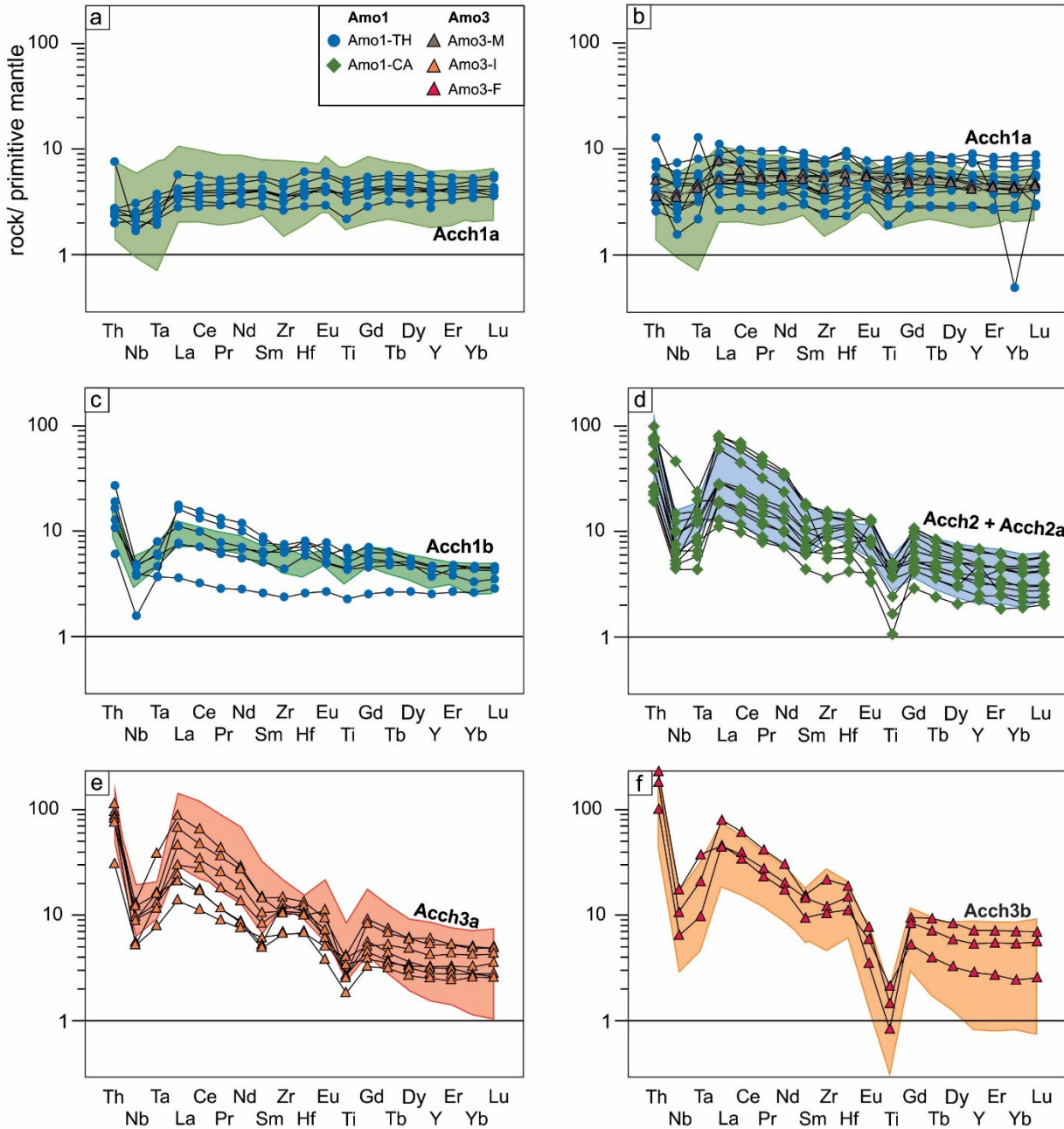


Fig. 3.17 Extended multi element plots for the volcanic units of the Lac des Montagnes belt, superimposed over the Colomb-Chaboulié fields.

Assigning the Colomb-Chaboullié greenstone belt to either the Opatica or the Nemiscau subprovince will require additional geochronology. Particular attention will have to be paid to the issue of inherited zircons to make sure that in all cases, crystallisation ages are being compared.

3.8 Conclusions

In this paper, the stratigraphy, volcanology, and geochemistry of the volcanic units of the Colomb-Chaboullié greenstone belt in the James Bay area of Quebec were refined and interpreted. Pillowed and massive basaltic flows are dominant. They alternate with variably porphyritic, pillowed and non-pillowed andesitic flows as well as intermediate to felsic volcaniclastic rocks. The pillow facies and hyaloclastite material indicates that these rocks were emplaced in a submarine environment. A number of Au-Ag-Cu sulphide showings are known in the belt and were shown to have a synvolcanic origin.

Five types of basalts have been defined geochemically. Given the current map scale and sample density, it was not possible to distinguish map units for these basalt types, but this should become possible when the scale is eventually increased. For example the basalt-basalt contact identified at the Lac Marcaut massive sulphide lens may be favourable to VMS mineralisation elsewhere in the belt.

The geochemical separation of the basalts is also valuable for petrogenetic interpretations, where *Acch1a* are most similar to MORB, whereas *Acch1b* and *Acch1c* show progressively more contaminated geochemical signatures. The major element trends for the basalts are mostly explained by crystal fractionation, not by AFC. In contrast, *Acch2* and *Acch2a* (intermediate lavas), *Acch3a* (intermediate volcaniclastic rocks), and *Acch3b* (felsic volcaniclastic rocks) share geochemical properties, including major elements, with possible contaminants from the Opatica Subprovince. As these intermediate to felsic rocks are interstratified with the basalt flows, we propose that the former were produced via crustal contamination and mixing processes within a pre-

existing magma chamber. The basalts on the other hand had a more direct passage from the mantle to the surface. Our model works regardless of the prevailing tectonic style during the Archean.

The Colomb-Chaboullié volcanic rocks have been compared to those of the Frotet-Evans and Lac des Montagnes greenstone belts. Although the ages of the Colomb-Chaboullié and Frotet-Evans belts are comparable, the Frotet-Evans belt is more geochemically diverse and complex, with limited units showing similar geochemical characteristics to the Colomb-Chaboullié belt. The Lac des Montagnes volcanic units are geochemically analogous to those of the Colomb-Chaboullié, however the significant difference in age means that these two greenstone belts cannot be correlated at present. Yet there is not enough modern U-Pb geochronological data from the three greenstone belts to make any definitive statements about correlations at this stage.

REFERENCES

- Activation Laboratories Ltd (2017) Lithogeochemistry. Retrieved from
<http://www.actlabs.com/page.aspx?menu=74&app=244&cat1=595&tp=2&lk=no>
- Agrawal S, Guevara M, Verma SP (2008) Tectonic discrimination of basic and ultrabasic volcanic rocks through log-transformed ratios of immobile trace elements. International Geology Review 50: 1057-1079
- Almberg LD, Larsen JF, Eichelberger JC, Vogel Ta, Patino LC (2008) Comparison of eruptive and intrusive samples from Unzen Volcano, Japan: Effects of contrasting pressure-temperature-time paths. Journal of Volcanology and Geothermal Research 175: 60-70
- Altigani MAH, Merkle RKW, Dixon RD (2016) Geochemical identification of episodes of gold mineralisation in the Barberton Greenstone Belt, South Africa. Ore Geology Reviews 75: 186-205
- Aoki A, Shuto K, Itaya T (1999) Stratigraphy and K-Ar ages of Tertiary volcanic rocks in the Hamamasu area northwestern Hokkaido, Japan. Journal of the Geological Society of Japan 105: 341-351
- Arndt NT, Lesher CM, Czamanske GK (2005) Mantle-derived magmas and magmatic Ni-Cu-(PGE) deposits. Economic Geology 100th Anniversary Volume: 5-23
- Bandayera D, Sharma KM (2001) Minéralisations en Ni-Cu+ÉPG dans la bande volcano-sédimentaire de Frotet-Evans (SNRC 32K). Ministère des Ressources naturelles, Québec; report MB 2001-06, 74 p.

Bandayera D, Daoudene Y, Bourassa S (2015) Geologie- Region du Lac Nemiscau, Secteur du Lac Rodayer. Ministère des Ressources naturelles, Québec; map CG 2015-05, 1 : 85 000 scale

Bandayera D, Daoudene Y (2017) Geologie de la Region du Lac Rodayer (SNRC 32K13-32K14-32N03 et 32N04-SE). Ministère des Ressources naturelles, Québec; report RG 2017-01, 57 p.

Bandayera D, Daoudene Y (in preparation) Géologie de la région du Lac Nemiscau, secteur ouest de la rivière Rupert (SNRC 32N06, 32N07 et 32N11). Ministère des Ressources naturelles, Québec

Barrett TJ, MacLean WH (1999) Volcanic sequences, lithogeochemistry, and hydrothermal alteration in some bimodal volcanic-associated massive sulfide systems. *In:* Barrie CT, Hannington Md (eds) Volcanic-associated massive sulfide deposits: processes and examples in modern and ancient settings Society of Economic Geologists, Reviews in Economic Geology 8: 101-131

Bédard LP, Ludden JN (1997) Nd-isotope evolution of Archaean plutonic rocks in southeastern Superior Province. Canadian Journal of Earth Sciences 34: 286-298

Bédard JH, Harris LB (2014) Neoarchean disaggregation and reassembly of the Superior craton. Geology 42: 951-954

Bédard JH, Harris LB, Thurston PC (2013) The hunting of the snArc. Precambrian Research 229: 20-48

Benn K, Sawyer EW, Bouchez J-L (1992) Orogen parallel and transverse shearing in the Opatica belt, Quebec: implications for the structure of the Abitibi Subprovince. Canadian Journal of Earth Sciences 29: 2429-2444

Benn K, Moyen JF (2008) The Late Archean Abitibi-Opatica terrane, Superior Province; A modified oceanic plateau. *In:* Condie KC, Pease V (eds) When Did Plate Tectonics Begin on Planet Earth? Geological Society of America, Special Paper 440: 173-197

Bickle M, Nisbet E, Martin A (1994) Archean greenstone belts are not oceanic crust. Journal of Geology 102: 121-137

Boily M (1999) Géochimie et tectonique des volcanites du segment de Frotet-Troïlus et de la bande de la rivière Eastmain. Ministère des Ressources naturelles, Québec; report MB 99-11, 81 p.

Boily M (2000) Géochimie des volcanites des ceintures volcano-sédimentaires de Frotet-Evans (CVFE) et de la Moyenne-Eastmain. Ministère des Ressources naturelles, Québec; report MB 2000-12, 74 p.

Boily M, Dion C (2002) Geochemistry of boninite-type volcanic rocks in the Frotet-Evans greenstone belt, Opatica subprovince, Quebec: implications for the evolution of Archaean greenstone belts. Precambrian Research 115: 349-371

Boulerice A (2016) Volcanology of the Lemoine Member of the Waconichi Formation, Abitibi Subprovince, Chibougamau, Quebec. Unpublished MSc thesis, Institut National de la Recherche Scientifique, Centre Eau Terre Environnement, Québec, 193 p.

Brisson H, Gosselin C, Fallara F, Gaulin R, Dion DJ (1998) Géologie de la région du lac Théodat (SNRC 32K/16). Ministère des Ressources naturelles, Québec; report RG 98-07, 24 p.

Calvert AJ, Ludden JN (1999) Archean continental assembly in the southeastern Superior Province of Canada. Tectonics 18: 412-429

Calvert AJ, Sawyer EW, Davis WJ, Ludden JN (1995) Archean subduction inferred from seismic images of a mantle suture in the Superior Province. *Nature* 375: 670-674

Card KD (1990) A review of the Superior Province of the Canadian Shield, a product of Archean accretion. *Precambrian Research* 48: 99-156

Card KD, Ciesielski A (1986) DNAG #1. Subdivisions of the Superior Province of the Canadian Shield. *Geoscience Canada* 13: 5-13

Caté A, Mercier-Langevin P, Ross P-S, Duff S, Hannington MD, Dubé B, Gagné S (2015) Geology and Au enrichment processes at the Paleoproterozoic Lalor auriferous volcanogenic massive sulphide deposit, Snow Lake Manitoba. *In:* Peter JM, Mercier-Langevin P., ed., Targeted Geoscience Initiative 4: Contributions to the understanding of volcanogenic massive sulphide deposit genesis and exploration methods development: Geological Survey of Canada, Open File 7853: 131-145

Condie KC (1981) Archean greenstone belts. *Developments in Precambrian Geology*, Vol. 3. Elsevier, Amsterdam, 434 p.

Crawford AJ, Falloon TJ, Green DH (1989) Classification, petrogenesis, and tectonic setting of boninites. *In:* Crawford AJ., ed., Boninites and related rocks. Unwin-Hyman, London: 1-49

Davis WJ, Gariépy C, Sawyer EW (1994) Pre-2.8 Ga crust in the Opatica gneiss belt: A potential source of detrital zircons in the Abitibi and Pontiac subprovinces, Superior Province, Canada. *Geology* 22: 1111-1114

Davis WJ, Machado N, Gariépy C, Sawyer EW, Benn K (1995) U-Pb geochronology of the Opatica tonalite-gneiss belt and its relationship to the Abitibi greenstone belt, Superior Province, Quebec. *Canadian Journal of Earth Sciences* 32: 113-127

Debreil JA (2014) Évolution volcanologique et chimico-stratigraphique du district minier de matagami, Sous-province de l’Abitibi, Québec. Unpublished PhD thesis, Institut National de la Recherche Scientifique, Centre Eau Terre Environnement, Québec, 279 p.

Dubé B, Gosselin P, Mercier-Langevin P, Hannington M, Galley A (2007) Gold-rich volcanogenic massive sulphide deposits. *In:* Goodfellow, W.D., ed., Mineral deposits of Canada: A synthesis of major deposit types, district metallogeny, the evolution of geological provinces, and exploration methods: Geological Association of Canada, Mineral Deposits Division, Special Publication 5: 75-94

Eckstrand OP, Hulbert LJ (2007) Magmatic nickel-copper-platinum group element deposits. *In:* Goodfellow, W.D., ed., Mineral deposits of Canada: A synthesis of major deposit types, district metallogeny, the evolution of geological provinces, and exploration methods: Geological Association of Canada, Mineral Deposits Division, Special Publication 5: 205-222

Ernst WG (2017) Earth’s thermal evolution, mantle convection, and Hadean onset of plate tectonics. *Journal of Asian Earth Sciences* 145: 334-348

Ewart A, Bryan WB, Chappell BW, Rudnick RL (1994) Regional geochemistry of the Lau-Tonga arc and backarc systems. *Proceedings of the Ocean Drilling Program, Scientific Results* 135: 385-425

Franklin JM, Lydon JW, Sangster DF (1981) Volcanic-associated sulfide deposits. *Economic Geology* 75th Anniversary Volume: 485-627

Franklin J, Gibson H, Jonasson I, Galley A (2005) Volcanogenic massive sulfide deposits. *Economic Geology* 100th Anniversary Volume: 523-560

Fraser (1993) The Lac Troilus gold-copper deposit, northwestern Quebec: A possible Archean porphyry system. *Economic Geology* 88: 1685-1699

Frolova TI, Plechov PY, Tikhomirov PL, Churakov SV (2001) Melt inclusions in minerals of allivalites of the Kuril-Kamchatka island arc. *Geochemistry International* 39: 336-346

Galley AG (1993) Semi-conformable alteration zones in volcanogenic massive sulphide districts. *Journal of Geochemical Exploration* 48: 175-200

Galley AG, Hannington MD, Jonasson IR (2007) Volcanogenic Massive Sulphide Deposits. In: Goodfellow, W.D., ed., *Mineral deposits of Canada: A synthesis of major deposit types, district metallogeny, the evolution of geological provinces, and exploration methods*: Geological Association of Canada, Mineral Deposits Division, Special Publication No. 5: 141-161

Galloway S, Ross P-S, Bandyayera D, Daoudene Y (2017) The volcanic stratigraphy of the Colomb-Chaboullié greenstone belt and the emplacement context of the volcanogenic massive sulphides, James Bay: preliminary results. Ministère de l'Énergie et des Ressources naturelles, Québec, report MB-2017-10, 25 p.

Galloway S, Ross P-S, Bandyayera D, Daoudene Y (2018) Chimico-stratigraphie volcanique et minéralisation volcanogène de la Ceinture archéenne de Colomb-Chaboullié, Baie James. Ministère de l'Énergie et des Ressources naturelles, Québec, report MB-2018-06, 37 p.

Gariépy CA, Allègre CJ (1985) The lead isotope geochemistry of late kinematic intrusives from the Abitibi greenstone belt and their implications for late Archean crustal evolution. *Geochimica et Cosmochimica Acta* 49: 2371-2384

Gifkins C, Herrmann W, Large R (2005) Altered volcanic rocks; a guide to description and interpretation. Centre for Ore Deposit Research, University of Tasmania, Australia, 275 p.

Goldfarb RJ, Baker T, Dubé B, Groves DI, Hart CJR, Gosselin P (2005) Distribution, character, and genesis of gold deposits in metamorphic terranes. Society of Economic Geologists, Economic Geology 100th Anniversary Volume: 407-450

Goodman S, Williams-Jones AE, Carles P (2005) Structural controls on the Archean Troilus gold-copper deposit, Quebec, Canada. Economic Geology 100: 177-582

Gosselin C (1996) Synthèse géologique de la région de Frotet-Troilus. Ministère des Richesses naturelles, Québec; report ET 96-02, 22 p.

Gosselin P, Dubé B (2005) Gold deposits of the world: Distribution, geological parameters and gold content. Geological Survey of Canada, Open File 4895, 1 CD-ROM

Gross GA (1995) Stratiform iron. In: Eckstrand OR, Sinclair WD, Thorpe RI (eds) Geology of Canadian mineral deposit types, Geological Survey of Canada, Geology of Canada 8: 41-54

Groves DI, Goldfarb RJ, Gebre-Mariam M, Hagemann SG, Robert F (1998) Orogenic gold deposits: A proposed classification in the context of their crustal distribution and relationship to other gold deposit types. Ore Geology Reviews 13: 7-27

Guernina S, Sawyer EW (2003) Large-scale melt-depletion in granulite terranes: an example from the Archean Ashuanipi Subprovince of Quebec. Journal of Metamorphic Geology 21: 181-201

Hamilton WB (1998) Archean magmatism and deformation were not products of plate tectonics. Precambrian Research 91: 143-179

Hannington MD, de Ronde CD, Petersen S (2005) Sea-floor tectonics and submarine hydrothermal systems. Society of Economic Geologists, Economic Geology 100th Anniversary Volume: 111-141

Hart TR, Gibson HL, Lesher CM (2004) Trace element geochemistry and petrogenesis of felsic volcanic rocks associated with volcanogenic massive Cu-Zn-Pb sulfide deposits. Economic Geology 99: 1003-1013

Hocq M (1994) La Province du Supérieur. In: Dubé C (ed) Géologie du Québec. Les publications du Québec: 7-20

Hoffman PF (1988) United plates of America, the birth of a craton: Early Proterozoic assembly and growth of Laurentia. Annual review of earth and planetary sciences 16: 543-603

Huston DL, Relvas JM, Gemmell JB, Drieberg S (2011) The role of granites in volcanic-hosted massive sulphide ore-forming systems: an assessment of magmatic-hydrothermal contributions. Mineralium Deposita 46: 473-507

Kerrich R, Polat A (2006) Archean greenstone-tonalite duality: Thermochemical mantle convection models or plate tectonics in the early Earth global dynamics? Tectonophysics 415: 141-165

Kerr DJ, Gibson HL (1993) A comparison of the Horne volcanogenic massive sulfide deposit and intracauldron deposits of the Mine sequence, Noranda, Quebec. Economic Geology 88: 1419-1442

Kröner A (1981) Precambrian plate tectonics. In: Kröner A (ed) Precambrian plate tectonics. Elsevier, Amsterdam: 57-90

Irvine TN, Baragar WRA (1971) A guide to the chemical classification of common volcanic rocks. Canadian journal of Earth Sciences 8: 523-548

Large R, Gemmel B, Paulick H, Huston L (2001) The alteration box plot: a simple approach to understanding the relationship between alteration mineralogy and lithogeochemistry associated with volcanic-hosted massive sulfide deposits. Economic Geology 96: 957-971

Lacroix S, Sawyer E (1995) An Archean fold-thrust belt in the northwestern Abitibi Greenstone Belt: structural and seismic evidence. Canadian Journal of Earth Sciences 32: 97-112

Laflèche MR, Dupuy C, Bourgault H (1992) Geochemistry and petrogenesis of Archean mafic volcanic rocks of the southern Abitibi belt, Québec. Precambrian Research 57: 207-241

Ludden J, Hubert C, Barnes A, Milkereit B, Sawyer EW (1992) A three dimensional perspective on the evolution of Earth's largest Archaean greenstone belt: results from the Abitibi-Grenville LITHOPROBE project. Lithos 30: 357-372

Lydon (1988) Volcanogenic massive sulphide deposits part 2: Genetic models. Geoscience Canada 15: 43-65

MacLean WH, Barrett TJ (1993) Lithgeochemical techniques using immobile elements. Journal of Geochemical Exploration 48: 109-133

Maier WD, Groves DI (2011) Temporal and spatial controls on the formation of magmatic PGE and Ni-Cu deposits. Mineralium Deposita 46: 841-857

Mercier-Langevin P, Dubé B, Lafrance B, Galley AG, Moorhead J (2007) A group of papers devoted to the LaRonde Penna Au-rich volcanogenic massive sulfide deposit, eastern Blake River Group, Abitibi greenstone belt, Quebec. *Economic Geology* 102: 577-583

Mercier-Langevin P, Gibson HL, Hannington MD, Goutier J, Monecke T, Dubé B, Houlé MG (2014) A special issue on Archean Magmatism, volcanism, and ore deposits: Part 2. Volcanogenic massive sulfide deposits. *Economic Geology* 109: 1-9

Miyoshi M, Hasenaka T, Sano T (2005) Genetic relationship of the compositionally diverse magmas from Aso post-caldera volcanism. *Bulletin of the Volcanological Society of Japan* 50: 269-283

Miyoshi M, Fukuoka T, Sano T, Hasenaka T (2008) Subduction influence of Philippine Sea plate on the mantle beneath northern Kyushu, SW Japan : An examination of boron contents in basaltic rocks. *Journal of Volcanology and Geothermal Research* 171: 73-87

Miyoshi M, Furukawa K, Shinmura T, Shimono M, Hasenaka T (2009) Petrography and whole-rock geochemistry of pre-Aso lavas from the caldera wall of Aso volcano, central Kyushu. *Journal of the Geological Society of Japan* 115: 672-687

Miyoshi M, Shimono M, Hasenaka T, Sano T, Mori Y, Fukuoka T (2010) Boron systematics of Hisatsu and Kirishima basaltic rocks from southern Kyushu, Japan. *Geochemical Journal* 44: 359-369

Morfin S, Sawyer EW, Bandyayera D (2014) The geochemical signature of a felsic injection complex in the continental crust: Opinaca Subprovince, Quebec. *Lithos* 196-197: 339-355

Moyen J-F, Laurent O (2018) Archean tectonic systems: A view from igneous rocks. *Lithos* 302-303: 99-125

O'Neil J, Francis D, Carlson RW (2011) Implications of the Nuvvuagittuq greenstone belt for the formation of Earth's early crust. *Journal of Petrology* 52: 985-1009

O'Neil J, Carlson RW, Paquette J-L, Francis D (2012) Formation age and metamorphic history of the Nuvvuagittuq greenstone belt. *Precambrian Research* 220-221: 23-44

O'Neil J, Boyet M, Carlson RW, Paquette J-L (2013) Half a billion years of reworking of Hadean mafic crust to produce the Nuvvuagittuq Eoarchean felsic crust. *Earth and Planetary Science Letters* 379: 13-25

Pearce JA (2008) Geochemical fingerprinting of oceanic basalts with applications to ophiolite classification and the search for Archean oceanic crust. *Lithos* 100: 14-48

Pearson WN, Trinder IA, Henderson DN, Wahl DG (1993) Prefeasibility study, Hordon Lake deposit, Quebec, for Kingswood Resources Inc. Statutory report submitted to Ministère des Ressources naturelles, Québec; GM 53039, 118 p.

Percival J, Mortenson JK, Stern RA, Card KD (1992) Giant granulite terranes of northeastern Superior Province: the Ashuanipi complex and Minto block. *Canadian Journal of Earth Sciences* 29: 2287-2308

Percival J, Skulski T, Sanborn-Barrie M, Stott G, Leclair A, Corkery M, Boily M (2012) Geology and tectonic evolution of the Superior Province, Canada. In: Percival J, Cook F, Clowes R., eds., *Tectonic styles in Canada: The Lithoprobe Perspective*, . Geological Association of Canada, Special Paper 49: 321-378

Polat A, Kerrich R (2001) Geodynamic processes, continental growth, and mantle evolution recorded in late Archean greenstone belts of the southern Superior Province, Canada. *Precambrian Research* 112: 5-25

Poulsen KH, Robert F, Dubé B (2000) Geological classification of Canadian gold deposits. *Geological Survey of Canada, Bulletin* 540, 106 p.

Powell WG, Carmichael DM, Hodgson CJ (1995) Conditions and timing of metamorphism in the southern Abitibi greenstone belt, Quebec. *Canadian Journal of Earth Sciences* 32: 787-805

Riopel J (1994) Rapport technique des travaux, campagne 1994, propriété Lac Marcaut. Statutory report submitted by Cambiex Exploration to Ministère des Ressources naturelles, Québec, GM 53629, 328 p.

Rogers R, Ross P-S, Goutier J, Mercier-Langevin P (2014) Using physical volcanology, chemical stratigraphy, and pyrite geochemistry for volcanogenic massive sulfide exploration : An example from the Blake River Group, Abitibi Greenstone Belt. *Economic Geology* 109: 61-88

Ross P-S, Bédard JH (2009) Magmatic affinity of modern and ancient subalkaline volcanic rocks determined from trace element discriminant diagrams. *Canadian Journal of Earth Sciences* 46: 823-839

Rowins SM (2000) Reduced porphyry copper-gold deposits: A new variation on an old theme. *Geology* 28: 491-494

Rudnick RL, Fountain DM (1995) Nature and composition of the continental crust: A lower crustal perspective. *Reviews of Geophysics* 33: 267-309

Sawyer EW, Benn K (1992) Geochemistry, Metamorphism and Structure of the Opatica Belt. Abitibi-Grenville Transect. Lithoprobe: 159-162

Sawyer E, Benn K (1993) Structure of the high-grade Opatica Belt and adjacent low-grade Abitibi Subprovinces, Canada: an Archaean mountain-front. Journal of Structural Geology 15: 1443-1458

Sigmarsson O, Vlastelic I, Andreasen R, Bindeman I, Devidal J-L, Moune S, Keiding JK, Larsen G, Höskuldsson A, Thordarson Th (2011) Remobilization of silicic intrusion by mafic magmas during the 2010 Eyjafjallajökull eruption. Solid Earth 2: 271-281

Smithies RH, Ivanic TJ, Lowery JR, Morris PA, Barnes SJ, Wyche S, Lu Y-J (2018) Two distinct origins for Archean greenstone belts. Earth and Planetary Science Letters 487: 106-116

Stolz AJ, Varne R, Davies GR, Wheller GE, Foden JD (1990) Magma source components in an arc-continent collision zone: The Flores-Lembata sector, Sunda Arc, Indonesia. Contributions to Mineralogy and Petrology 105: 585-601

Sun S-S, McDonough WF (1989) Chemical and isotopic systematics of oceanic basalts: implications for mantle composition and processes. In: Saunders AD, Norry MJ (eds) Magmatism in the Ocean Basins. Geological Society, London, Special Publication 42: 313-345

Takagi T, Orihashi Y, Naito K, Watanabe Y (1999) Petrology of a mantle-derived rhyolite, Hokkaido, Japan. Chemical Geology 160: 425-445

Tawarayewicz J, White RS, Woods AW, Brandsdottir B, Gudmundsson MT (2012) Magma mobilization by downward-propagating decompression of the Eyjafjallajökull volcanic plumbing system. Geophysical Research Letters 39, L19309

Tomlinson KY, Condie KC (2001) Archean mantle plumes: Evidence from greenstone belt geochemistry. *In:* Ernst RE, Buchan KL, eds Mantle plumes: Their identification through time: Boulder, Colorado. Geological Society of America, Special Paper 352: 341-357

Thorsen K, Taquet B, Lamothe G, Burk R, Tarnocai D (1993) Assessment report on the 1991-1992 exploration program, Lac Marcaut property. Statutory report submitted by Teck Exploration Ltd. to Ministère des Ressources naturelles Québec. GM 52214, p. 231

Thurston PC (2002) Autochthonous development of Superior Province greenstone belts? Precambrian Research 115: 11-36

Thurston PC, Ayer JA, Goutier J, Hamilton MA (2008) Depositional gaps in Abitibi Greenstone Belt stratigraphy: a key to exploration for syngenetic mineralization. Economic Geology 34: 677-680

Tsvetkov AA, Sukhanov MK, Govorov GI (1985) Regular evolution of magmatism in recent and Paleogene arcs (for instance Kuril Islands and northern Caucasus). *In:* Bogatikov OA, eds Oceanic magmatism: Evolution, geological correlation: Nauka, Moscow: 185-218

Turner S, Rushmer T, Reagan M, Moyen J-F (2014) Heading down early on? Start of subduction on Earth. Geology 42: 139-142

Voliquette (1975) Région de la rivière Nemiscau. Ministère des Ressources naturelles, Québec; report RG 158, 156 p.

Westall F, de Ronde C. E. J, Southam G, Grassineau N, Colas M, Cockell C, Lammer H (2006) Implications of a 3.472-3.333 Gyr-old subaerial microbial mat from the Barberton greenstone belt, South Africa for the UV environmental conditions on the early Earth. Philosophical Transactions of the Royal Society of London B: Biological Sciences 361: 1857-1876

Winchester JA, Floyd PA (1977) Geochemical discrimination of different magma series and their differentiation products using immobile elements. Chemical Geology 20: 325-343

Windley BF (1996) The evolving continents, 3rd edn, Wiley, 785 p.

Winter JD (2001) An introduction to igneous and metamorphic petrology. Prentice Hall, 697 p.

Wood DA (1980) The Application of a Th-Hf-Ta diagram to problems of tectonomagmatic classification and to establishing the nature of crustal contamination of basaltic lavas of the British Tertiary volcanic province. Earth and planetary science letters 50: 11-30